

WARSAW UNIVERSITY OF TECHNOLOGY

DISCIPLINE OF SCIENCE - CHEMICAL ENGINEERING /
FIELD OF SCIENCE - ENGINEERING AND TECHNOLOGY

Ph.D. Thesis

Zuzanna Bojarska, M.Sc.

**Production and characterization methods
of hybrid nanostructures based on molybdenum disulfide and
carbon nanomaterials for catalytic and lubricating applications**

Supervisor

Łukasz Makowski, Prof. WUT, Ph.D., D.Sc.

Co-supervisor

Marta Mazurkiewicz-Pawlicka, Ph.D.

WARSAW 2022

Special thanks to people without whom this work would not have been possible

Łukasz Makowski, Prof. WUT, Ph.D. D.Sc.

Marta Mazurkiewicz-Pawlicka, Ph.D.

Artur Małolepszy, Ph.D.

Michał Wojtalik, Ph.D.

Janusz Kopytowski, M.Sc.

Jakub Zabrzycycki, Eng.

Abstract of the Doctoral Thesis

Production and characterization methods of hybrid nanostructures based on molybdenum disulfide and carbon nanomaterials for catalytic and lubricating applications

This doctoral dissertation is devoted to developing a new method for synthesizing hybrid nanostructures based on molybdenum disulfide and carbon nanomaterials (MoS₂/CNMs). The first stage of the work was to determine the influence of the synthesis parameters of pure molybdenum disulfide obtained using impinging jet reactors on the properties of the product. The obtained results made it possible to establish favorable process conditions for the production of hybrid nanostructures. As a result of the heterogeneous nucleation, MoS₂ nanoparticles are formed on the surface of carbon nanomaterials. The foreign substance present in the supersaturated solution reduces the nucleation energy, so heterogeneous nucleation occurs earlier than homogeneous nucleation. In this way, the surface of carbon nanomaterials is covered with MoS₂ nanoparticles. Wet chemical synthesis can be carried out in commonly used tank reactors, but also in the impinging jet reactors. The latter, in particular, are suitable for the controlled production of such particles. The high mixing intensity is related to the formation of an area with a high energy dissipation rate in the contact zone of the inlet streams. This allows to obtain materials with the desired and repeatable properties in an inexpensive, continuous, and easy to scale way. Due to the potential use of MoS₂ as a hydrogen evolution catalyst, the properties of hybrid nanostructures were tested for this application. The maximum current density obtained at a potential of 0.2 V vs. RHE for the best hybrid sample was 16 times higher than in the case of pure molybdenum disulfide. Furthermore, MoS₂ is commonly used as a lubricant. Therefore, it was checked how hybrid nanostructures affect the lubricating properties of engine oil. Studies of the size distribution of particulate matter in the engine exhaust gas showed that the use of oil with the addition of MoS₂/CNMs allowed to reduce the total volume of particulate matter in the exhaust gas by 91% and 49% under idling conditions and with load compared to work with the base oil.

Keywords: molybdenum disulfide, carbon nanomaterials, impinging jet reactors, hydrogen evolution reaction, nanoadditives for engine oils

Streszczenie rozprawy doktorskiej

Metody wytwarzania i charakteryzacji nanostruktur hybrydowych na bazie disiarczku molibdenu i nanomateriałów węglowych do zastosowań katalitycznych i smarnych

Niniejsza rozprawa doktorska poświęcona jest opracowaniu nowej metody syntezy hybrydowych nanostruktur na bazie disiarczku molibdenu i nanomateriałów węglowych (MoS_2/CNMs). Pierwszym etapem pracy było określenie wpływu parametrów prowadzenia syntezy czystego disiarczku molibdenu otrzymywanego z wykorzystaniem reaktorów zderzeniowych na właściwości produktu. Uzyskane wyniki umożliwiły określenie korzystnych warunków procesowych wytwarzania hybrydowych nanostruktur. W wyniku heterogenicznej nukleacji nanocząstki MoS_2 powstają na powierzchni nanomateriałów węglowych. Obecna substancja obecna w roztworze przesyconym zmniejsza energię zarodkowania, dzięki czemu nukleacja heterogeniczna następuje wcześniej niż homogeniczna. W ten sposób powierzchnia nanomateriałów węglowych pokryta zostaje nanocząstkami MoS_2 . Moką syntezę chemiczną można przeprowadzić w powszechnie stosowanych reaktorach zbiornikach, ale także w reaktorach zderzeniowych. W szczególności te drugie nadają się do kontrolowanej produkcji takich cząstek. Wysoka intensywność mieszania związana jest z tworzeniem się obszaru o dużej szybkości rozpraszania energii w strefie kontaktu strumieni wlotowych. Pozwala to uzyskać materiały o pożądanym i powtarzalnym właściwościach w tani, ciągły oraz łatwy do przeskalowania sposób. Ze względu na potencjalne zastosowanie MoS_2 jako katalizatora reakcji wydzielania wodoru, sprawdzono właściwości hybrydowych nanostruktur pod kątem tej aplikacji. Maksymalna gęstość prądu uzyskiwana przy potencjale 0.2 V vs. RHE dla najlepszej próbki hybrydowej wynosi 16 razy więcej niż w przypadku czystego disiarczku molibdenu. Ponadto MoS_2 powszechnie jest stosowany jako lubrykant, dlatego też sprawdzono jak hybrydowe nanostruktury wpływają na właściwości smarne oleju silnikowego. Badania rozkładu rozmiarów cząstek stałych w spalinach silnika wykazały, że użycie oleju z dodatkiem MoS_2/CNMs pozwoliły na zmniejszenie całkowitej objętości cząstek stałych w spalinach o 91% i 49% w warunkach biegu jałowego i z obciążeniem w stosunku do pracy z olejem bazowym.

Słowa kluczowe: disiarczek molibdenu, nanomateriały węglowe, reaktory zderzeniowe, reakcja wydzielania wodoru, nanododatki do olejów silnikowych

Table of Contents

Abstract of the Doctoral Thesis.....	5
Streszczenie rozprawy doktorskiej.....	6
List of publications included in the doctoral dissertation	10
Author's contribution to specific papers.....	11
List of other publications created during the Ph.D. candidate's research activities	12
Patent applications.....	13
List of projects that research has been included in the dissertation	14
List of projects that research has not been included in the dissertation	15
Awards	16
Conference presentations related to the topic of the doctoral dissertation.....	17
Conference presentations not related to the topic of the doctoral dissertation.....	19
Abbreviations and formulas	21
List of symbols.....	23
Introduction	25
Purpose	27
Scope... ..	28
1. Carbon nanomaterials.....	29
1.1 Graphene oxide	29
1.2 Reduced graphene oxide	30
1.3 Carbon nanotubes.....	31

2.	Molybdenum disulfide-based materials	32
2.1	Transition metal dichalcogenides	32
2.2	Molybdenum disulfide	32
2.3	Hybrid nanostructures based on molybdenum disulfide and carbon nanomaterials	34
2.4	Preparation methods of hybrid nanostructures MoS ₂ /CNMs	35
3.	Hydrogen evolution reaction catalysis	36
3.1	Hydrogen evolution reaction	36
3.2.4	Electrochemically active surface area	41
3.3	Hydrogen evolution reaction catalysts based on MoS ₂	42
4.	Engine oil additives	44
4.2	Rheology	46
4.3	Engine oils	47
4.3	Oil additives based on MoS ₂	48
5.	Preparation of molybdenum disulfide through wet chemical synthesis	50
5.1	Influence of annealing temperature	51
5.2	Influence of reducing agent	53
5.3	Influence of reactor geometry and process mode	56
5.4	Influence of process conditions	59
6.	Preparation of hybrid nanostructures based on MoS ₂ and CNMs via wet chemical synthesis	61
7.	Catalytic properties of hybrid nanostructures based on MoS ₂ and CNMs	66
7.1	Electrochemical analysis of the synthesized MoS ₂ -based materials	66

7.2	Electrochemical analysis of reference MoS ₂	69
7.3	Hydrogen production.....	71
8.	Lubricating properties of hybrid nanostructures based on MoS ₂ and CNMs	74
8.1	Tribological properties of MoS ₂ -based additives.....	74
8.2	Rheological properties of MoS ₂ -based additives	77
8.3	Particle size distribution in the engine exhaust gas.....	81
9.	Conclusions	86
	List of Figures	88
	List of Tables.....	91
	References	92

List of publications included in the doctoral dissertation (*data from 2022)

P1 – Michał Wojtalik, **Zuzanna Bojarska**, Łukasz Makowski. Experimental studies on the chemical wet synthesis for obtaining high-quality MoS₂ nanoparticles using impinging jet reactor. *Journal of Solid State Chemistry*. 2020; 285: 121254. DOI:10.1016/j.jssc.2020.121254. (*IF: 3.656; CS: 5.2; ministerial points: 70)

P2 – **Zuzanna Bojarska**, Mateusz Mężydło, Marta Mazurkiewicz-Pawlicka, Łukasz Makowski. Influence of process parameters and reducing agent on the size of MoS₂ nanoparticles obtained in impinging jet reactor. *Applied Sciences*. 2022; 12: 11293. DOI:10.3390/app122111293. (*IF: 2.838; CS: 3.7; ministerial points: 100)

P3 – **Zuzanna Bojarska**, Marta Mazurkiewicz-Pawlicka, Stanisław Gierlotka, Łukasz Makowski. Production and properties of molybdenum disulfide/graphene oxide hybrid nanostructures for catalytic applications. *Nanomaterials*. 2020; 10(9): 1865. DOI:10.3390/nano10091865. (*IF: 5.719; CS: 6.6; ministerial points: 100)

P4 – **Zuzanna Bojarska**, Marta Mazurkiewicz-Pawlicka, Bogusław Mierzwa, Tomasz Płociński, Łukasz Makowski. Effect of the carbon support on MoS₂ hybrid nanostructures prepared by an impinging jet reactor for hydrogen evolution reaction catalysis. *Journal of Environmental Chemical Engineering*. 2022, 10(4): 108038. DOI:10.1016/j.jece.2022.108038. (*IF: 7.968; CS: 7.7; ministerial points: 100)

P5 – **Zuzanna Bojarska**, Janusz Kopytowski, Marta Mazurkiewicz-Pawlicka, Stanisław Gierlotka, Antoni Rozeń, Łukasz Makowski. Molybdenum disulfide-based hybrid materials as new types of oil additives with enhanced tribological and rheological properties. *Tribology International*. 2021; 160: 106999, DOI:10.1016/j.triboint.2021.106999. (*IF: 5.62; CS: 9.3; ministerial points: 200)

P6 – Łukasz Makowski, **Zuzanna Bojarska**, Antoni Rozeń. Rheological properties of engine oil with nano-additives based on MoS₂ materials. *Nanomaterials*. 2022; 12(4): 581. DOI:10.3390/nano12040581. (*IF: 5.719; CS: 6.6; ministerial points: 100)

Author's contribution to specific papers

P1 – Secondary author – Formulating some of the conclusions from the XRD analysis; performing and partially developing TGA analysis of the purified product and the MoS₂ reference; preparing figures 9, 10; separating of particles by exfoliation, performing measurements and research on their electrochemical properties; preparing and editing the manuscript.

P2 – Lead author – Developing research concepts, consulting and interpreting research results; drawing conclusions from the research; preparing figures 9 – 13; preparing and editing the manuscript.

P3 – Lead author – Developing research concepts; conducting the experiments (synthesis in both reactors) and measurements (PSD, TGA, FTIR, and LSV); interpreting research results; drawing conclusions from the research; preparing all figures; preparing and editing the manuscript.

P4 – Lead author – Developing research concepts; conducting the experiments (synthesis of MoS₂/CNMs) and physicochemical analysis (PSD, TGA); participating in electrochemical measurements (LSV, CV, EIS, stability); drawing conclusions from the research; preparing all figures; preparing and editing the manuscript.

P5 – Lead author – Developing research concepts; conducting the experiments (synthesis of MoS₂/CNMs), physicochemical analysis (PSD, FTIR, TGA), and tribological and rheological measurements; drawing conclusions from the research; preparing all figures (except figure 2); preparing and editing the manuscript.

P6 – Secondary author – Participating in developing research concepts; developing the physicochemical analysis (density and specific heat capacity); drawing conclusions from the research; preparing figure 1; preparing and editing the manuscript.

List of other publications created during the Ph.D. candidate's research activities

1 – Monika Jałowiecka, **Zuzanna Bojarska**, Artur Małolepszy, Łukasz Makowski. Mass transport enhancement in direct formic acid fuel cell with a novel channel design. *Chemical Engineering Journal*. 2023; 451 (1): 138474, DOI:10.1016/j.cej.2022.138474. (IF: 16.744; CS: 19.4; ministerial points: 200)

2 – Michał Wojtalik, Przybysław Przybył, Katarzyna Zubańska, Monika Żuchowska, **Zuzanna Bojarska**, Monika Arasimowicz-Andres, Antoni Rozeń, Łukasz Makowski. Otrzymywanie syntetycznych cząstek MoS₂ za pomocą metody mokrej [Production of synthetic particles of MoS₂ using wet chemical synthesis *Przemysł Chemiczny*. 2019; 98(11), 1817-1821, DOI:10.15199/62.2019.11.24. (IF: 0.49; ministerial points: 70)

3 – **Zuzanna Bojarska**, Marta Mazurkiewicz-Pawlicka, Łukasz Makowski. Graphene oxide-based nanomaterials as catalysts for oxygen reduction reaction. *Chemical and Process Engineering*. 2019; 40 (4): 361–376, DOI:10.24425/cpe.2019.130212. (IF: 0.679; CS: 1.4; ministerial points: 100)

Patent applications

1 – *Elementy turbulizujące w kanałach dystrybuujących reagenty w niskotemperaturowym ogniwie paliwowym z membraną protonoprzewodzącą*

[Turbulence elements in the channels distributing the reactants in a low-temperature fuel cell with a proton-conducting membrane];

application no. P.440498;

Łukasz Makowski, **Zuzanna Bojarska**, Monika Jałowiecka, Artur Małolepszy;

date of filing the invention 2022/02/28

2 – *Sposób wytwarzania nanocząstek dwusiarczku renu i zastosowanie nanocząstek dwusiarczku renu wytworzonych tym sposobem w elektrokatalizie i fotokatalizie*

[The method of producing rhenium disulfide nanoparticles and the use of rhenium disulfide nanoparticles produced by this method in electrocatalysis and photocatalysis];

application no. P.440673;

Łukasz Werner, **Zuzanna Bojarska**, Kamil Czelej, Marta Mazurkiewicz-Pawlicka, Karol Ćwieka, Leon Gradoń;

date of filing the invention 2022/03/17

List of projects that research has been included in the dissertation



Badanie kinetyki powstawania kryształów disiarczku molibdenu w celu uzyskania produktu o pożądanych właściwościach w reaktorach zderzeniowych

[Investigation of the kinetics of molybdenum disulfide particles to obtain product of desired properties in jets reactors]

OPUS, NCN, DEC-2017/27/B/ST8/01382 (2018-2021)



Nowoczesne hybrydowe katalizatory na bazie nanomateriałów węglowych i disiarczku molibdenu do reakcji wydzielania wodoru

[Novel hybrid catalysts based on carbon nanomaterials and molybdenum disulfide for hydrogen evolution reaction]

TechMat-1, Excellence Initiative – Research University, 1820/11/Z01/POB5/2020



Novel hybrid materials based on molybdenum disulfide with enhanced photocatalytic properties for hydrogen evolution reaction

[Nowoczesne materiały hybrydowe na bazie disiarczku molibdenu ze zwiększonymi właściwościami fotokatalicznymi do reakcji wydzielania wodoru]

8th Polish - Taiwanese/Taiwanese-Polish Joint Research Call, PL-TW/VIII/2020/9



Nowe hybrydowe nanostruktury na bazie disiarczku molibdenu i nanomateriałów węglowych do zastosowań smarnych

[Novel Hybrid Nanostructures Based on Molybdenum Disulfide and Carbon Nanomaterials for Lubricating Applications]

PRELUDIUM, NCN, 2021/41/N/ST8/03764

List of projects that research has not been included in the dissertation



Opracowanie nowej geometrii kanałów z wykorzystaniem obliczeniowej mechaniki płynów do optymalizacji wydajności ogniwa paliwowego zasilanego kwasem mrówkowym
[Development of new channel geometry using computational fluid dynamics to optimize the efficiency of the direct formic acid fuel cell]

ENERGYTECH-1, Excellence Initiative – Research University, 1820/29/Z01/POB7/2020



Synteza i charakterystyka nanokatalizatorów na bazie dwuwymiarowego dwusiarczku renu (ReS_2) do fotokatalitycznej produkcji wodoru
[Synthesis and characterization of nanocatalysts based on two-dimensional rhenium disulfide (ReS_2) for photocatalytic hydrogen production]

TechMat-2, Excellence Initiative – Research University, 1820/19/Z01/POB5/2021



Wytwarzanie katalizatorów do reakcji redukcji tlenu opartych na zredukowanym tlenku grafenu przy użyciu płynów w stanie nadkrytycznym
[Manufacture of oxygen reduction catalysts based on reduced graphene oxide using supercritical fluids]

TechMat-2, Excellence Initiative – Research University



Wysokowydajny układ przepływowy do fotokatalitycznej produkcji wodoru z biomasy
[High-performance flow system for photocatalytic production of hydrogen from biomass]

Lider, NCBR, LIDER/19/0069/L 11/19/NCBR/2020

Awards

- 1.** My research was the basis for awarding the 1st prize to the Warsaw University of Technology in the 3W Competition - 3W World Leader in the SCIENCE category 2022.
- 2.** II Award for the best presentation of a young scientist during European Technical Coatings Congress, July 12-14, 2022, Krakow.
- 3.** Team Award of the 1st degree of the Rector of the Warsaw University of Technology for scientific achievements in 2019-2020.
- 4.** Dean's Award for scientific achievements and exceptional social activity in the 2020/2021 academic year.
- 5.** Dean's Award for scientific achievements and exceptional social activity in the 2019/2020 academic year.

Conference presentations related to the topic of the doctoral dissertation

1. 26th International Congress of Chemical and Process Engineering, August 21-25, 2022, Prague, Czech Republic, with **oral presentation** entitled “Nonadditives for engine oil based on molybdenum disulfide with enhanced tribological properties and their impact on environment”. **Zuzanna Bojarska**, Łukasz Makowski;
2. European Technical Coatings Congress, July 12-14, 2022, Krakow, Poland, with **oral presentation** entitled “Designing hybrid nanocomposites based on molybdenum disulphide and carbon nanomaterials for enhanced photo electrocatalytic properties”. **Zuzanna Bojarska**, Marta Mazurkiewicz-Pawlicka, Łukasz Makowski;
3. European Technical Coatings Congress, July 12-14, 2022, Krakow, Poland, with **poster presentation** entitled “Nanosized MoS₂ deposited on carbon nanomaterials as the new lubricant additive for engine oils”. **Zuzanna Bojarska**, Marta Mazurkiewicz-Pawlicka, Łukasz Makowski;
4. X Kongres Technologii Chemicznej, Maj 11-14, 2022, Wrocław, Poland, with **oral presentation** entitled “Nowoczesne nanododatki MoS₂/CNMs do olejów silnikowych i ich wpływ na środowisko”. **Zuzanna Bojarska**, Łukasz Makowski;
5. 10th European Young Engineers Conference, April 4-6, 2022, online, with **oral presentation** entitled “Highly efficient hybrid nanostructures based on MoS₂ for hydrogen evolution”. **Zuzanna Bojarska**, Marta Mazurkiewicz-Pawlicka, Łukasz Makowski;
6. 10th European Young Engineers Conference, April 4-6, 2022, online, with **poster presentation** entitled “Preparation of MoS₂/carbon nanomaterials catalysts for hydrogen evolution reaction”. Jakub Zabrzycki, **Zuzanna Bojarska**, Marta Mazurkiewicz-Pawlicka;
7. 5th International Caparica Symposium on Nanoparticles/Nanomaterials and Applications, January 24-27, 2022, Caparica, Portugal, with **oral presentation** entitled “Novel hybrid nanostructures based on molybdenum disulfide and carbon nanomaterials for energy conversion applications”. **Zuzanna Bojarska**, Marta Mazurkiewicz-Pawlicka, Łukasz Makowski;
8. European Congress of Chemical Engineering and European Congress of Applied Biotechnology, September 20-23, 2021, online, with **oral presentation** entitled "Molybdenum disulfide-based hybrid materials as new types of oil additives with

- enhanced tribological and rheological properties". **Zuzanna Bojarska**, Janusz Kopytowski, Antoni Rozeń, Łukasz Makowski;
9. 9th European Young Engineers Conference, April 19-21, 2021, online, with **oral presentation** entitled "MoS₂/CNMs hybrid nanostructures for photo-electrocatalytic applications"; **Zuzanna Bojarska**, Marta Mazurkiewicz-Pawlicka, Łukasz Makowski;
 10. 4th International Conference on Nanotechnology based innovative applications for the environment, March 28-31, 2021, online, with **oral presentation** entitled "Production and properties of molybdenum disulfide/carbon nanomaterials hybrid nanostructures"; **Zuzanna Bojarska**, Marta Mazurkiewicz-Pawlicka, Łukasz Makowski;
 11. 4th International Conference on Nanotechnology based innovative applications for the environment, March 28-31, 2021, online, with **oral presentation** entitled "Molybdenum disulfide based engine oil nanosuspensions with enhanced tribological and rheological properties". **Łukasz Makowski**, **Zuzanna Bojarska**, Janusz Kopytowski, Antoni Rozeń;
 12. 24th International Congress of Chemical and Process Engineering, March 15-18, 2021, online, with **oral presentation** entitled "Synthesis of molybdenum disulfide-carbon nanomaterials nanocomposites in the impinging jet reactor and their electrochemical performance". **Zuzanna Bojarska**, Marta Mazurkiewicz-Pawlicka, Łukasz Makowski
 13. Baltic University Programme VII PhD Students Training, November 24-28, 2019, Rogow, Poland, with **oral presentation** entitled "Designing hybrid nanostructures based on molybdenum disulfide for enhanced photoelectrocatalytic properties". **Zuzanna Bojarska**, Marta Mazurkiewicz-Pawlicka, Łukasz Makowski;
 14. 12th European Congress of Chemical Engineering, September 15-19, 2019, Florence, Italy, with **poster presentation** entitled "Designing hybrid nanocomposites of molybdenum disulphide/carbon nanomaterials". **Zuzanna Bojarska**, **Łukasz Makowski**, Marta Mazurkiewicz-Pawlicka, Monika Arasimowicz;
 15. 23rd Polish Conference of Chemical and Process Engineering, June 2-5, 2019, Jachranka-Warszawa, Polska with **poster presentation** entitled "Graphene oxide-based materials as supports for photocatalyst nanoparticles". **Zuzanna Bojarska**, Marta Mazurkiewicz-Pawlicka, Łukasz Makowski;
 16. 8th European Young Engineers Conference, April 08-10, 2019, Warsaw, Poland, with **oral presentation** entitled "Graphene oxide-based materials as supports for catalyst nanoparticles". **Zuzanna Bojarska**, Marta Mazurkiewicz-Pawlicka, Łukasz Makowski.

Conference presentations not related to the topic of the doctoral dissertation

1. American Advanced Materials Congress, October/November 29-05, 2022, Miami, USA, with **oral presentation** entitled “Sustainable hydrogen production in flow systems over supported plasmonic photocatalysts: Recent advances and future perspectives”. Karol Ćwieka, Kamil Czelej, **Zuzanna Bojarska**, Łukasz Werner, Katarzyna Jabłczyńska, Krzysztof Wojtas, Leon Gradoń, Juan Carlos Colmenares
2. 26th International Congress of Chemical and Process Engineering, August 21-25, 2022, Prague, Czech Republic, with **oral presentation** entitled “Numerical and experimental study on the improvement of Direct Formic Acid Fuel Cell channel design”. Monika Jałowiecka, **Zuzanna Bojarska**, Artur Małolepszy, Łukasz Makowski;
3. MRS Spring Meeting, May 8-13, Honolulu, Hawai’i, with **poster presentation** entitled “Synthesis of MoS₂/CNMs/TiO₂ hybrid nanostructures as potential HER catalysts”. Zuzanna Bojarska, Marta Mazurkiewicz-Pawlicka, Artur Malolepszy, Łukasz Makowski;
4. MRS Spring Meeting, May 8-13, Honolulu, Hawai’i, with **poster presentation** entitled “Preparation of WO₃/MoS₂/Carbon nanomaterials hybrid structures for potential energy applications”. Marta Mazurkiewicz-Pawlicka, **Zuzanna Bojarska**, Artur Malolepszy, Łukasz Makowski;
5. X Kongres Technologii Chemicznej, Maj 11-14, 2022, Wrocław, Poland, with **oral presentation** entitled “Badania doświadczalne i modelowanie CFD transportu masy w ogniwie paliwowym”. Monika Jałowiecka, **Zuzanna Bojarska**, Artur Małolepszy, Łukasz Makowski;
6. 10th European Young Engineers Conference, April 4-6, 2022, online, with **oral presentation** entitled “Computational Fluid Dynamics modelling and experimental research on the development of fuel cell channel design”. Monika Jałowiecka, **Zuzanna Bojarska**, Artur Małolepszy, Łukasz Makowski;
7. European Fuel Cells and Hydrogen Conference Virtual Conference, December 15-17, 2021, online, with **poster presentation** entitled "Computational and experimental research on enhancement of direct formic acid fuel cell performance via novel channel design". Monika Jałowiecka, **Zuzanna Bojarska**, Łukasz Makowski, Artur Małolepszy;

8. European Congress of Chemical Engineering and European Congress of Applied Biotechnology, September 20-23, 2021, online, with **poster presentation** entitled "Computational analysis of a direct formic acid fuel cell performance with innovative channel design". Monika Jałowiecka, **Zuzanna Bojarska**, Łukasz Makowski, Artur Małolepszy;
9. 9th European Young Engineers Conference, April 19-21, 2021, online, with **poster presentation** entitled: "Computational Fluid Dynamics modeling of a direct fuel cell with a novel channel design". Monika Jałowiecka, **Zuzanna Bojarska**, Łukasz Makowski, Artur Małolepszy.

Abbreviations and formulas

AS	– Ammonium sulfide
CA	– Citric acid
CFD	– Computational fluid dynamics
CNMs	– Carbon nanomaterials
CNTs	– Carbon nanotubes
CO ₂	– Carbon dioxide
CV	– Cyclic voltammetry
CVD	– Chemical vapor deposition
ECSA	– Electrochemically active surface area
E _{HER}	– Equilibrium HER potential
EIS	– Electrochemical impedance spectroscopy
FA	– Formic acid
FAPES	– Fast aerosol particle emission spectrometry
GHG	– Greenhouse gas
GO	– Graphene oxide
HER	– Hydrogen evolution reaction
HMA	– Ammonium molybdate tetrahydrate
H ₂	– Hydrogen
LSV	– Linear sweep voltammetry
MoS ₂	– Molybdenum disulfide
MoS ₂ /CNMs	– Hybrid nanostructure
NASA	– National Aeronautics and Space Administration
NPs	– Nanoparticles
PSD	– Particle size distribution
RES	– Renewable energy sources
rGO	– Reduced graphene oxide
RHE	– Reversible hydrogen electrode
SAE	– Society of Automotive Engineers
STEM	– Scanning transmission electron microscopy
SOCNTs	– Strongly oxidized carbon nanotubes

- TGA – Thermogravimetric analysis
- TMDs or TMDCs – Transition metal dichalcogenides
- UE – European Union
- XRD – X-Ray powder diffraction

List of symbols

a	– Constant in Tafel equation [V]
b	– Tafel slope [$V \cdot \text{dec}^{-1}$]
D_p	– Particle diameter [m]
F_N	– Normal force [N]
F_R	– Friction force [N]
I	– Current [A]
j, i_0	– Current density [$A \cdot \text{cm}^{-2}$]
j_0	– Exchange current density [$A \cdot \text{m}^{-2}$]
k	– Electrochemical equivalence [$\text{g} \cdot \text{C}^{-1}$], flow consistency index [$\text{Pa} \cdot \text{s}^n$]
L_{10}	– Mean size (arithmetic mean) [μm]
L_{32}	– Mean size (surface-weighted mean size) [μm]
L_{43}	– Mean size (volume-weighted mean size) [μm]
m	– Mass of hydrogen released at the electrode [g]
N	– Particle concentration [$\# \cdot \text{m}^{-3}$]
n	– Flow behavior index [-]
P	– Load [$N \cdot \text{m}^{-1}$]
R_{ct}	– Charge transfer resistance [Ω]
R_{mt}	– Mass transfer resistance [Ω]
t	– Time [s]
V	– Particle volume [m^3]
Y	– Hydrogen yield [$\text{mmol} \cdot \text{g}_{\text{cat}}^{-1} \cdot \text{h}^{-1}$]
Z'	– Real part of impedance [Ω]
$-Z''$	– Negative, imaginary part of impedance [Ω]

$\dot{\gamma}$	– Shear rate [s^{-1}]
ΔG_{H^*}	– Gibbs' adsorption energy [eV]
η	– Dynamic viscosity [$\text{Pa}\cdot\text{s}$], overpotential [V]
η_1	– Overpotential at $1 \text{ mA}\cdot\text{cm}^{-2}$ [V vs. RHE]
η_{10}	– Overpotential at $10 \text{ mA}\cdot\text{cm}^{-2}$ [V vs. RHE]
η_{100}	– Overpotential at $100 \text{ mA}\cdot\text{cm}^{-2}$ [V vs. RHE]
μ	– Friction factor [-]
v	– Sliding velocity [$\text{m}\cdot\text{s}^{-1}$]
τ	– Shear stress [Pa]

Introduction

Due to the changing climatic conditions that directly and indirectly affect human life, European Union (UE) has started the fight against greenhouse gas (GHG) emissions. UE has an ambitious plan to achieve climate neutrality by 2050, along with an interim emission reduction target of 55% by 2030 [1]. The GHG targets apply to every EU country in sectors not covered by the Emissions Trading System, i.e., transport, agriculture, construction, and waste management. In order to achieve climate neutrality, different approaches are taken into account. One of the ideas is carbon dioxide (CO₂) sinks. They are defined as any system that absorbs more CO₂ than it emits, e.g., forests and oceans. However, the artificial carbon dioxide sinks are not sufficient on the scale needed to fight global warming [2]. Thus, it is necessary to reduce GHG emissions to achieve the aforementioned targets. For this purpose, investments in renewable energy, energy efficiency, or other clean, low-carbon technologies are made. Among renewable energy technologies, hydrogen has been distinguished as the fuel of the future [3, 4]. In the political and business environment, clean hydrogen is gaining unprecedented momentum. Nowadays, hydrogen is mainly produced from natural gas, obtaining grey and blue types (Figure 1). The new paradigm is to obtain hydrogen using renewable energy sources (RES), a green attempt [5]. Accompanying water splitting with RES is a promising way to obtain a sustainable and balanced energy economy [5, 6].

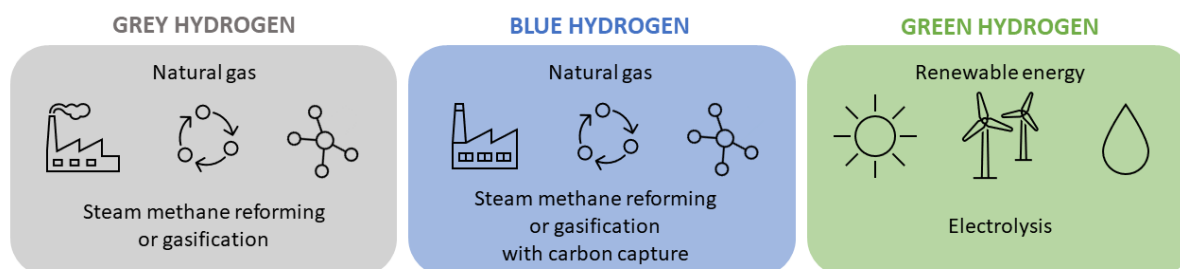


Figure 1. Types of hydrogen and methods of its production

However, the high cost or/and insufficient efficiency of the aforementioned technologies limit the usability of green hydrogen. Meeting the market requirements, novel, low-cost, and accessible catalysts for hydrogen production are sought. Herein, molybdenum disulfide (MoS₂) can be distinguished as a promising option. MoS₂ is an exciting example of a two-dimensional material due to its low toxicity, relatively low cost, and electrochemical activity. In addition, MoS₂ nanoparticles (NPs) have been considered a noteworthy alternative for widely used but expensive platinum. The use of MoS₂-based catalyst for hydrogen evolution reaction (HER) in water splitting may be a way to lower the cost of green hydrogen production.

The transition period between the common usage of green hydrogen and the present time, which according to the EU, is approximately 20-30 years, requires focusing on current transportation issues, one of which is to limit engine exhaust emissions. Nowadays, specialists propose the use of electric and hybrid vehicles. Yet, their prices prevent their fast exchange with combustion engine cars. The solution for the above problem may be fuel and oil additives that extend engine lifetime and mitigate the negative effects on the environment. MoS₂ has also found its application for these purposes. Owing to its layered structure, often compared to graphite, MoS₂ is considered an excellent lubricant. The addition of MoS₂ to engine oil significantly enhanced its tribological and rheological properties, thus improving engine combustion conditions and reducing environmental emissions.

Certainly, MoS₂ is a material with unique properties, with the potential to be used in many fields, not only for hydrogen production and lubricant additives. However, the obstacle to overcome is that MoS₂ changes its properties with the particle size. In both applications, better results are obtained for nanoparticles. There are many methods to reduce the size of MoS₂. An interesting approach is adding carbon nanomaterials (CNMs) while synthesizing molybdenum disulfide forming hybrid nanostructures – MoS₂/CNMs. Adding carbon nanomaterials during MoS₂ precipitation results in decreased particle size, expands the surface area, and has many other advantages discussed in detail in this dissertation.

There are many methods to produce hybrid nanostructures. Nevertheless, most of them are not scalable and/or associated with high technological costs, which causes problems with the widespread use of these materials. Designing a scalable and low-cost production method would allow for further development of these materials and their applications. Moreover, due to the variety of uses of these materials, which require different characteristics, their production method should make it possible to control the properties of the obtained particles. Therefore, one method would allow the preparation of hybrid nanostructures for advanced applications such as catalysis and more vast fields, such as lubricants.

Purpose

The purpose of the research conducted as part of this doctoral dissertation was to develop new hybrid nanostructures based on molybdenum disulfide and carbon nanomaterials (MoS₂/CNMs) and the method of their production to use them as hydrogen evolution reaction catalysts and engine oils nanoadditives.

Scientific dissertation theses

T1 – Wet chemical synthesis can be used for preparation of MoS₂-based materials. This reaction is based on an aqueous solution leading to particle precipitation. To improve the properties of MoS₂, carbon nanomaterials may be added during the synthesis as a support for nanoparticle growth. Due to the lower energy of heterogeneous nucleation (compared to homogeneous), MoS₂ deposits directly on the carbon surface, resulting in smaller particle sizes.

T2 – The wet chemical synthesis can also be carried out in an impinging jet reactor. Due to the high energy dissipation in the reactor mixing area, nanoparticles with desired and reproducible properties are obtained. With the use of impinging jet reactor, this method should enable to control the properties, such as morphology, structure, and size of particles, giving the possibility to select the best option for a given application. The proposed synthesis is a novel method to prepare MoS₂/CNMs that, in addition, can be easily transferred to a bigger scale than the laboratory.

T3 – Thanks to the unique properties of molybdenum disulfide, it can be used as a potential catalyst for hydrogen evolution reaction. Moreover, the addition of carbon nanomaterials as a support for MoS₂ growth is proposed to enhance its electrocatalytic properties. CNMs improve charge transport and expose the active sites of MoS₂ by reducing particle sizes.

T4 – Molybdenum disulfide is also a valuable additive to engine oils. Hybrid nanostructures MoS₂/CNMs improve the engine oils lubricating properties due to reduced size and a synergetic effect of two materials with great tribological behavior.

Scope

The scope of the research in this work included (i) preparation and physicochemical analysis of MoS₂ obtained through wet chemical synthesis; (ii) the determination of influence of process parameters on preparation of MoS₂ in the impinging jet reactors; (iii) development of the preparation method of MoS₂/CNMs in the impinging jet reactor; (iv) investigation of these materials as the potential hydrogen evolution reaction catalyst; and (v) investigation of these materials as engine oil additives.

In this dissertation, six publications [P1-P6] were summarized and sorted out, presenting the results obtained as a part of doctoral activities. This dissertation has been divided into III parts:

I part – Literature review (chapters 1– 4)

The motivation to start research on this topic has been clarified in this part of the dissertation. The properties and preparation methods of molybdenum disulfide have been described. The advantages of hybrid nanostructures MoS₂/CNMs over pure MoS₂ were also indicated. The basics of hydrogen evolution reaction catalysis and MoS₂ catalytic properties have been discussed. In the last part of the literature review, the tribological and rheological basics as well as MoS₂ lubricating properties have also been presented.

II part – Results and discussion (chapter 5 – 8)

Six publications created during the doctoral activities were summarized and reorganized to form a complete whole. This part has been divided into four main chapters. The first is devoted to the influence of various parameters on the synthesis of molybdenum disulfide particles. The second describes a novel method for the synthesis of hybrid nanostructures based on MoS₂ and carbon nanomaterials with the use of impinging jet reactor. The third and fourth chapters are devoted to their applications, i.e. catalysts for hydrogen evolution reaction and engine oil additives.

III part – Conclusions (chapter 9)

This part of the dissertation summarizes all research results and draws the most important conclusions. This part also answers the research problems formulated in the research theses.

1. Carbon nanomaterials

The novelty and outstanding properties of two- and one-dimensional materials have aroused tremendous interest in various fields. The Discovery of carbon nanomaterials (in particular, fullerenes in 1985, carbon nanotubes in 1991, and graphene in 2004) sparked a revolution in the field of nanotechnology [7, 8]. Their use can be found almost in every field of science, from medicine to space technologies. The wide application of carbon nanomaterials meant that scientists from various disciplines create novel hybrid, functionalized, and doped structures, leading to the emergence of new interdisciplinary scientific and engineering trends [9]. Depending on the CNMs structure, their properties may differ. Due to their various properties and availability, in this dissertation, carbon nanomaterials such as graphene oxide (GO), reduced graphene oxide (rGO), and carbon nanotubes (CNTs) were taken into account.

1.1 Graphene oxide

Graphene oxide is a form of oxidized graphene flakes. The most common method of producing it is oxidation, followed by exfoliation of graphite. Through the oxidation process, the typical graphite structure containing carbon atoms in sp^2 hybridization is disrupted. New oxygen-containing functional groups are formed at points where the carbon network is broken. Hydroxyl and epoxy groups are mainly formed on the GO basal plane, while carboxyl, carbonyl, phenol, and lactone groups form on the edges of the graphene structure (Figure 2) [10].

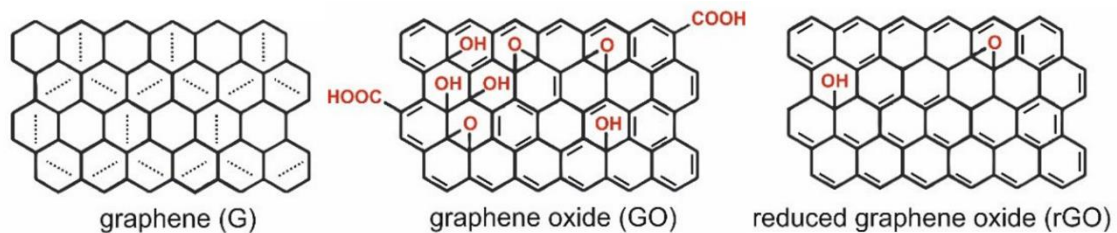


Figure 2. Graphene and graphene oxide structure [11]

A large number of functional groups and partially changed hybridization from sp^2 to sp^3 of graphene oxide caused the electrical conductivity to be much lower than in the case of other carbon nanomaterials [9, 10], [P4]. This limits its direct use in electrical and electronic applications. However, the presence of many functional groups provides a large active surface area and hydrophilic nature of graphene oxide. Therefore, GO forms stable dispersion in various polar solvents, especially in water, which distinguishes it from other carbon nanomaterials. Moreover, structure defects and functional groups of GO may serve as nucleation sites for

the deposition of other compounds and active sites for chemical modification or functionalization [10], [P3-P5]. The possibility of changing the GO chemical composition by chemical, thermal or electrochemical treatments allows for controlling its physicochemical properties [10, 12] and thus finding applications in various fields, such as solar cells [13], drug delivery [14], membranes [15], water purification [16], and many others.

However, due to the different production methods of GO, it does not have a clearly defined structure, and its properties may differ from batch to batch. This can cause problems achieving a homogeneous sample or duplicating the properties for individual batches obtained by the same method.

1.2 Reduced graphene oxide

Reduced graphene oxide is another example of graphene derivatives. It is mainly produced by GO reduction (Figure 2). This method is much cheaper than graphene production. Its properties, such as good electric conductivity and mechanical strength, are similar to those of graphene. Therefore, rGO is a compromise between relatively cheap GO and graphene with unique properties [17].

Unlike GO, rGO has a hydrophobic nature, which depends on the degree of oxidation and thus the reduction method used. There are many methods (chemical [18], electrochemical [19], thermal [20], and microwave [21]) to reduce graphene oxide. Depending on the method, a more or less reduced graphene oxide with a different number of layers is obtained. Nevertheless, even a small amount of functional groups makes it dispersible in many solvents [22]. In addition, as in the case of GO, these defects and functional groups may be active sites for its further modifications, which is another advantage over graphene [P4, P5].

However, similar problems as in the case of GO with poorly defined structure concern rGO. In addition, reduced graphene oxide tends to agglomerate during reduction treatment, resulting in a smaller surface area and deteriorated properties [17]. Yet, the above problems did not prevent many applications from being found, such as in fuel cells [23], gas sensors [24], hydrogen production [25], and much more.

1.3 Carbon nanotubes

Due to the shape and simple composition, carbon nanotubes stand out with their properties among carbon nanomaterials. CNTs form seamless cylinders coiled from graphene flakes. Among the CNTs, two groups can be distinguished: single-walled carbon nanotubes (SWNTs) and multi-walled carbon nanotubes (MWNTs). SWNT was formed from only one graphene sheet, while MWNT from multiple sheets (Figure 3) [9]. Both MWNTs and SWNTs are mainly produced via arc discharge [26], chemical vapor deposition [27], and laser- ablation [28].

Due to their high Young's modulus and tensile strength, which resulted from sp^2 hybridization, carbon nanotubes have drawn great attention as additives for composites and hybrid structures to improve their mechanical properties [29]. Moreover, these properties and their unique shape have made CNTs also desired lubricants [30–32] [P5-P6]. Carbon nanotubes also present excellent electrical properties, better than GO or rGO. This allowed CNTs to find use in electronic applications, such as batteries [33], supercapacitors [34], fuel cells [35], and catalyst supports [P3-P4].

Despite many advantages, a significant problem of carbon nanotubes is the difficulty of their dispersion in aqueous solutions due to their structure consisting only of carbon. Moreover, the presence of van der Waals interactions between the tubes causes a strong tendency towards agglomeration [36]. These cause the main problems which limit their applications. Therefore, much work is devoted to functionalizing and stabilizing carbon nanotubes [37–39].

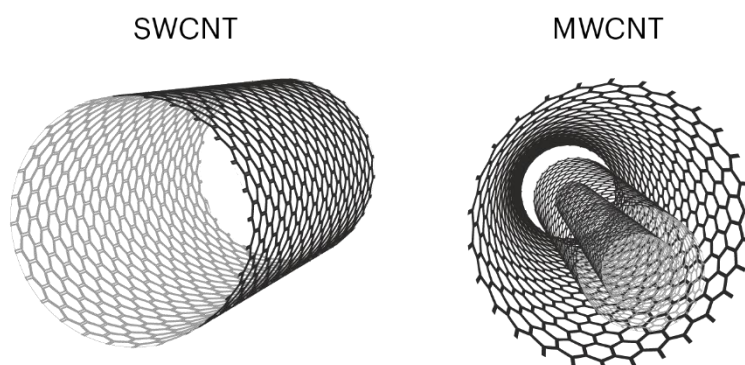


Figure 3. Single-wall carbon nanotube and multi-wall carbon nanotube structures [40]

2. Molybdenum disulfide-based materials

2.1 Transition metal dichalcogenides

With the development of carbon nanomaterials, research was also undertaken on the subject of other 2D materials. Among them, transition metal dichalcogenides (TMDCs or TMDs) can be distinguished. Due to their layered structure, they are often compared to graphite. However, their chemical structure differs significantly. TMDCs are compounds with the general formula MX_2 . The M corresponds to the transition metal element, like Mo, Re, W, and X to two chalcogenous planes made of atoms, such as S and Se [41], [P1, P2].

2.2 Molybdenum disulfide

In particular, an exciting example of TMDCs is molybdenum disulfide (MoS_2). Its monolayer consists of an S-Mo-S layer held together by strong covalent bonds, while these monolayers are bonded by weak Van der Waals forces (Figure 4) [P1, P2]. Therefore, MoS_2 layers can easily slide in relation to each other, resulting in a low friction factor. This phenomenon caused that MoS_2 became a suitable lubricant. It gained its publicity mainly as a dry lubricant. In this application, it has been heavily studied by the National Aeronautics and Space Administration (NASA) [42–44]. Due to its ability to work in critical conditions such as low or very high temperatures and an oxygen-poor environment, molybdenum disulfide has become a desirable lubricant for space application [44, 45], [P2]. In addition, MoS_2 NPs are also added to liquid lubricants to improve their properties [46], [P5-P6].

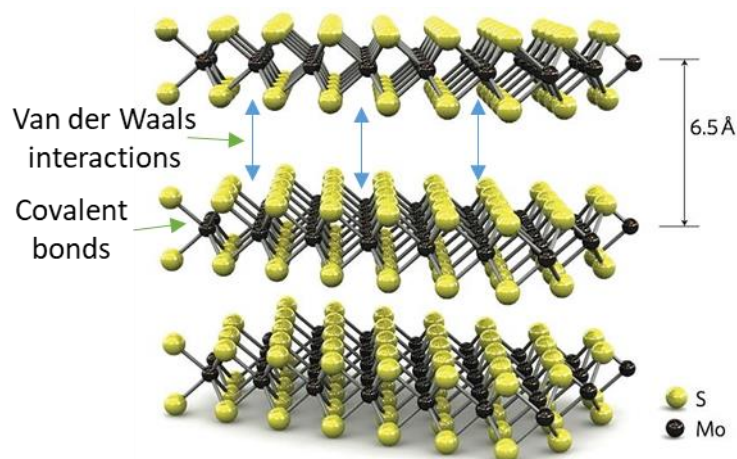


Figure 4. Molybdenum disulfide structure [47]

MoS₂ is most commonly found in crystalline form. Ramsdell's notation shows it has several crystalline forms, such as 3R, 2H, and 1T, in which 2H is the most often (Figure 5). 2H MoS₂ is a p-type semiconductor. Furthermore, its monolayer has a direct band gap equal to 1.8 eV with significant photoluminescence intensity. The above features allowed MoS₂ to be used in optical applications, such as photodetectors [48], solar cells [49], and photocatalysis [50]. Molybdenum disulfide NPs have also drawn significant attention as the catalyst for several reactions, such as hydrodesulfurization [51], hydrogen evolution [P3-P4], [52], and oxygen reduction reactions [53]. Nanosized MoS₂ is an appreciated catalyst or co-catalyst as it has a large surface area and forms permeable two-dimensional channels for ion adsorption and transport [54]. Although nano-MoS₂ has many exciting features, its properties deteriorated with particle size (increased number of layers). Therefore, many studies are devoted to obtaining the nanometric MoS₂ [P1-P2].

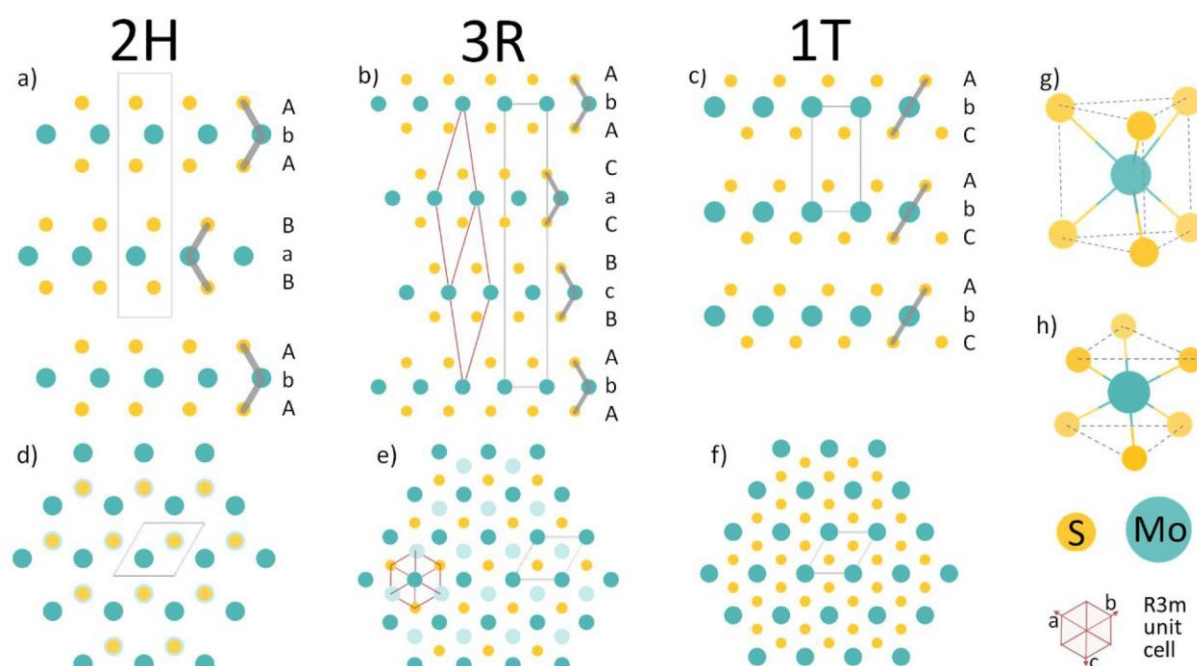


Figure 5. Crystalline forms of MoS₂ [55]

2.3 Hybrid nanostructures based on molybdenum disulfide and carbon nanomaterials

In the case of the molybdenum disulfide synthesis, nucleation and growth of particles occur. With the following agglomeration, particles obtained may be micrometric [P1, P2], [56]. To overcome this problem, ensuring good mixing conditions during the synthesis or further exfoliation can be proposed [P1, P2], [57]. The noteworthy alternative to reduce the number of MoS₂ layers is using carbon nanomaterials as the support for particle growth. The nucleation takes place on the carbon surface, and the formed particles begin to grow alongside carbon nanomaterials, thanks to which they have smaller sizes and a larger surface area (Figure 6) [P3], [58]. A new hybrid nanostructure MoS₂/CNMs with enhanced properties is then created. Moreover, the hybrid nanostructures tend to agglomerate less than their pure compounds. Adding CNMs to the MoS₂ structure also has many other advantages, such as enhanced catalytic and lubricating properties, which are discussed in detail later in this dissertation.

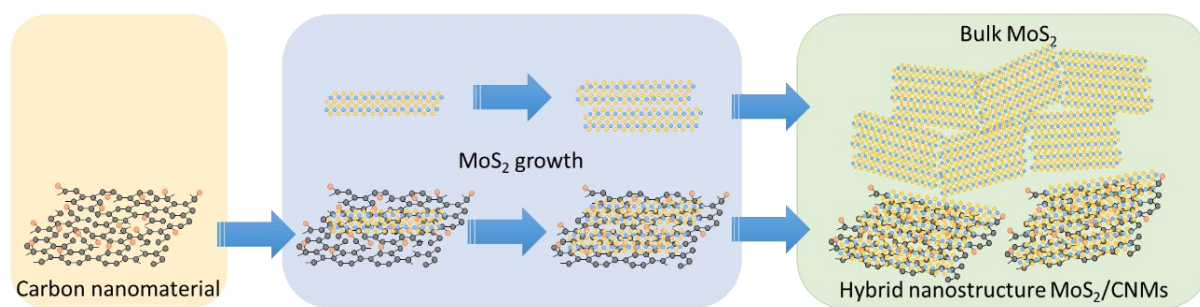


Figure 6. Preparation of hybrid nanostructures MoS₂/CNMs and bulk MoS₂

As mentioned before, carbon nanomaterials present various properties which can influence particle growth. Graphene oxide has many defects and functional groups that can serve as MoS₂ nucleation sites, leading to strong interactions between them. Moreover, the hydrophilic nature of GO may facilitate its dispersion in the reaction mixture, resulting in a larger surface area for the nucleation of the particles. However, its many oxygen-containing groups may oxidize MoS₂ changing its properties. While reduced graphene oxide with fewer functional groups, defects, and hydrophobicity may result in poorer dispersion of MoS₂ particles on its surface. However, it has much better conductivity and mechanical properties that can contribute to better catalytic and tribological features. Similarly carbon nanotubes, however, their specific geometry may cause different behavior during the reaction and facilitate nucleation of MoS₂ [P4, P5]. A vital aspect is checking how these materials affect the final properties of hybrid nanostructures, which have not been thoroughly studied so far.

2.4 Preparation methods of hybrid nanostructures MoS₂/CNMs

An extraction from a natural mineral – molybdenite is a primary method to produce molybdenum disulfide particles. Its properties vary depending on the quality of the ore and the extraction location [P1]. However, the synthetic methods for preparing MoS₂ are more effective in generating nanoparticles with reproducible and desired properties.

There are many synthetic preparation routes for MoS₂, such as chemical vapor deposition (CVD) [59], microwave-assisted [60], hydrothermal [61], and solvothermal [62] methods. However, they all can be characterized by a lack of process control, high energy, low throughput, no scalability possibility, a problem with reproducible properties of the obtained particles, or high costs. Additionally, adding carbon nanomaterials during the synthesis limits some preparation methods due to the impossibility of producing hybrid nanostructures.

Peng et al. presented a one-pot liquid-phase-exfoliation method for producing MoS₂/GO hybrids. MoS₂ was exfoliated by ultrasonication and stabilized by GO. However, their method demands 40 h for sonication and a further 48 h for the formation of agglomerates. This causes the proposed method to be very long and expensive [58]. Zhou et al. synthesized hierarchical MoS₂-rGO nanosheets. Their method involves keeping an autoclave in an electronic oven at 220 °C for 24 h, which makes it challenging to scale up [63]. The CVD is a very accurate method that produces materials with desired properties. Like Deokar et al., who produced hexagonal-shaped nanoplates of molybdenum disulfide on vertically aligned carbon nanotubes by CVD. They achieved a uniform coverage of MoS₂ with a thickness of around 20 nm [64]. However, this method is costly and has little throughput. More information about different ways to prepare MoS₂/CNMs can be found in [P3]. Therefore, methods of producing these hybrid materials are still being sought, which will ensure the possibility of their production on a large scale while maintaining the desired properties.

3. Hydrogen evolution reaction catalysis

3.1 Hydrogen evolution reaction

Due to the search for methods of obtaining hydrogen, water electrolysis is currently attracting tremendous attention. Water electrolysis or electrochemical water splitting is a process by which water is decomposed into oxygen and hydrogen by means of electricity (Figure 7). Powered by renewable energy can be a way to produce green hydrogen that can help find a way to conduct a sustainable energy economy. The electrochemical hydrogen evolution reaction (HER) is a half-reaction that occurs at the cathode during water splitting [65].

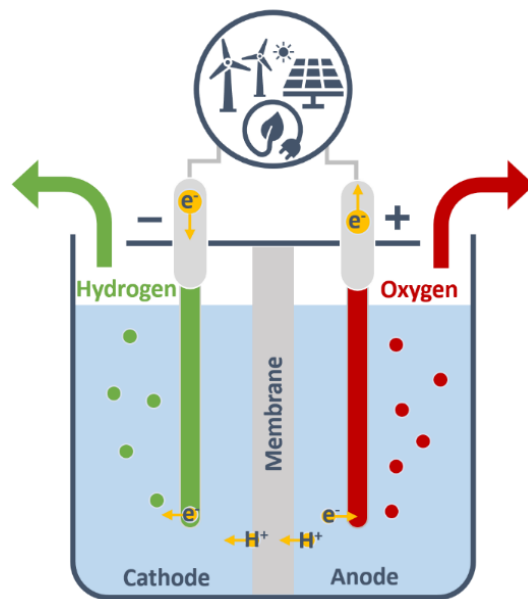
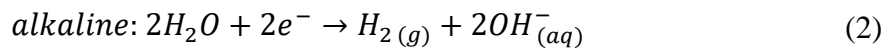
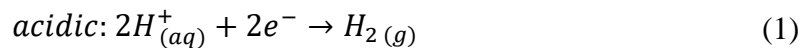
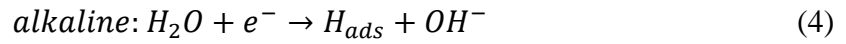


Figure 7. Water splitting (water electrolysis)

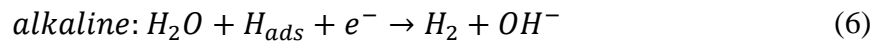
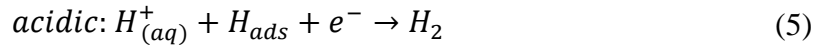
Depending on the reaction environment, HER reduces hydrogen ions or water molecules. In the case of an acidic electrolyte, the protons are reduced (Equation 1), and in turn, in an alkaline electrolyte, the reduction of water molecules takes place (Equation 2) [66].



The hydrogen evolution reaction can be divided into two steps. The first is the Volmer reaction, during which a single proton is reduced in the case of the acidic environment, resulting in the adsorption of the hydrogen atom on the electrode (Equation 3). In the case of the alkaline electrolyte, the adsorption of the hydrogen atom also takes place, but the molecule being reduced is water (Equation 4).



The formation and desorption of the hydrogen gas molecule then occur on the electrode surface in two ways: by the Heyrovsky reaction or by the Tafel reaction. The first one involves the reaction of the adsorbed hydrogen atom with the proton and an electron transfer – in the case of the acidic environment (Equation 5) or the reaction of the adsorbed hydrogen atom with the water molecule, also with the electron transfer – in the case of the alkaline medium (Equation 6).



While the Tafel reaction consists of the recombination of two adsorbed hydrogen atoms in the same way for both acidic and alkaline electrolytes (Equation 7). A schematic presentation of the above reactions is presented in Figure 8.



The slowest step determines the rate of the hydrogen evolution reaction. Which of the steps control the HER rate is influenced by the electrode material and catalyst used. Two HER mechanisms can be distinguished: Volmer-Heyrovsky and Volmer-Tafel, depending on the course of the second step of the reaction [66].

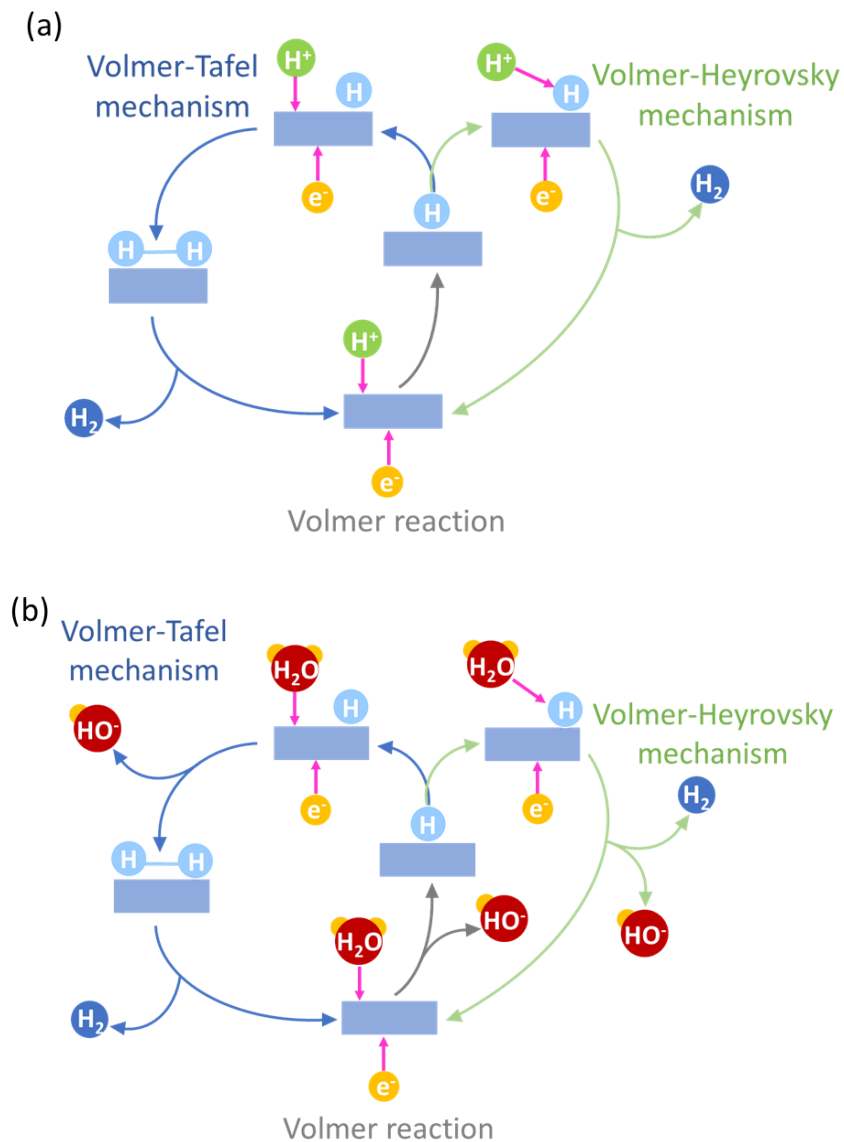


Figure 8. Mechanism of hydrogen evolution on the electrode surface in (a) acidic and (b) alkaline solutions

The hydrogen evolution reaction can be significantly improved through the catalysts used. The more activity a catalyst has, the less energy the process will require to obtain a certain amount of hydrogen. The catalyst activity can be estimated by measuring different parameters, such as overpotential, Tafel slope, stability, electrochemically active surface area (ECSA), and performing electrochemical impedance spectroscopy (EIS).

3.2 Hydrogen evolution reaction parameters

3.2.1 Overpotential

Like any electrode reaction, hydrogen evolution occurs at a specific electric potential value. The HER potential (E_{HER}) corresponds to the equilibrium potential of the electrode, i.e., the potential for which the anode current density and the cathode current density flowing through the electrode-solution interface are the same and are equal to an exchange current density. The exchange current density is a characteristic feature of a given half-cell in an equilibrium state and describes the current density generated by the flow of charges from the electrode to the solution and the flow of charges from the solution to the electrode at equilibrium i.e., when the rates of both processes are equal. In this situation, no current flows through the electrode, so the total current density is zero [67].

To initiate the electrolysis process, applying a voltage to the system equal to at least the difference of the equilibrium potentials of the electrodes is needed. It follows that the potential equal to the E_{HER} should be applied to the cathode to induce the electrochemical reaction of hydrogen evolution. However, the HER rarely occurs at the equilibrium potential because, like most electrochemical reactions, it requires the supply of additional energy to cross an activation energy barrier. Additional energy is provided by applying an extra potential to the cathode, called overpotential, defined as the difference between the potential applied to the electrode during the flow of current forced by this potential and its equilibrium potential [56].

Typically, the evaluation of the HER catalyst is based on the overpotential values determined for the current density of 1, 10, or 100 $\text{mA}\cdot\text{cm}^{-2}$, respectively η_1 , η_{10} , or η_{100} . The η_{10} is most often used to compare the activity of various catalysts. The smaller the absolute value of the overpotential η_{10} of the given catalyst, the more active it is, and lower energy must be supplied to the electrolyzer. The comparison of the activity of three exemplary catalysts in accordance with the described criterion is shown in Figure 9 [66].

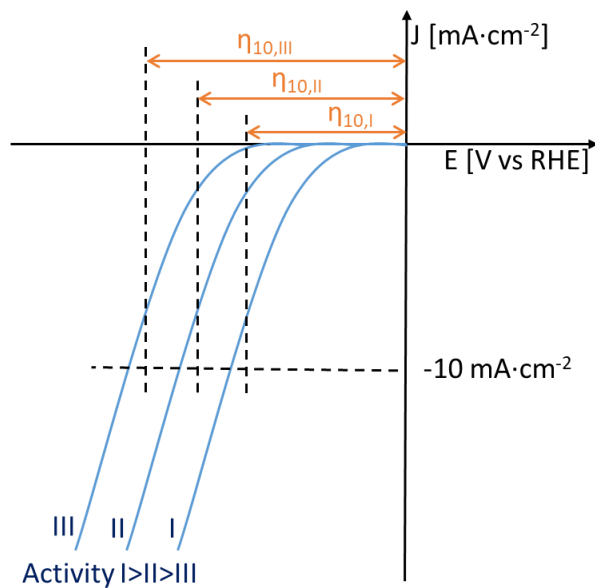


Figure 9. Comparison of catalyst activity based on the comparison of η_{10} values

In the case of HER, the overpotential can be easily determined by measuring the potential difference between the working electrode and a constant potential reference electrode (e.g., a silver chloride electrode – Ag/AgCl). Knowing the value of the reference electrode potential with respect to the reversible hydrogen electrode (RHE), the HER overpotential can be determined as the measured potential difference to which the potential of the reference electrode versus RHE has been added [66].

3.2.2 Tafel slope

The greater the overpotential is applied to the electrode (i.e., the higher the voltage in the electrolyzer), the more significant current density flows through the system. The Butler-Volmer equation gives the exact relationship between these two quantities. This equation can be simplified for small values of the overpotential. Then it turns out that the overpotential is linearly related to the current density. In turn, for large values of overpotential, the Butler-Volmer equation can be simplified to the equation known as the Tafel equation (Equation 8) [56].

$$\eta = a + b \cdot \log \left| \frac{j}{j_0} \right| \quad (8)$$

where η is overpotential [V]; a is constant [V]; b is Tafel slope [$V \cdot \text{dec}^{-1}$]; j is current density [$A \cdot m^{-2}$]; j_0 is exchange current density [$A \cdot m^{-2}$].

The Tafel equation can be plotted in the coordinate system, yielding a Tafel plot. The constants a and b in Equation 8 depend on the temperature and the electrode used. Of particular importance is the value of the constant b , known as the Tafel slope, as it plays a crucial role in evaluating the HER activity of the catalyst. A small value of the Tafel slope means a sharp increase in the current density and, thus, the efficiency of hydrogen production, with a slight rise of the overpotential, i.e., a slight increase in the energy supplied to the system [56, 68].

The value of the Tafel slope also enables the determination of the limiting stage of the hydrogen evolution reaction. Theoretical Tafel slope at room temperature for Volmer, Heyrovsky, and Tafel step is 120, 40, 30 $\text{mV}\cdot\text{dec}^{-1}$, respectively [69].

3.2.3 Stability

The stability is another crucial factor of HER catalyst. It can be performed by multiplying cyclic voltammetry (CV) or linear sweep voltammetry (LSV) cycles. Comparing the changes in the overpotential between the first measurement and after specific cycles enables checking the electrode's stability. A minor shift in the overpotential indicates that the catalyst is stable during the measurement time. It is also possible to check the catalyst stability by galvanostatic or potentiostatic methods. The potential or current density is measured over a long period (at least a few hours). The catalyst can be recognized as stable if no significant changes are visible [66].

3.2.4 Electrochemically active surface area

Electrochemically active surface area can be explained as the catalyst surface that is accessible to the electrolyte. The larger the contact surface of the catalyst with the electrolyte, the greater the system's ability to transport the charge and the greater the number of active centers that can participate in the reaction [70].

3.2.5 Electrochemical impedance spectroscopy

Electrochemical impedance spectroscopy mainly relies on plotting the so-called Nyquist plots. This plot shows the negative and the imaginary part $-Z''$ versus the real part Z' of the complex impedance of individual electrodes or cells (Figure 10). Moreover, the Nyquist plot enables estimating the catalyst charge transfer resistance R_{ct} , which is related to the electrode interface charge transfer. Low R_{ct} means low catalyst overpotential. The semicircle at low frequencies also refers to the mass transfer resistance R_{mt} of adsorbed species on the electrode surface. Therefore, the smaller R_{mt} , the more active catalyst is [66].

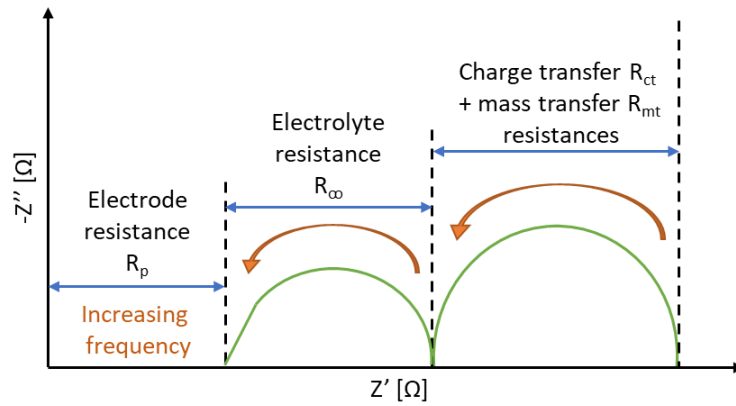


Figure 10. An example of Nyquist plot

3.3 Hydrogen evolution reaction catalysts based on MoS₂

The best-known catalyst for the hydrogen evolution reaction is platinum, which corresponds to a very low overpotential η_{10} and a low Tafel slope. Its excellent catalytic ability can be explained by its position on the graph of current density i_0 versus Gibbs' adsorption energy ΔG_{H^*} , called the volcano curve, as shown in Figure 11. It shows that platinum corresponds to a very high exchange current density value at the point where $\Delta G_{H^*} \cong 0$ eV. The above-mentioned diagram also shows that metals such as palladium, ruthenium, rhodium, and iridium have a high catalytic activity towards HER. However, their price and scarcity significantly limit their large-scale production [66, 70].

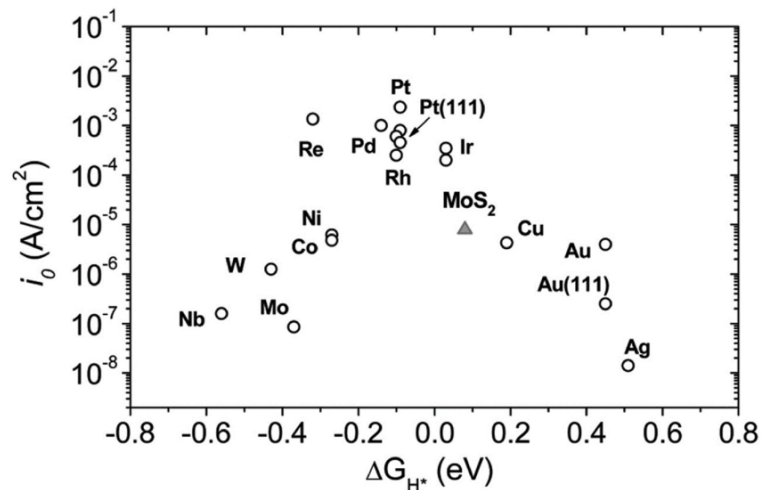


Figure 11. Exchange current density as a function of Gibbs energy for selected materials [71]

Recently, molybdenum disulfide has been particularly popular in the context of HER catalysis. It is characterized by a relatively high catalytic activity. Although its basal plane is catalytically neutral, edges on which sulfur atoms are exposed exhibit a particular catalytic activity. Figure 11 shows that the Gibbs energy of hydrogen adsorption for MoS₂ is close to zero, also at the high exchange current density. Therefore, it seems to be a promising alternative for noble-metal catalysts [56, 66, 72].

Molybdenum disulfide has amorphous and crystalline structures. Among the crystalline forms, the 2H and 1T structures present the highest catalytic activity of HER, the latter having better conductive properties [66]. The amorphous form of MoS₂ also presents a very good activity. Long-range disorganization and the resulting structural defects, such as sulfur vacancies, favor the exposure of active sites [73], [P4]. Tang et al. synthesized SWCNT-supported amorphous MoS₂ via a microwave heating process. They established that the overpotential η_{10} of amorphous MoS₂@SWCNT is 99 mV lower than crystalline MoS₂@SWCNT [74]. As previously mentioned, MoS₂ in the form of nanoparticles will be more catalytically active than its counterpart in bulk form due to the more significant amount of exposed edges. Therefore, when preparing HER catalysts based on MoS₂ NPs, care must be taken to ensure that these particles do not agglomerate. This is especially important as most disulfide nanomaterials tend to form closed fullerene structures, exposing catalytically neutral planes [56]. One of the solutions may be adding carbon nanomaterials as the support for MoS₂ growth. The main task of these supports is to expand the surface of the catalyst by keeping it in a state of high fragmentation, which contributes to a greater exposure of active sites. In addition, carbon nanomaterials have conductive properties, when combined with the MoS₂, can give a hybrid structure with increased electrical conductivity, which will result in greater electric charge transfer capacities. The latter feature is of particular importance in electrocatalysis [P3, P4]. Huang et al. synthesized leaves-and-branch structure of strongly coupled and porous MoS₂-carbon nanotube nanocomposite. This nanocomposite exhibits remarkably improved electrocatalytic activity toward HER [75].

Therefore, hybrid nanostructures MoS₂/CNMs have great potential for use in HER catalysis, and along with obtaining them by an easy-to-scale and cheap method can significantly reduce the cost of producing green hydrogen. Moreover, checking how different carbon nanomaterials affect the catalytic properties of MoS₂ may be crucial for obtaining a relatively low-cost catalyst with excellent activity toward HER.

4. Engine oil additives

4.1 Tribology

Friction is the resistance to motion created during the surface contact of two bodies that rub relative to each other. Ensuring adequate friction allows for the creation of reliable machines and devices with low wear ensuring their long service life and higher operational safety. Tribology is a branch of science that describes laws accompanying the lubrication process [76].

A vital parameter characterizing friction is the friction factor μ . It is determined experimentally and is a property of the tested system. The friction factor is the ratio of the friction force counteracting the movement of two contacting surfaces to the normal force pressing these surfaces together (Equation 9) [77].

$$\mu = \frac{F_R}{F_N} \quad (9)$$

where μ – friction factor [-]; F_R – friction force [N]; F_N – normal force [N].

In the field of tribology, the Stribeck curve is also an important aspect. This curve shows the variability of friction across the entire lubrication range (Figure **Figure 1212**). It also illustrates the three main regimes into which lubrication can be divided, i.e., boundary, mixed and hydrodynamic. The standard Stribeck curve shows the friction factor plotted as a function of the sliding velocity or the dimensionless Hersey number, defined by Equation 10 [77].

$$\text{Hersey number} = \frac{\eta \cdot v}{P} \quad (10)$$

where η – dynamic viscosity [Pa·s]; v – sliding velocity [m·s⁻¹]; P – load [N·m⁻¹].

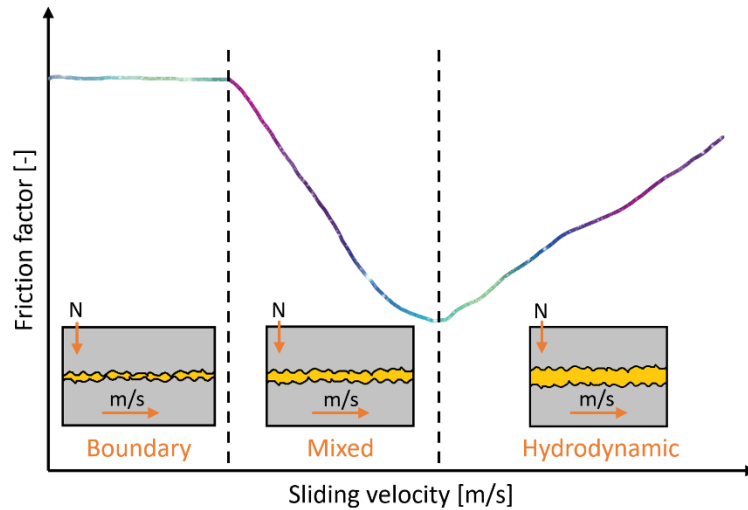


Figure 12. Stribeck curve and illustrations of the three lubricant regimes

Boundary lubrication occurs at low (close to zero) sliding velocities. In this regime, the lubricant film's thickness is insufficient to separate the friction surfaces completely, resulting in a high friction factor and significant material wear. Mixed lubrication also occurs at lower speeds, which are not able to ensure complete separation of the contact surfaces, but better than in the case of boundary lubrication. It is a transitional regime in which the friction factor decreases with increasing sliding velocity. In comparison, hydrodynamic lubrication occurs for high fluid velocities. The lubricant completely separates the friction surfaces, which minimizes wear. In addition, the occurring high pressures cause an increase in the liquid viscosity. Wear is thus controlled by viscous separation. In this regime, the lubricant film has the most significant thickness [77].

Tribology deals, inter alia, with the lubrication of engine oils and their additives, improving lubricating properties. Ensuring optimal lubrication, friction, and wear conditions is essential for proper engine operation [78]. In this field, MoS_2 plays a prominent role due to its excellent thermal, mechanical properties and low friction factor.

4.2 Rheology

Rheology is a branch of science which primary interest is the study of the deformation of materials and their flow under the influence of applied external forces. Deformation means the movement of parts or particles of a material body in relation to each other so that the continuity of the body is not broken. If the deformation of the body increases continuously over time and becomes irreversible, the material is said to flow. Rheology thus complements tribology, which studies the interaction of two moving bodies [79].

In rheology, the essential property of the material is its viscosity. It characterizes the fluid's internal resistance to deformation caused by the application of external forces. This concept was introduced by the Newtonian law of viscosity, in which the shear stress was related to the shear rate (Equation 11).

$$\tau = \eta \cdot \dot{\gamma} \quad (11)$$

where τ – shear stress [Pa]; η – dynamic fluid viscosity [Pa·s]; $\dot{\gamma}$ – shear rate [s^{-1}].

The first step in analyzing the rheological properties of liquids is to plot flow curves and viscosity curves (Figure 13). The flow curves show the relationship between the shear stress and the shear rate. Depending on their shape, the type of tested fluid can be determined. First, the fluids can be distinguished into shear thinning and thickening. Moreover, fluids can be divided into those that have yield stress and do not. Curves presenting fluids without yield stress pass through the origin of the coordinate system, such as Newtonian, pseudoplastic, and dilatant fluids. The yield stress is the existence of a specific limit value of the shear stress beyond which the fluid begins to flow. This group is known as plastic-viscous fluids (plastic and Bingham fluids). The flow curves obtained from rheological tests can be converted into viscosity curves of individual fluids. These curves then show the relationship between the dynamic viscosity of the tested fluid and the shear rate. Typical viscosity curves for fluids lacking a yield point are shown in Figure 13 [79, 80].

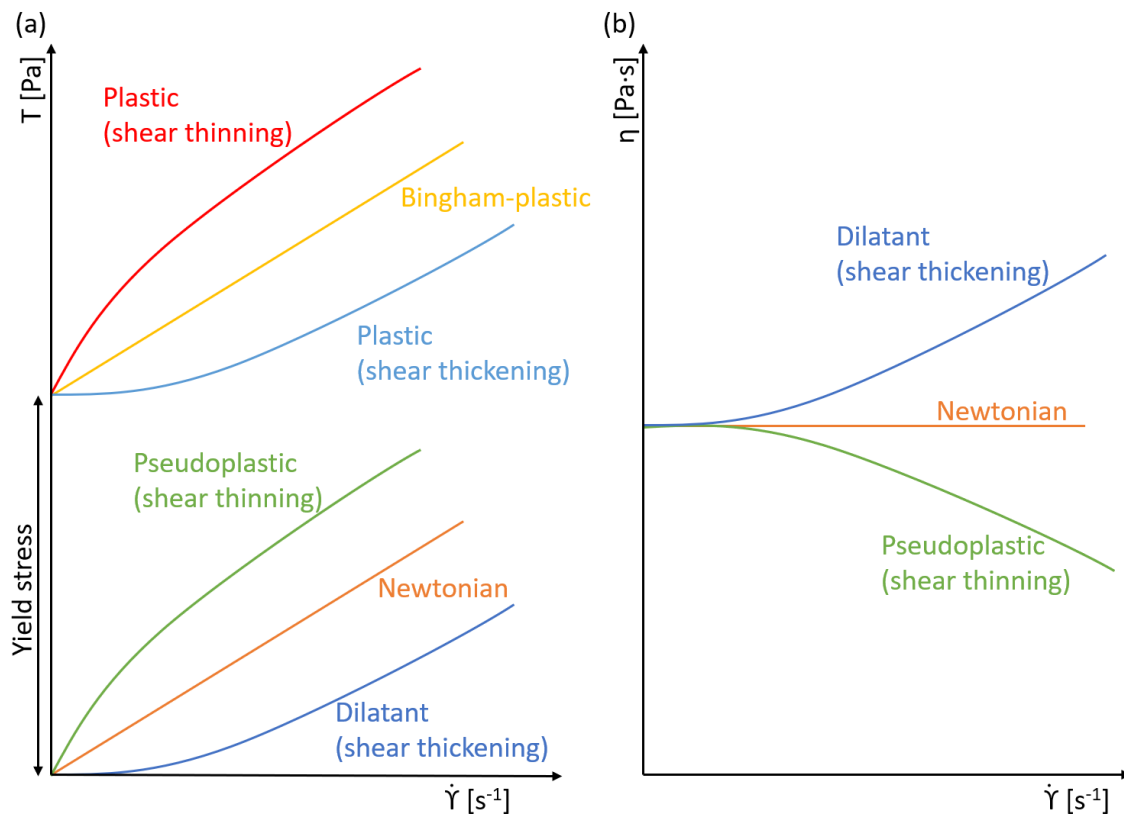


Figure 13. (a) Flow curves and (b) viscosity curves for different types of fluids

4.3 Engine oils

Engine oil is a fluid necessary for all types of vehicles. The task of the oil is to ensure low friction between the moving parts of the machine, creating a thin layer on them to prevent wear. The oil is also responsible for cooling the engine and ensuring that the piston rings are adequately sealed. Additionally, it neutralizes the acids and reduces the nanoparticle nucleation formed during engine operation. Therefore, engine oil is critical to maintaining proper engine performance [P5-P6], [81].

The vital parameter of engine oil is its viscosity, which characterizes the fluid's internal friction. Its appropriate value allows oil to be pumped at the lowest temperature that occurs during engine start-up while protecting the components during their operation at high temperatures. The Society of Automotive Engineers (SAE) has classified lubricants into two grades based on their viscosity. The winter class is marked with the letter "W" to indicate cold start conditions, e.g., 0W, 10W, 20 W, and 25 W oils. Numbers only describe the summer class. These include oils of the following type: SAE 20, 30, 40, 50, and 60. Nowadays, the most common are multigrade oil, marked, e.g., as 10W-40. The preceding number is, therefore, equal to the viscosity value of this oil in cold conditions. The smaller this number, the easier

the lubricant will flow. The following number indicates the oil viscosity at the engine operating temperature. On the other hand, the greater this number, the thicker and more stable the oil film will cover the individual engine components [82].

Engine oils must fulfill many other functions, both in the winter when the engine is cold and when the engine is warm and loaded. Moreover, the imposed operational criteria and environmental protection mean that the oil's required rheological and tribological properties are significantly diversified. Thus, developing an oil with the desired properties is a complex task.

4.3 Oil additives based on MoS₂

The use of additives is an effective way to improve the lubricating properties of engine oils. Additives are primarily used to mitigate friction phenomena, increase wear resistance, and reduce pollution caused by emitted gases. Among various additives, nanoadditives can be distinguished. Due to their size, they have easier access to rubbing parts and are more stable at oil suspensions. There are many oil nanoadditives, such as zinc dithiophosphate and tungsten disulfide, but molybdenum disulfide certainly deserves special attention [83], [P5-P6]. Van der Waals interactions between its monolayers and high mechanical strength made it a desirable lubricant additive [46, 84].

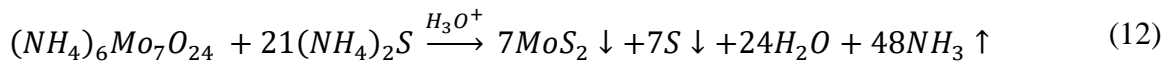
However, its particle agglomeration is still a problem to overcome. Hybrid nanostructures MoS₂/CNMs may be a solution. Due to the size reduction, not only is the dispersion of the lubricating suspensions improved, but there is also a synergistic effect between these two unique materials. Carbon nanomaterials are also desired lubricants due to their extraordinary mechanical properties and good thermal stability. Through CVD, Song et al. produced a composite based on MoS₂ and SOCNTs (strongly oxidized CNTs). They proved that dibutyl phthalate containing SOCNTs@MoS₂ composite exhibited the best tribological and antiwear properties among other DBP additives, such as SOCNTs, MoS₂, and SOCNT-MoS₂ mixtures [85]. More information about different additives based on molybdenum disulfide can be found in [P5-P6].

Therefore, hybrid materials have an advantage over their pure substances or mixture. So far, little work has been done on using MoS₂/CNMs hybrid nanostructures as additives to engine oils, creating a gap that needs to be filled.

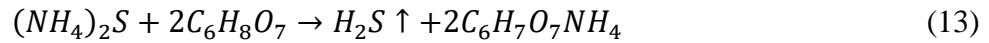
A scalable and low-cost production method would allow for the further development of hybrid nanostructures based on molybdenum disulfide and carbon nanomaterials and their uses. Due to the variety of applications of MoS₂/CNMs, which require different features, their production method should allow to control the particle properties. Therefore, one method would allow the preparation of hybrid nanostructures for advanced applications such as HER catalysts and more vast fields, such as oil additives. For catalytic applications, hybrid nanostructures should be characterized by a large surface area, exposed active sites, and superior charge transfer. On the other hand, for lubrication applications, the MoS₂/CNMs should primarily be nanometric in size, but also retain their layered structure that allows them to be easily rubbed. In both of these applications, these materials have great potential due to their unique and diverse properties.

5. Preparation of molybdenum disulfide through wet chemical synthesis

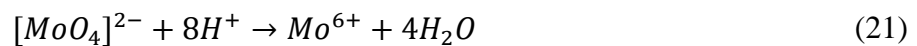
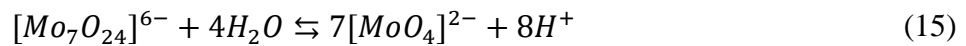
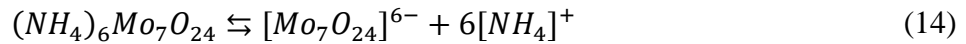
Wet chemical synthesis can be distinguished from synthetic preparation methods of MoS₂ (pointed out in section 2.4 *Preparation methods of hybrid nanostructures MoS₂/CNMs*). The wet chemical synthesis is based on the reaction in an aqueous environment, leading to the precipitation of MoS₂ nanoparticles. In this reaction, ammonium molybdate tetrahydrate (NH₄)₆Mo₇O₂₄·4H₂O (HMA) and ammonium sulfide (NH₄)₂S (AS) can be used as the precursor of molybdenum Mo and sulfur S, respectively [P1, P2]. An acid (e.g., citric (CA) or formic acid (FA)) is also needed for the synthesis, which serves as a reducing agent and provides an acidic environment [P1-P2]. Then the reaction takes the form of Equation 12.



A small amount of hydrogen sulfide H₂S is also produced during the synthesis. In the case of the use of citric acid as the reducing agent, the parallel reaction takes the form of Equation 13 [P1, P2].



The reaction mechanism is widely described in [86]. Wojtalik et al. presented a new mechanism that does not take into account the formation of molybdenum complex with citric acid, and MoS₂ is formed by the reduction reaction of molybdenum ions (Equations 14-24).



As a result of homogeneous nucleation in an oversaturated solution, amorphous MoS₂ is formed. The obtained particles are contaminated by by-products and unreacted reagents that must be purified and then annealed. The synthesized product suspension can be purified by either centrifugation or filtration. The schematic presentation of the wet chemical synthesis is shown in Figure 14, and the whole procedure is accurately described in [P1].

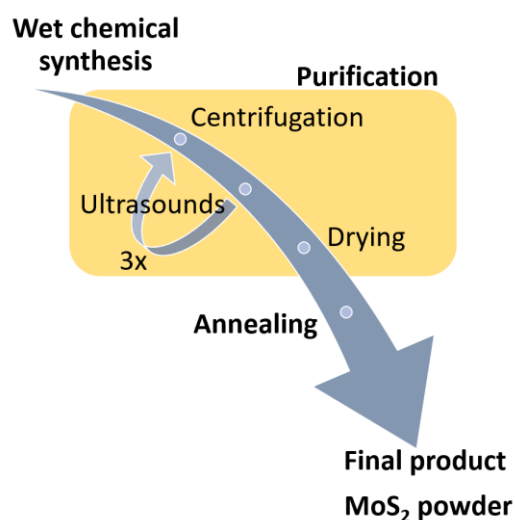


Figure 14. Schematic presentation of wet chemical synthesis

5.1 Influence of annealing temperature

Depending on the annealing temperature, it is possible to control the degree of MoS₂ crystallinity. Annealing for one hour at 850 °C is sufficient to obtain a high-quality and crystalline product. However, to maintain the mostly amorphous phase, but remove the unbonded sulfur from the product (Equation 12), annealing for one hour at 550 °C is adequate. Figure 15 shows an X-Ray powder diffraction (XRD) analysis of purified, annealed at 550 and 850 °C MoS₂ [P1-P2, P4].

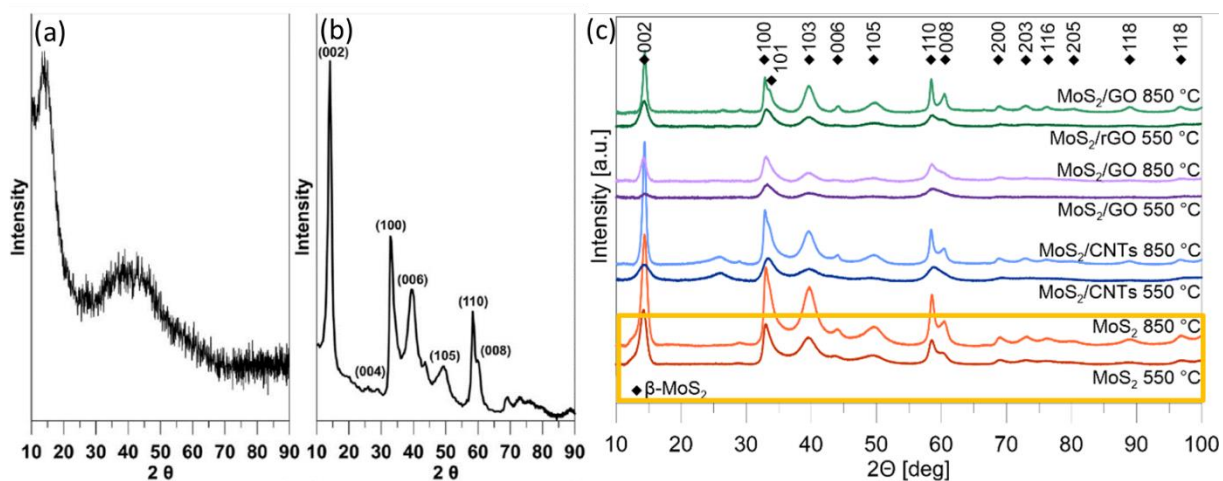


Figure 15. Diffractograms of (a) purified particles [P1], (b) annealed at 850 °C [P1], and 550 °C [P4] particles of MoS₂ obtained by wet chemical synthesis

The annealing temperatures were determined based on thermogravimetric analysis (TGA). Figure 16 shows the TG analysis of the purified synthesis product under argon and air flows. Annealing takes place in a stream of inert gas, therefore, in terms of selecting the appropriate temperature for this process, the mass change curve in the argon flow has been taken into account. Figure 16 shows that there is a decrease in mass in the temperature range of 400-600 °C, which may be caused by the boiling of unbounded sulfur and the removal of by-products that were not removed during purification [P1]. Therefore, the minimum temperature to produce a pure product, but with the maintenance of the mostly amorphous structure, is 550 °C [P4]. Molybdenum disulfide crystallization occurs at higher temperatures (above 800 °C), thus, the temperature of 850 °C was selected for the complete crystallization of MoS₂ [P1, P4].

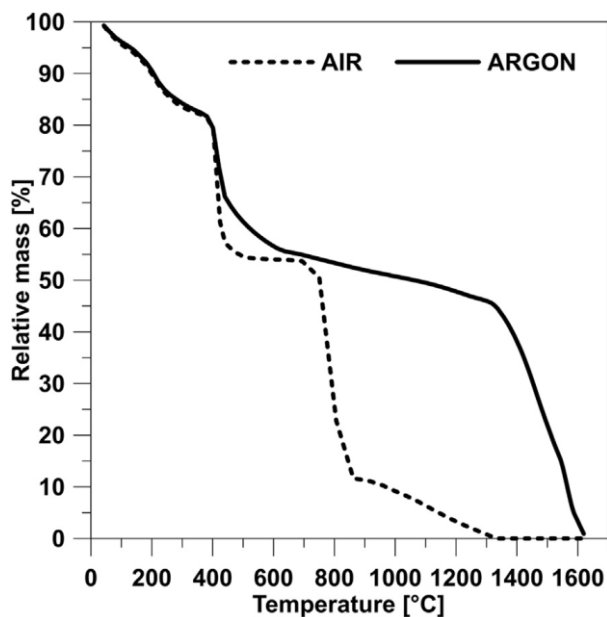


Figure 16. Thermogravimetric analysis of purified MoS₂ particles heated in the flow of air and argon [P1]

5.2 Influence of reducing agent

Also the used reducing agent influences the size and morphology of the obtained particles. For this reason, citric acid and formic acid have been tested as the reducing agent for the reaction presented in Equation 12. Particle size distributions (PSD) (by (a-b) number, (c-d) surface area, (e-f) volume) of MoS₂ prepared with citric and formic acid after each step of preparation (i.e., synthesis, purification, and annealing) are shown in Figure 17. As can be seen, the final synthesis product (annealed particles) obtained using formic acid is much smaller than this prepared with citric acid. The mean sizes (L_{10}) of the final products synthesized using CA and FA are 0.769 and 0.413 μm , respectively. Although FA initially caused the formation of agglomerates. Its smaller molecules are easier to remove. Hence during the purification, in which the particles are also subjected to ultrasounds, the agglomerates are broken up, and the particles' mean sizes are smaller [P2].

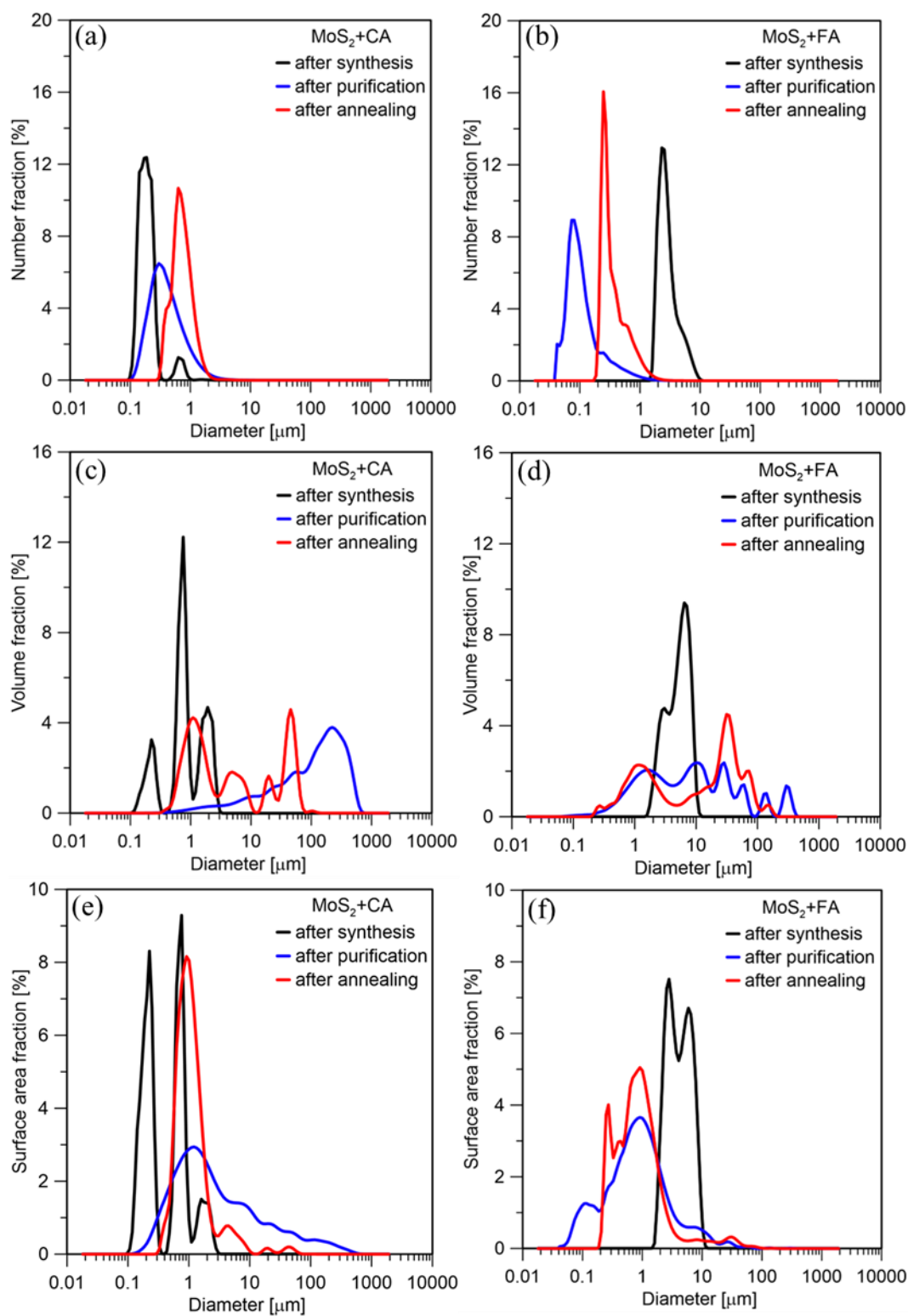


Figure 17. Particle size distributions (by (a-b) number, (c-d) surface area, (e-f) volume) for MoS₂ particles prepared with citric (CA) and formic acid (FA) after each step of preparation

[P2]

Raman spectroscopy (Figure 18) revealed that both samples showed similar vibrational modes, typical for MoS₂. Measurements for particles synthesized using FA and CA were performed under the same conditions (same laser power – 5%, same number of counts, same measurement area, and same length of exposure). However, in the case of the MoS₂ sample prepared with FA, 5% of the laser power was too high and the sample oxidized during the measurement. It was necessary to use a weaker laser power (1%) for the measurements. Then the measurements showed the presence of typical peaks for MoS₂ with no oxide contamination. Hence it can be concluded that the particles are smaller and less stable than particles after CA. On the other hand, the sample prepared with CA showed much lower susceptibility to laser oxidation. However, the sample was not homogeneous, and Mo-oxides were visible at some points where the measurements were taken. More information about the influence of the reducing agent used on the size and morphology of MoS₂ can be found in [P2]. The further results presented in this dissertation were obtained for particles prepared using citric acid.

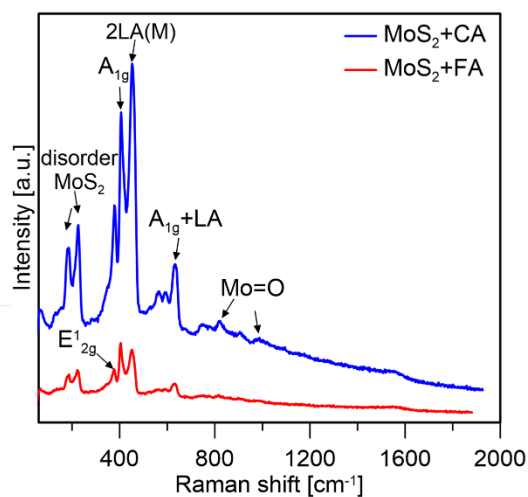


Figure 18. Raman spectra of MoS₂ prepared with the use of citric (CA) and formic acid (FA)

[P2]

5.3 Influence of reactor geometry and process mode

The wet chemical synthesis can be performed in commonly used semi-batch tank reactors and continuous flow reactors (i.e., impinging jet reactors). Figure 19 shows the schemes of MoS₂ synthesis using both of these reactors.

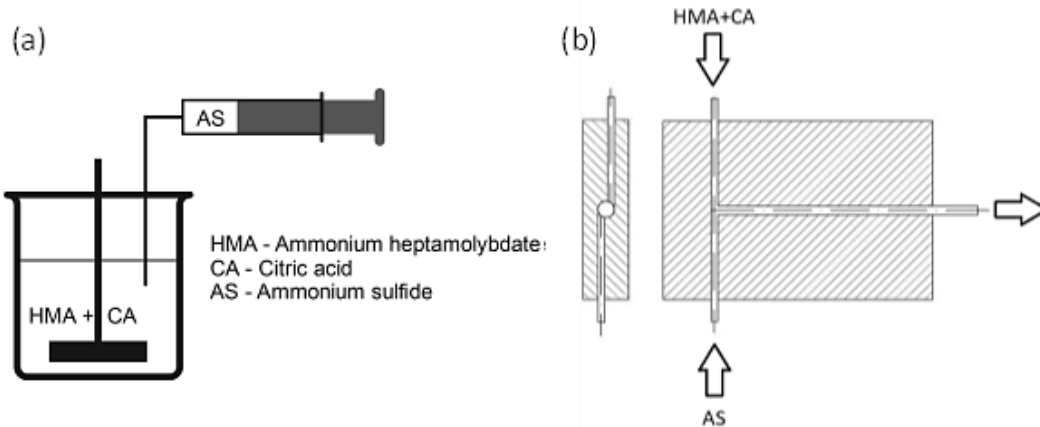


Figure 19. Scheme of (a) semi-batch and (b) continuous flow reactor used for the MoS₂ production through the wet chemical synthesis [P1]

Figure 20 shows the particle size distributions of molybdenum disulfide synthesized in the semi-batch and the continuous flow reactors. The size of particles obtained through the wet chemical synthesis can be controlled by either the initial concentration of molybdenum or the type of reactor used. Comparing the PSDs for agglomerates (Figure 20 a and c), it can be seen that their size is significantly smaller for the particles from the impinging jet reactor. The use of the jet reactor allows obtaining good mixing conditions due to the high energy dissipation in the mixing area. Due to the collision and change in streams' flow direction in a small volume, kinetic energy is converted into high turbulent motion. Thus, the agglomerates obtained in the impinging jet reactor are smaller than in the semi-batch reactor. However, there is no significant difference in the size of the primary particles synthesized in both reactors [P1].

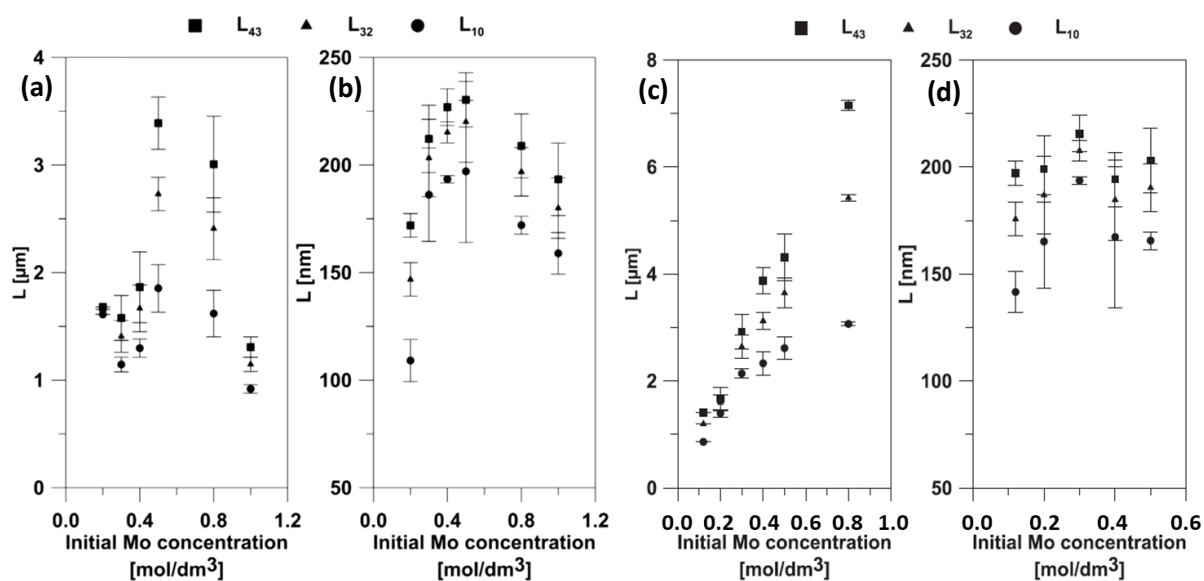


Figure 20. PSD of the MoS₂ obtained in the continuous flow reactor (a) agglomerates and (b) primary particles, and in the semi-batch system (c) agglomerates and (d) primary particles depending on the initial Mo concentration [P1]

The use of the impinging jet reactor has many advantages, such as (i) simple and scalable design, (ii) limited power consumption (compared to the traditional passive reactors), (iii) process control, and (iv) possibility of continuous production. The ability to run the process in a continuous mode is one of the paradigms of process intensification. Additionally, with the benefits of wet chemical synthesis, this method also allows controlling the properties of the obtained particles, such as (i) degree of crystallinity, (ii) morphology, (iii) size, (iv) surface properties, and (v) agglomeration. Wet chemical synthesis performed in the impinging jet reactor is relatively inexpensive and facile, not requiring special apparatus or process conditions, making it very attractive for the industrial market [P1, P2].

There are various geometries of the impinging jet reactors. From the previous studies [86–90], the S-type reactor has been chosen as the most prominent. However, in the industry, the most common is the T-type. Therefore, these two were investigated for MoS₂ particle production. The S-type reactor has inlets tangential to the outlet, and the T-type reactor normally (Figure 21).

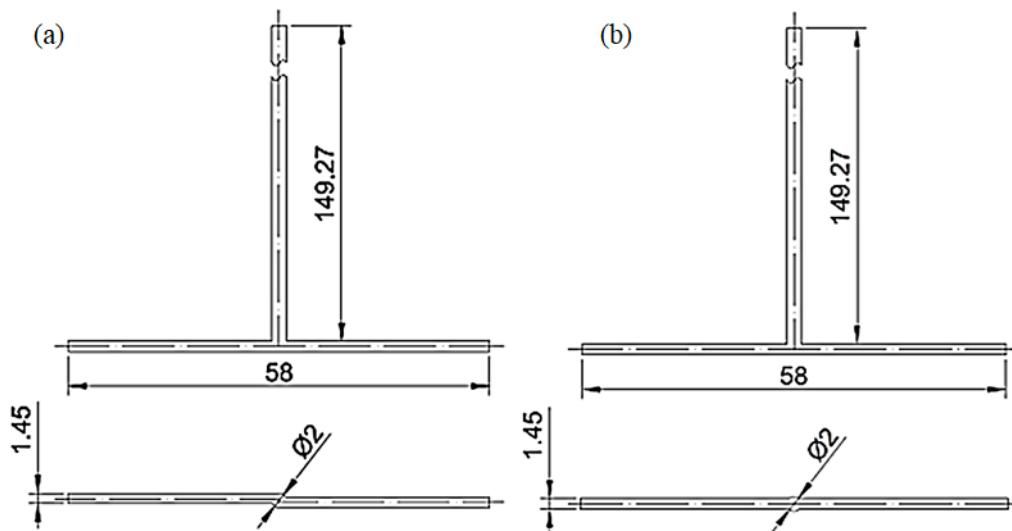


Figure 21. (a) S-type and (b) T-type reactors [P2]

The homogeneous precipitation is almost an instantaneous process. In order to limit the secondary precipitation and agglomeration, intensive mixing is required. To confirm that the S-type reactor is more suitable than the T-type for this process, areas of high mixing intensity in both reactors were determined based on computational fluid dynamics (CFD). The areas of high mixing intensity were defined as zones above 70% of the maximum value for turbulence intensity.

The CFD results for different reagents' flow velocities are presented in Figure 22. As can be seen, the size of these zones is much greater for the S-type reactor. The volume of high mixing intensity is 27 and 228 % greater than that of the T-type at 20 ml/min and 60 ml/min, respectively. Moreover, the shape of these zones differs. In the case of the S-type reactor, the inlet streams formed a vortex that is difficult for the inlet fluid elements to bypass. In contrast, in the T-type reactor, the vortex is created in the outlet pipe axis, especially at higher flow velocity values and in the collision area of the inlet streams. Therefore, the S-type impinging jet reactor has been found as the most suitable for the MoS₂ precipitation, ensuring the best mixing conditions. The comprehensive comparison is in [P2].

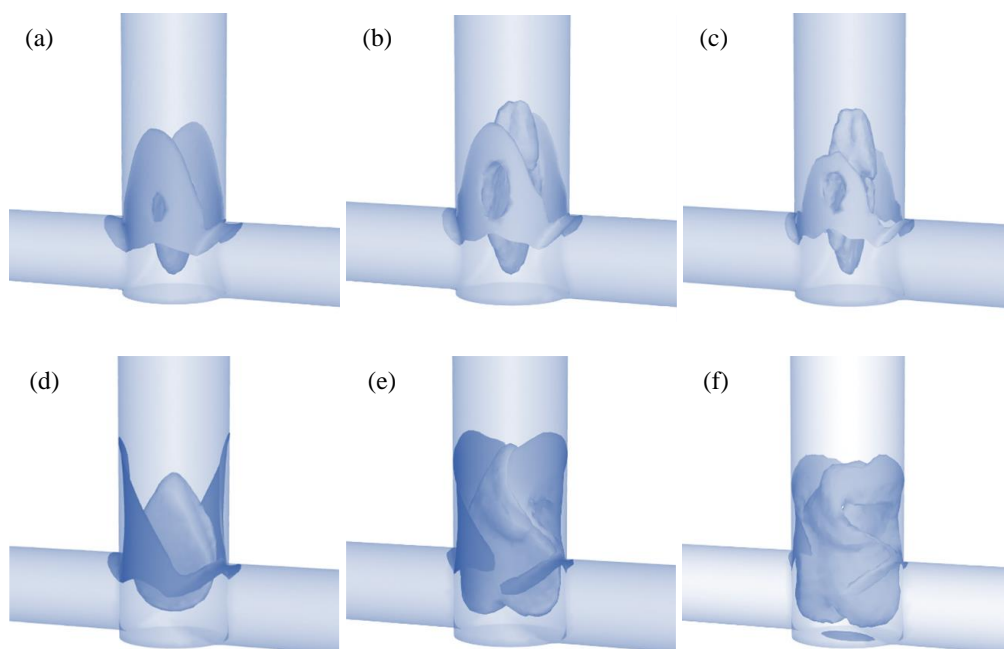


Figure 22. Mixing areas with turbulence intensity above 70% in the T-reactor for various flow velocities of CA (a) 20, (b) 40, and (c) 60 ml/min and in the S-reactor for (d) 20, (e) 40, and (f) 60 ml/min [P2]

5.4 Influence of process conditions

As was mentioned before (section 2.2 *Preparation methods of hybrid nanostructures MoS₂/CNMs*), MoS₂ has many prominent features, but its properties deteriorated with increasing particle size. It is crucial to ensure such process conditions to obtain the smallest possible particles. For this purpose, various parameters were tested, such as initial molybdenum concentration, reagent flow velocity, and reaction temperature.

Figure 23 shows how the process conditions influence the particles' mean sizes, which were determined based on the entire PSDs, including primary particles and agglomerates. Therefore, as the initial molybdenum concentration increases, the particle size also increases (Figure 23 a). A higher concentration of Mo favors secondary over homogeneous precipitation. Thus, particle agglomeration can be observed. The reagent flow velocity and temperature do not have such a significant effect on the particle size as the Mo concentration. The smallest particle sizes were obtained for the highest values of flow velocities due to the greater turbulence dissipation rate in the mixing area (Figure 23 b). This result was consistent with numerical simulations (section 5.3 *Influence of reactor geometry and process mode*). However, during the synthesis, a small amount of hydrogen sulfide is also produced (Equation 13). To remain safe and reduce the risk of uncontrolled release of this hazardous gas, running

the process at slightly lower flow rates than 40 ml/min is wiser. With increasing temperature, the average particle size decreases due to the greater mobility of the particles (Figure 23 c). However, at 25 °C, a slight increase in the mean size of the particles can be observed. This temperature is closer to the ammonium sulfide flash point (32 °C). Therefore, AS vapor pressure is higher, and less sulfur precursor is in the reacting solution, promoting particle growth and formation of Mo-oxides over the homogenous nucleation of MoS₂. From the obtained results, it can be concluded that the process conditions, such as an initial concentration of 0.2 M with a reagent flow of 20 ml/min at 20 °C, are the best and ensure the smallest possible particle size [P2].

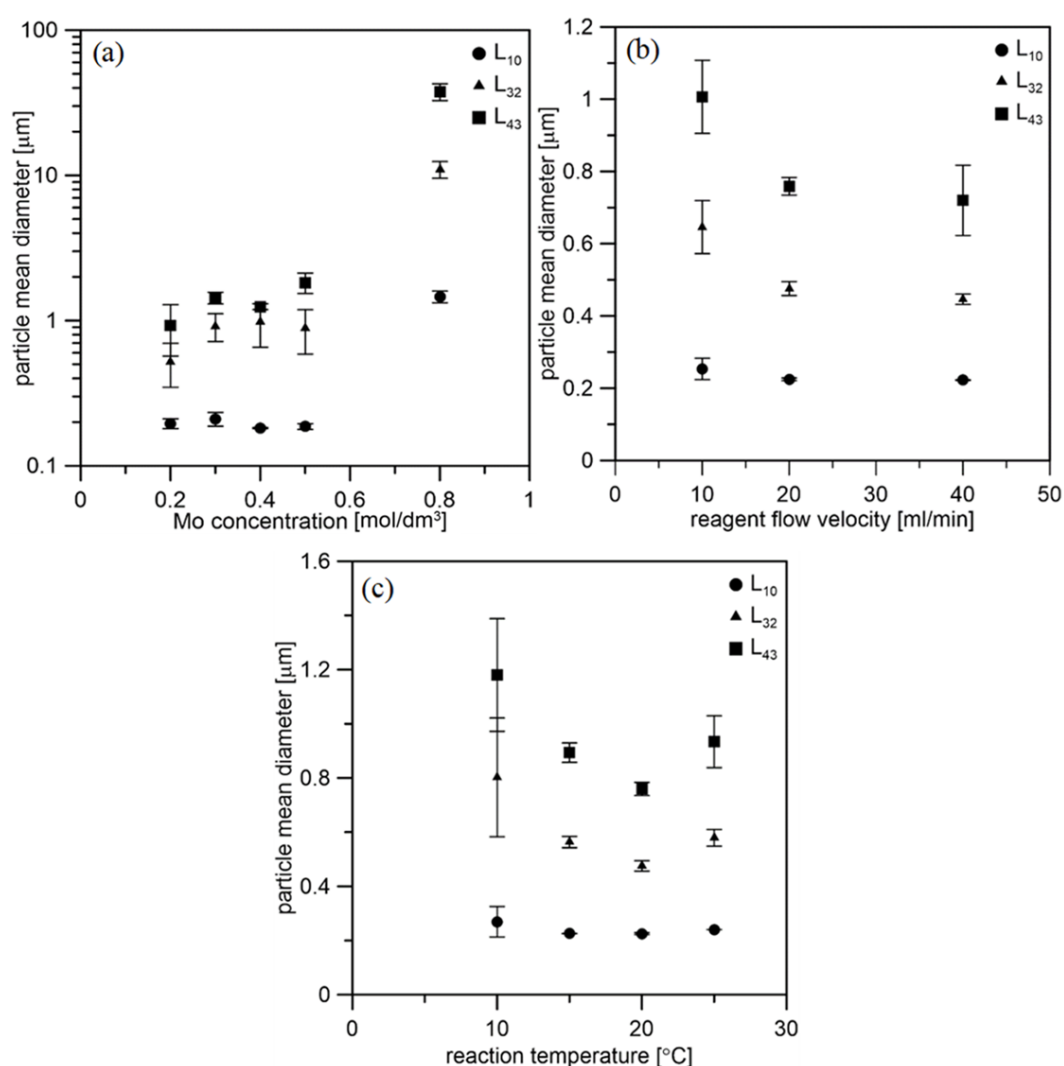


Figure 23. Influence of the process conditions on the particle mean size (a) initial molybdenum concentration at 20 °C and with a flow velocity of 20 ml/min, (b) reagent flow velocity at 20 °C and with Mo concentration of 0.2 M, (c) reaction temperature with a flow velocity of 20 ml/min and with Mo concentration of 0.2 M [P2]

6. Preparation of hybrid nanostructures based on MoS₂ and CNMs via wet chemical synthesis

To reduce molybdenum disulfide size and thus improve its properties, particle precipitation can occur on the carbon surface. The newly formed nanoparticles grow alongside the carbon nanomaterials, creating hybrid nanostructures MoS₂/CNMs. These materials can also be prepared by the wet chemical synthesis performed in the impinging jet reactor. The proposed approach is a novel method that has not yet been tested.

In the first synthesis approach, a semi-batch reactor (Figure 24 a) was used to determine whether heterogeneous nucleation was taking place on the surface of the carbon nanomaterials. For this purpose, graphene oxide was used. GO is hydrophilic and easily forms a well-dispersed aqueous suspension, thanks to which a large surface for particle precipitation is provided. Additionally, its defects and numerous functional groups can be used as nucleation sites for particle growth. Subsequently, the wet chemical synthesis with the use of GO was transferred to be used in the continuous reactor, i.e., S-type impinging jet reactor, which was selected as the most suitable (Figure 24 b). Additionally, hybrid nanostructures were synthesized in different assumed weight ratios of MoS₂:GO, i.e., 10:1, 30:1, and 50:1. The samples were purified and then annealed at 550 °C to maintain the mostly amorphous structure. The procedures of the wet chemical synthesis carried out in both reactors are accurately described in [P3].

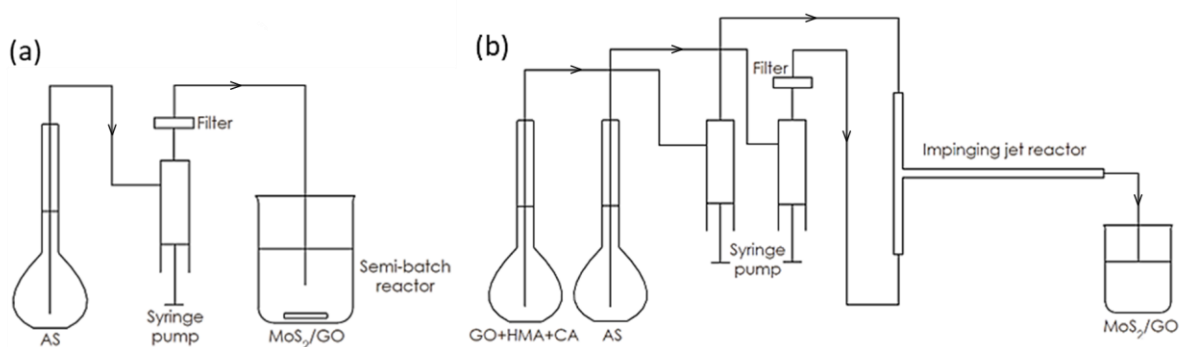


Figure 24. Schemes of the wet chemical synthesis carried out in (a) semi-batch and (b) continuous flow reactor (i.e., impinging jet reactor) [P3]

SEM images were taken to check whether the particles were deposited directly on the carbon surface or whether homogeneous nucleation had occurred and the particles were formed separately. SEM images of the samples were taken in two modes: the secondary electrons (SE) mode and the bright-field scanning transmission electron microscopy (BF-STEM). Figure 25 presents SEM images of materials prepared in the semi-batch system. The images confirmed that heterogeneous nucleation had taken place, and the GO flakes were covered with particles.

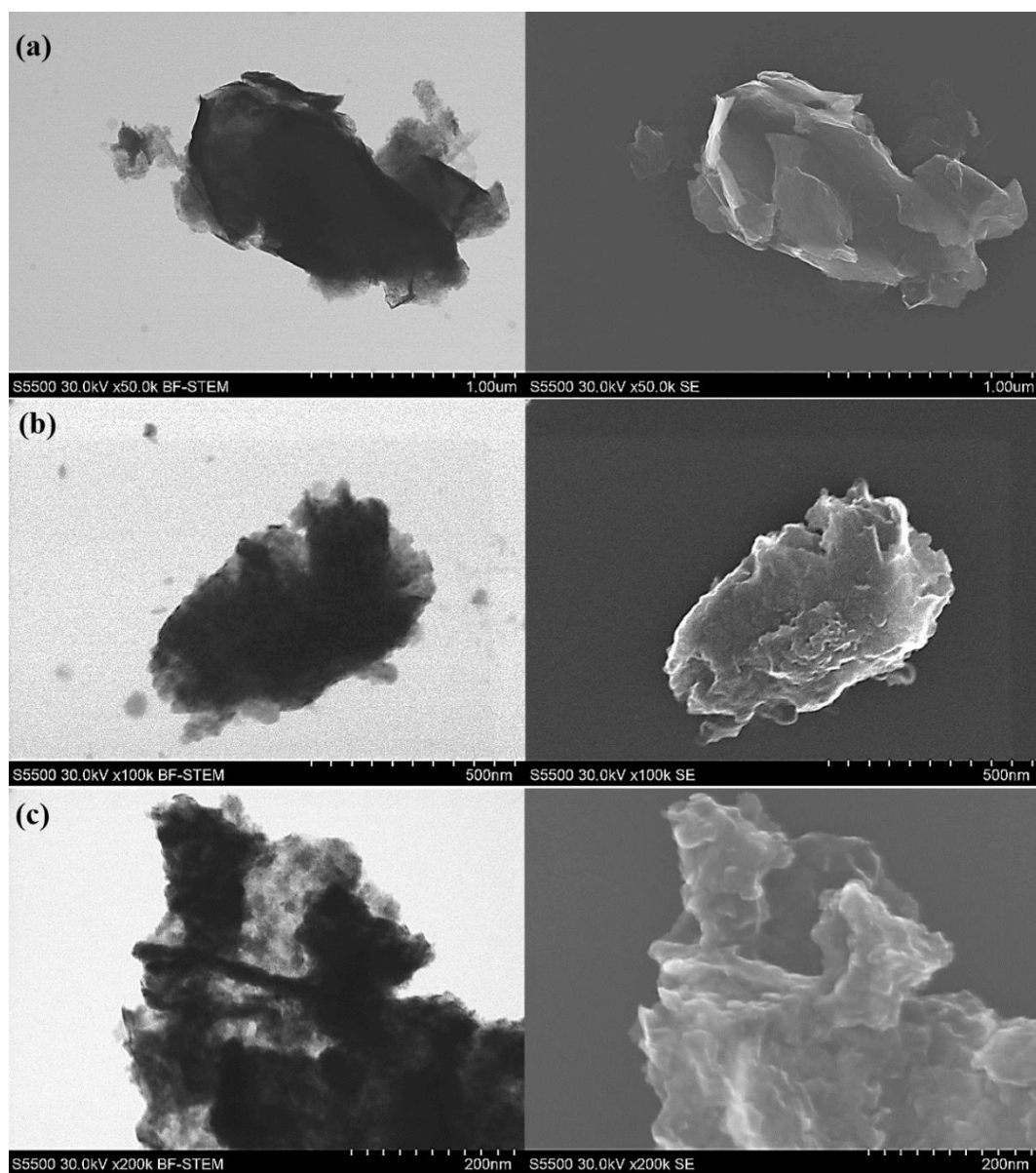


Figure 25. Images of MoS₂/GO formed in the semi-batch reactor in weight ratios of (a) 10:1, (b) 30:1, (c) 50:1 in SE and BF-STEM modes [P3]

The images of samples prepared in the impinging jet reactor also showed that heterogeneous nucleation had occurred (Figure 26). However, the particles are much smaller and better dispersed than those obtained in the semi-batch reactor, most probably due to better mixing conditions in the impinging jet reactor. Moreover, it was observed that the hybrid nanostructures tend to agglomerate less than the pure MoS₂ [P3].

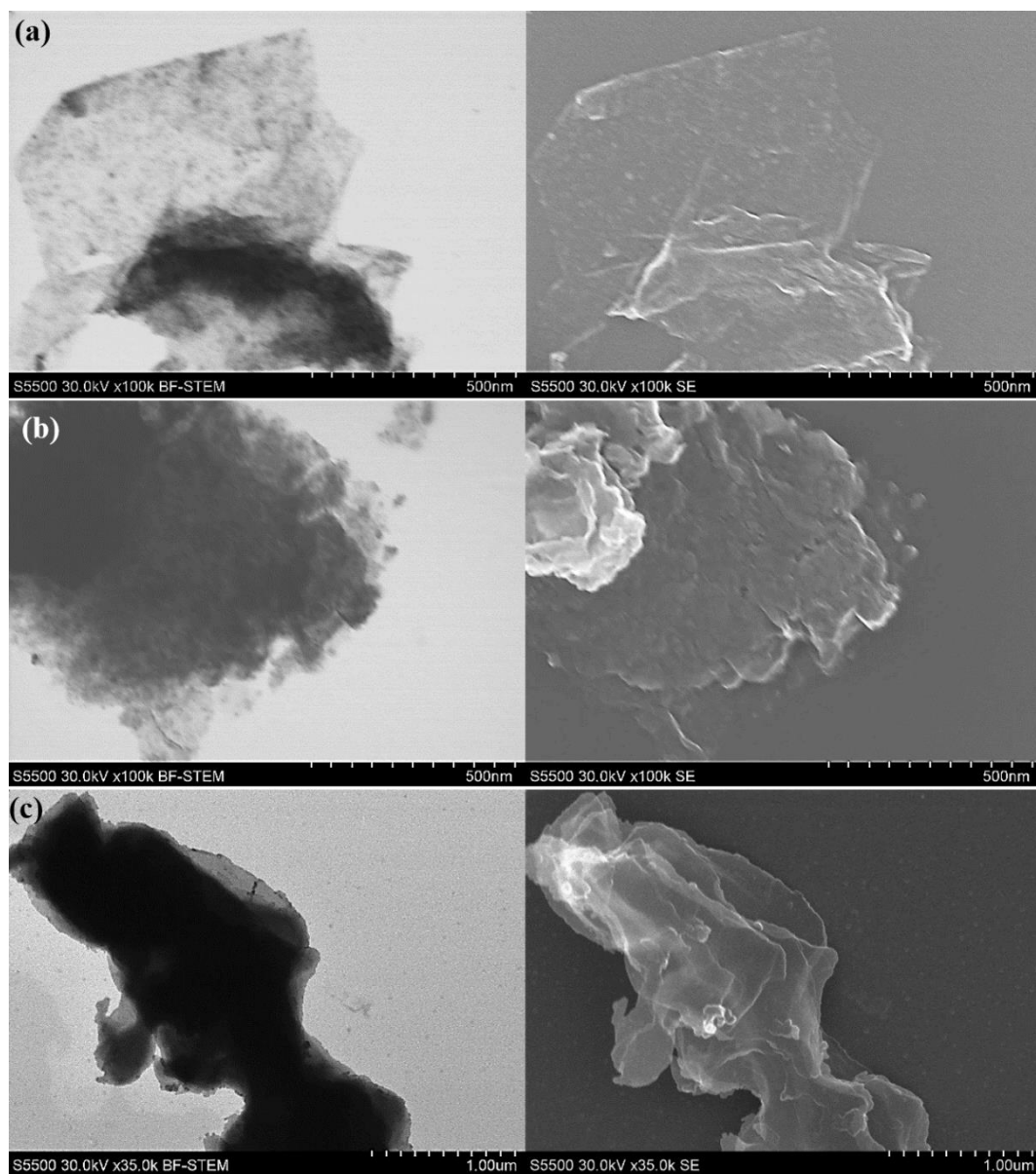


Figure 26. Images of MoS₂/GO formed in the impinging jet reactor in weight ratios of (a) 10:1, (b) 30:1, (c) 50:1 in SE and BF-STEM mode [P3]

The produced materials were subjected to XRD analysis and compared with the typical form of molybdenum disulfide, i.e., 2H crystalline. Diffractograms presented in Figure 27 confirmed that the synthesized products are based on molybdenum disulfide, showing typical peaks for this material. The average size of the 2H-MoS₂ crystallites is 9 nm in the c-direction and 12 nm in the a-direction. The size of the molybdenum disulfide deposited on graphene oxide is much smaller. The one from the semi-batch reactor is 3.1 nm in the c-direction and 7.4 nm in the a-direction, and from the impinging jet reactor is ~1.6 nm in the c-direction. In addition, the difference in crystallinity can be observed. Due to the lower annealing temperature of the hybrid nanostructures, both samples of MoS₂/GO have shown lower crystallinity. The most amorphous is the material obtained from impinging jet reactor [P3].

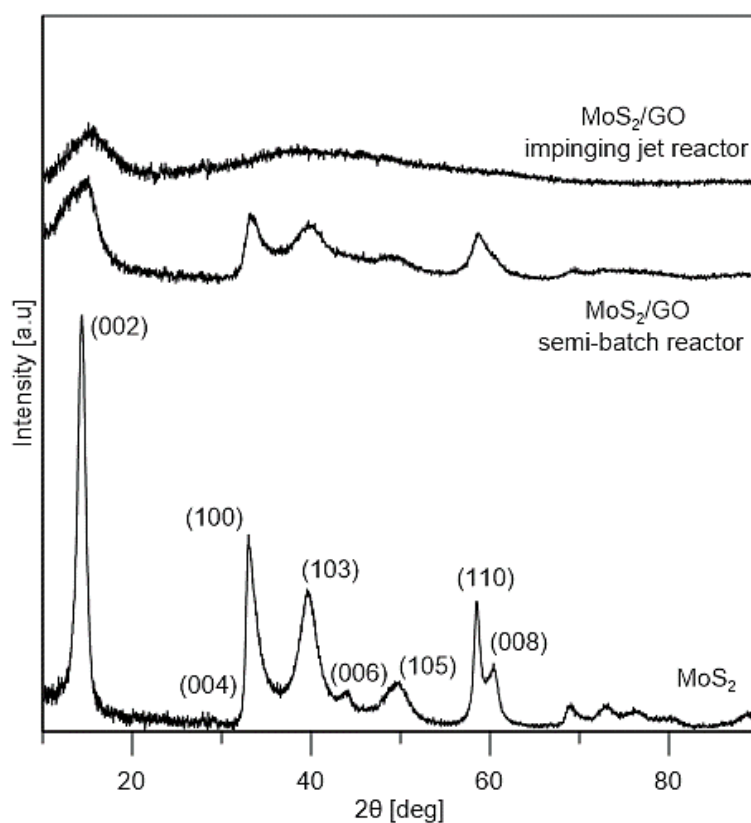


Figure 27. Diffractograms of MoS₂, MoS₂/GO prepared in the semi-batch reactor and impinging jet reactor [P3]

More information about the production of hybrid nanostructures based on molybdenum disulfide and carbon nanomaterials is presented in [P3]. These results are consistent with the assumed two first theses [T1-T2] presented in this dissertation. Wet chemical synthesis is a proper method for obtaining hybrid nanostructures based on molybdenum disulfide and carbon nanomaterials. In this approach, the particles precipitate directly on the carbon surface due to the lower energy of heterogenous than homogenous nucleation. The addition of GO to the synthesis allowed obtaining well-dispersed MoS₂ nanoparticles on the carbon flakes. The wet chemical synthesis can also be carried out in the impinging jet reactor. Due to the high energy dissipation in the reactor mixing area, particles were obtained with smaller sizes and thus a lower tendency to agglomerate. The proposed synthesis is a novel method to prepare MoS₂/CNMs that can be easily transferred to a bigger scale than the laboratory.

7. Catalytic properties of hybrid nanostructures based on MoS₂ and CNMs

7.1 Electrochemical analysis of the synthesized MoS₂-based materials

Research on the use of MoS₂ as a catalytically active material has recently become popular. Molybdenum disulfide is a promising catalyst for hydrogen evolution reaction. Due to climate change, research aimed at finding alternatives to expensive catalysts based on noble metals seems particularly important. Therefore, in this doctoral dissertation, it was decided to test the materials produced by this novel method whether they show good catalytic activity for hydrogen evolution reaction. Wet chemical synthesis allowed to check various parameters, such as the influence of various carbon supports (GO, rGO, CNTs), the different assumed weight ratios of MoS₂:CNMs (5:1, 30:1, 50:1), two annealing temperatures (550 and 850 °C). The procedures for synthesizing these materials and the methods for carrying out the analyses are presented in [P4].

The HER activity of the obtained MoS₂ and MoS₂/CNMs was studied through iR-corrected linear sweep voltammetry (Figure 28). Molybdenum disulfide samples annealed at both temperatures presented similar electrochemical performances (Figure 28 a). However, in the case of hybrid nanostructures, there is a noticeable difference between materials annealed at these two temperatures. For all GO and CNT-based samples, hybrid nanostructures annealed at 550 °C perform better. This temperature is insufficient to fully crystallize the wet chemical synthesis amorphous product. Whereby the obtained materials are mostly amorphous with smaller particle sizes, shorter Mo-Mo bonds, and higher amounts of exposed active sites, which was confirmed by high-resolution scanning transmission electron microscope (STEM) images (Figures 29-30). Therefore, the lower annealing temperature has resulted in superior catalytic activity.

Adding carbon nanomaterials during the synthesis of MoS₂ is also a promising approach to enhance its catalytic activity. Due to the good electrical conductivity of CNMs, better LSV results were achieved for the hybrid nanostructures. Moreover, the lower energy of heterogenous than the homogenous nucleation allowed obtaining highly dispersed nanosized MoS₂ particles with exposed catalytically active edges.

The best results were obtained for the hybrid nanostructures based on graphene oxide and carbon nanotubes. Very interesting are the electrochemical performances of samples based on rGO (Figure 28 b). Due to the high electronic conductivity of rGO, the catalytic activity of these

samples was surprisingly low. Due to its hydrophobic properties, there was a problem with obtaining good dispersion of rGO in the HMA+CA solution. This led to a smaller surface area available, which resulted in heterogeneous nucleation and precipitation of MoS₂ particles with poorer dispersion and larger sizes. Removal of excess rGO during purification and annealing, which was not covered with MoS₂, lowered the electrical conductivity of the sample.

In the case of hybrid nanostructures based on GO (Figure 28 c), the best electrochemical performance was shown by a sample with an assumed weight ratio of 50/1 and annealed at 550 °C. The overpotential and Tafel slope for this hybrid nanostructure were the best and equal to -0.217 V vs. RHE and 84.3 mV·dec⁻¹, respectively. Raman spectroscopy and TGA revealed [P4] that this sample had the highest content of MoS₂ and Mo-oxides among other GO-based materials. Graphene oxide flakes have poor electronic conductivity. However, its additional reduction may have occurred during annealing, which is why the MoS₂/GO 50/1 exhibit such good properties. Moreover, during annealing, some MoS₂ particles oxidized. Molybdenum oxides, especially MoO₃, can enhance the catalytic activity towards HER of molybdenum disulfide by promoting water dissociation and enhancing interfacial electron transfer [91].

The hybrid nanostructures based on carbon nanotubes also exhibit excellent electrocatalytic activity (Figure 28 c). The best sample, and slightly worse than this based on GO, was with the assumed weight ratio of 5/1 annealed at 550 °C. The overpotential was equal to -0.227 V vs. RHE, and the Tafel slope was equal to 87.4 mV·dec⁻¹. These samples owe their good catalytic activity to the carbon nanotubes, which have excellent electronic conductivity and specific geometry. The comprehensive electrochemical analysis (stability, CV, ECSA, EIS) is extensively described in [P4].

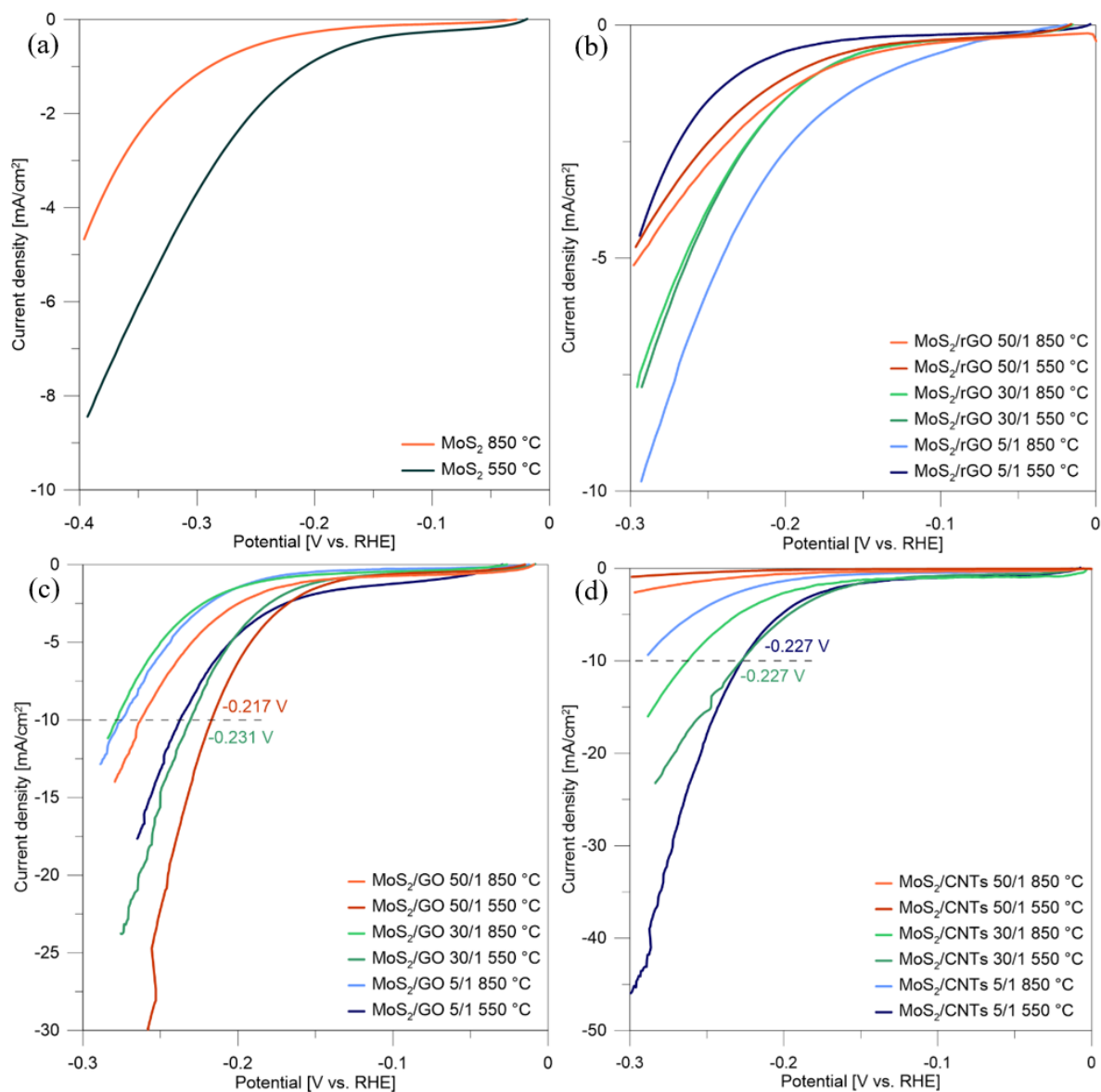


Figure 28. LSV curves of (a) MoS₂ and hybrid nanostructures (b) MoS₂/rGO; (c) MoS₂/GO; (d) MoS₂/CNTs with assumed weight ratios of 5/1, 30/1, 50/1 annealed at 550 and 850 °C

[P4]

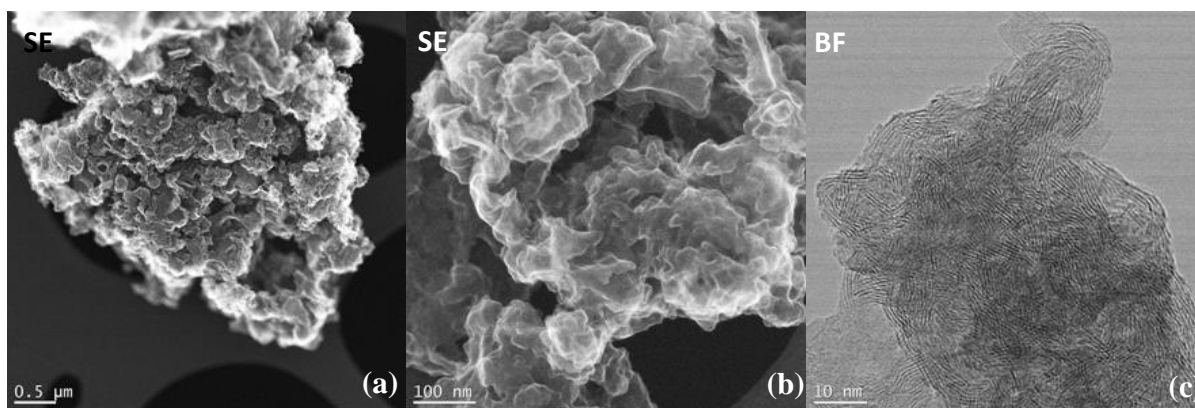


Figure 29. STEM images of MoS₂/GO 50/1 550 °C [P4]

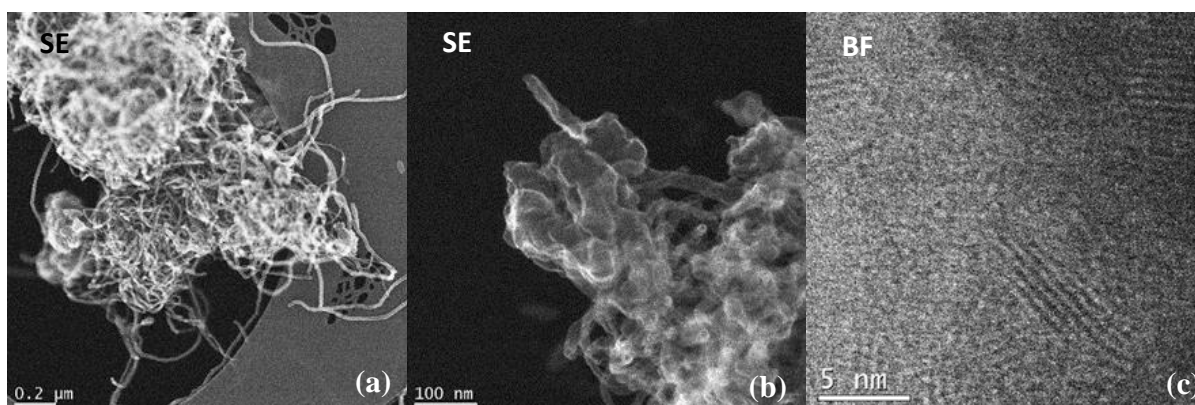


Figure 30. STEM images of MoS₂/CNTs 5/1 550 °C [P4]

7.2 Electrochemical analysis of reference MoS₂

In the previous section and publication [P4], it was proved that the addition of carbon nanomaterials as well as the amorphous structure of hybrid nanostructures resulted in an improvement of the catalytic properties. Moreover, it was decided to compare the obtained results with the electrochemical properties of commercially available molybdenum disulfide. The reference powder was purchased from Sigma-Aldrich (<2 μm, 98%). This section supplements the results presented in the publication [P4]. To compare the obtained linear sweep voltammetry curves with the new sample, the analysis conditions and methodology to prepare an electrode based on reference molybdenum disulfide were the same as in [P4].

From Figure 31 can be seen that the electrochemical performance of the purchased MoS_2 is much worse than the synthesized products. The maximum current density obtained for a potential equal to 0.4 V vs. RHE was worse than mostly amorphous and crystalline MoS_2 by 71% and 48%, respectively. Poor electrochemical properties may result from the structure of the reference sample, which is presented in Figure 32. The commercial materials had a form of well-defined agglomerates of flakes with smooth surfaces, resulting in poorly exposed active edges. STEM images of the reference MoS_2 were taken during the research described in [P5].

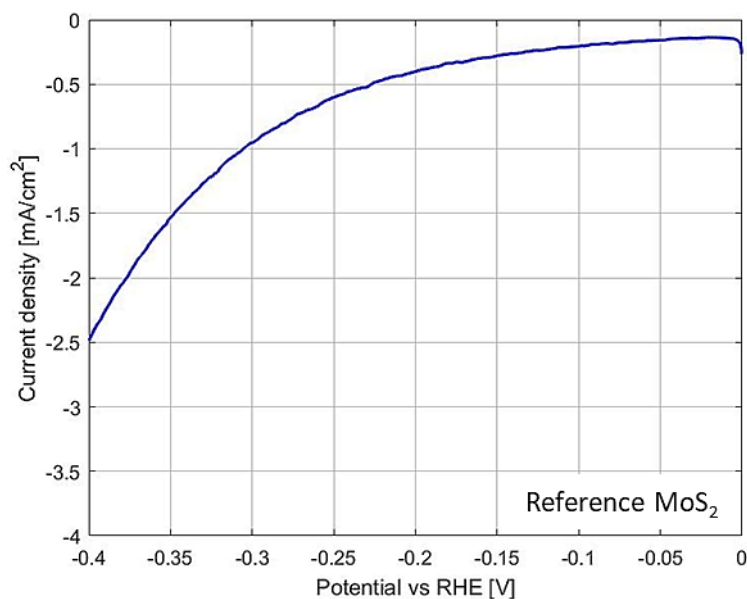


Figure 31. LSV curve of reference MoS_2

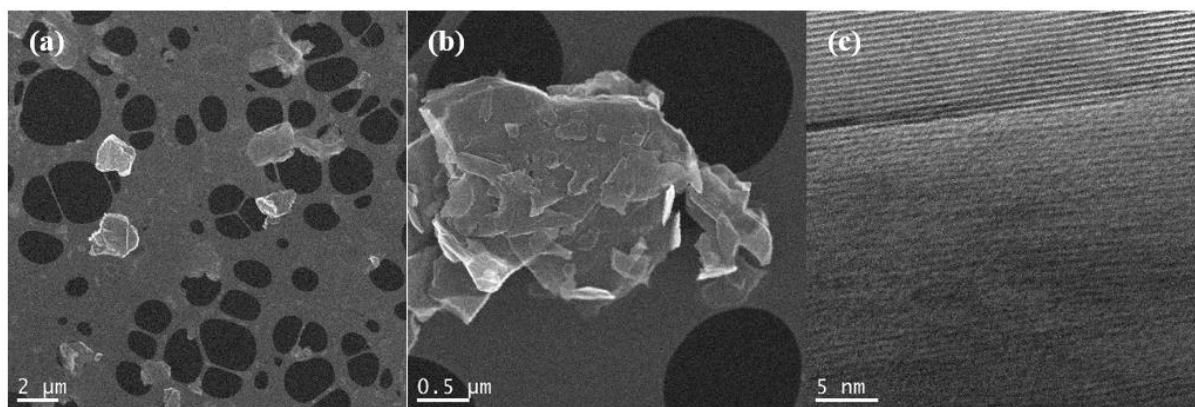


Figure 32. STEM images of reference MoS_2 [P5]

7.3 Hydrogen production

Due to the lack of equipment enabling direct measurement of hydrogen production, it was decided to perform chronoamperometric tests that allow estimating HER yield. Of all the samples described in sections 7.1 and 7.2, only the best samples (i.e., MoS₂, MoS₂/GO 50/1, MoS₂/CNTs 5/1, all annealed at 550 °C) and reference were tested. The electrodes for chronoamperometric measurements were prepared similarly and with the same materials as in the publication [P4]. Tests were conducted for the potential values close to overpotential η_{10} . The current density values were measured for 60 min. Chronoamperometric results are shown in Figure 33. All samples were stable during the measurements. In the case of all the tested materials, some deviations were visible. These irregularities are related to the formation and detachment of gas bubbles from the electrode surface during the measurement. In these conditions, the most stable sample was the hybrid nanostructure based on graphene oxide.

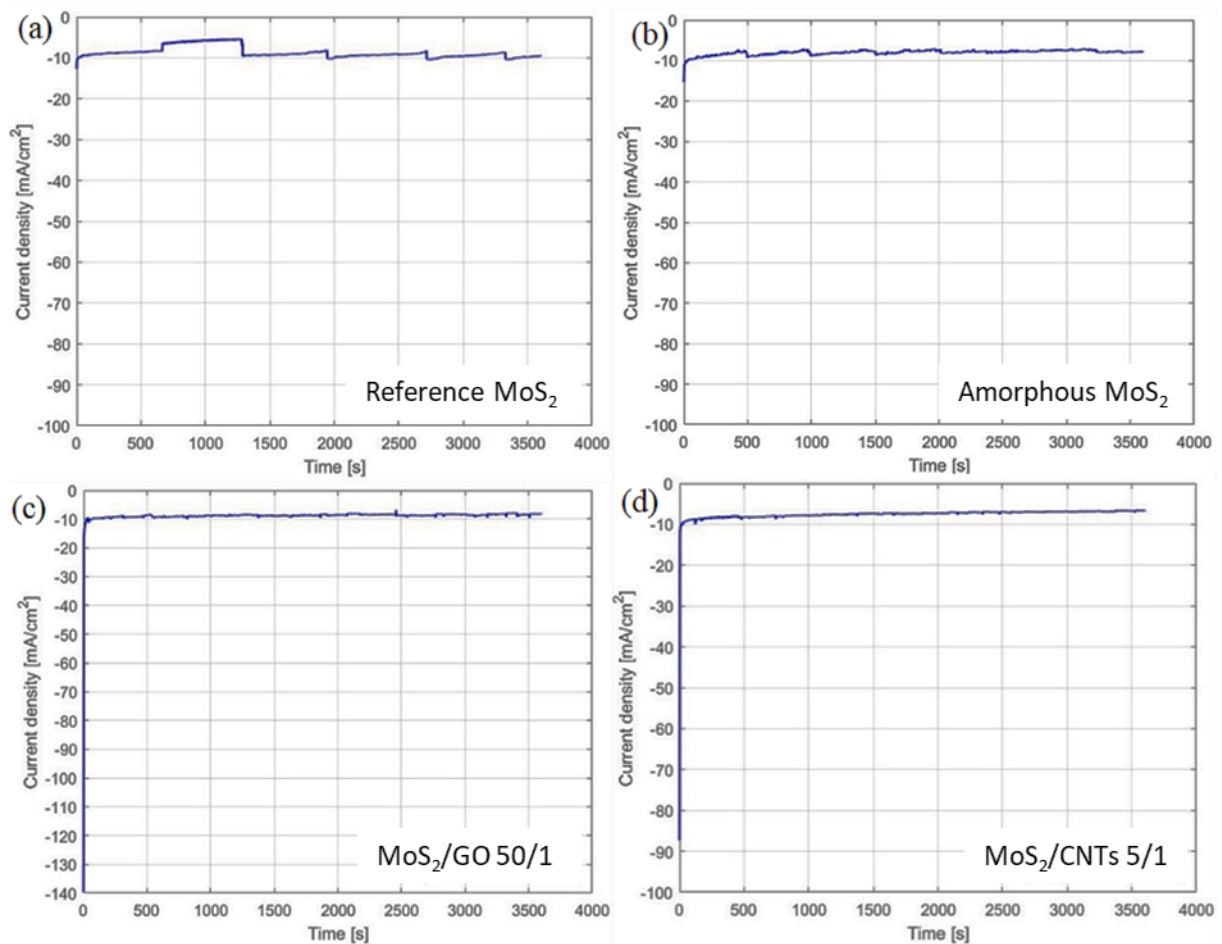


Figure 33. Chronoamperometric measurements of (a) reference and (b) amorphous MoS₂, hybrid nanostructures based on (c) GO and (d) CNTs

On the basis of chronoamperometric measurements, hydrogen yield Y [$\text{mmol} \cdot \text{g}_{\text{cat}}^{-1} \cdot \text{h}^{-1}$] was estimated. The number of moles of hydrogen released at the electrode was determined using I Faraday's law of electrolysis (Equation 25). The results are presented in Table 1.

$$m = k \cdot I \cdot t \quad (25)$$

where m – mass of hydrogen released at the electrode [g]; k – electrochemical equivalence [$\text{g} \cdot \text{C}^{-1}$]; I – current [A]; t – time [s].

The highest production while maintaining the lowest applied potential was obtained for the MoS₂/GO sample. The high hydrophilicity, the large number of defects, and the functional groups allowed obtaining hybrid nanostructures with well-dispersed MoS₂ nanoparticles and exposed active edges. Additional reduction during annealing and formation of Mo-oxides also enhanced the charge transport of GO. Therefore, the best sample was MoS₂/GO with the assumed mass ratio of 50/1 and annealed at 550 °C giving the highest hydrogen yield. Slightly worse was the sample based on CNTs. Its good catalytic activity owes to carbon nanotubes' excellent electrical conductivity and unique geometry. From Table 1 can be clearly seen that the synthetic materials presented significantly better catalytic properties. To obtain hydrogen production at a similar level using reference MoS₂, much more energy must be applied to the system.

Table 1. The estimated hydrogen yield

	Reference MoS₂	Mostly amorphous MoS₂	MoS₂/CNTs 5/1 550 °C	MoS₂/GO 50/1 550 °C
Y [$\text{mmol} \cdot \text{g}_{\text{cat}}^{-1} \cdot \text{h}^{-1}$]	143	132	124	145
E [mV]	-740	-560	-480	-460

The presented results in the publication [P4] and sections 7.2-7.3 confirmed the thesis [T3] assumed in this doctoral dissertation. The use of carbon nanomaterials as support for MoS₂ growth enhances its catalytic properties, confirmed by electrochemical analysis. CNMs improve charge transport and expose the active sites of MoS₂ by reducing particle sizes, which is visible in the STEM images. The proposed novel method for obtaining MoS₂-based materials is cheap, scalable and allows obtaining products with the desired catalytic properties.

8. Lubricating properties of hybrid nanostructures based on MoS₂ and CNMs

8.1 Tribological properties of MoS₂-based additives

Molybdenum disulfide is a well-known dry lubricant. However, it can also be used as an additive to engine oils. Although liquid lubricants with the addition of MoS₂ are available on the market, this is not a widely researched topic by scientists. Therefore, in this dissertation, the tribological properties of oil nanosuspensions with the addition of MoS₂ and hybrid nanostructures MoS₂/CNMs were checked. As in the case of the catalytic application, wet chemical synthesis allowed to check various parameters, such as the influence of various carbon supports, different assumed weight ratios of MoS₂:CNMs, and two annealing temperatures.

Three different carbon supports (GO, rGO, CNTs) were tested in the first attempts. Their different structures may affect the tribological and rheological properties of the obtained suspensions in various ways. The procedures for synthesizing these materials, oil suspensions, and the methods for conducting the analyses are presented in [P5].

To test whether the additives based on MoS₂ improve the lubricating properties of the base oil (10W-40), the tribological measurements were performed at various temperatures corresponding to both engine operating and starting conditions. Stribeck curves of the base oil and 1 wt.% suspensions are presented in Figure 34. For the lower temperatures (−10 and 0 °C), the friction factors decreased with increasing sliding speed. Thus tested oils flow in the mixed lubrication regime. At these temperatures, all the additives improve the tribological properties of the base oil. At low sliding velocities, the lowest friction factor is exhibited by the nanosuspensions with hybrid nanostructures. However, with the increase of sliding velocity, the differences between the friction factor of each sample are less significant. The best results are obtained for the nanosuspension containing reference MoS₂. For higher temperatures (25 and 75 °C) in the entire range of sliding velocity, the best tribological properties are obtained by nanosuspensions with the addition of each hybrid nanostructure. The additives reduced the friction factor of base oil up to 55%. Yet, the nanosuspension containing synthesized molybdenum disulfide exhibited the worst lubricating properties. A complete analysis of the lubricating properties of the prepared nanosuspensions can be found in [P5].

The low friction factors of the suspension containing reference MoS₂ result from its layered and arranged structure (Figure 32). Its individual layers can move freely in relation to each other, giving good lubricating properties. In the case of synthesized MoS₂, its structure is completely different. Despite smaller particles than the reference, it shows worse lubricating properties, especially at higher temperatures. This may be due to a more chaotic structure and tendency to agglomeration, which is greater at higher temperatures. Very promising are tribological properties of nanosuspensions containing hybrid nanostructures, i.e., MoS₂/GO, MoS₂/rGO, MoS₂/CNTs. Molybdenum disulfide nanoparticles deposited on carbon nanomaterials' surface enable improved tribological properties of the oil due to the smallest particle sizes and synergetic effect between these two unique materials. Carbon nanomaterials increased the molybdenum disulfide's dispersion stability, enhancing its positive impact on the tribological properties and reducing agglomeration and sedimentation from suspensions.

It is worth noting that there is no apparent difference between the tribological properties of particular additives based on MoS₂/CNMs. At 75 °C and higher values of the sliding speed, the best results were obtained for the suspension containing MoS₂/GO. This is probably due to the most petite sizes of these particles. In addition, the effect of the MoS₂:CNMs ratio was tested, but no significant differences between the suspensions were found. However, the annealing temperature showed an influence on the suspension friction factor. Due to their smaller size, the mostly amorphous particles (annealed at 550 °C) exhibit better tribological properties.

Upon addition, the hybrid nanostructures were produced at a different time than those tested for catalytic applications. Interestingly, as in the case of samples based on GO and CNTs, they were synthesized from the same batches of carbon nanomaterials, and a different rGO was used. Although it was produced with the same technique, the MoS₂/rGO hybrid nanostructure differed from the one studied catalytically. This time, MoS₂ particles were successfully deposited on the carbon surface, and the carbon content in this sample was also much higher, confirmed by TGA [P5]. This would mean that the carbon nanomaterial had a lower degree of reduction than the one taken for catalytic tests, resulting in lower hydrophobicity. Thus it was possible to obtain a better dispersion of MoS₂ NPs on the rGO flakes. This confirms the problem with the reproducibility of the properties of carbon nanomaterials mentioned in Section 1. *Carbon nanomaterials*. Therefore, it is crucial to analyze the carbon nanomaterials before proceeding to further research and synthesis.

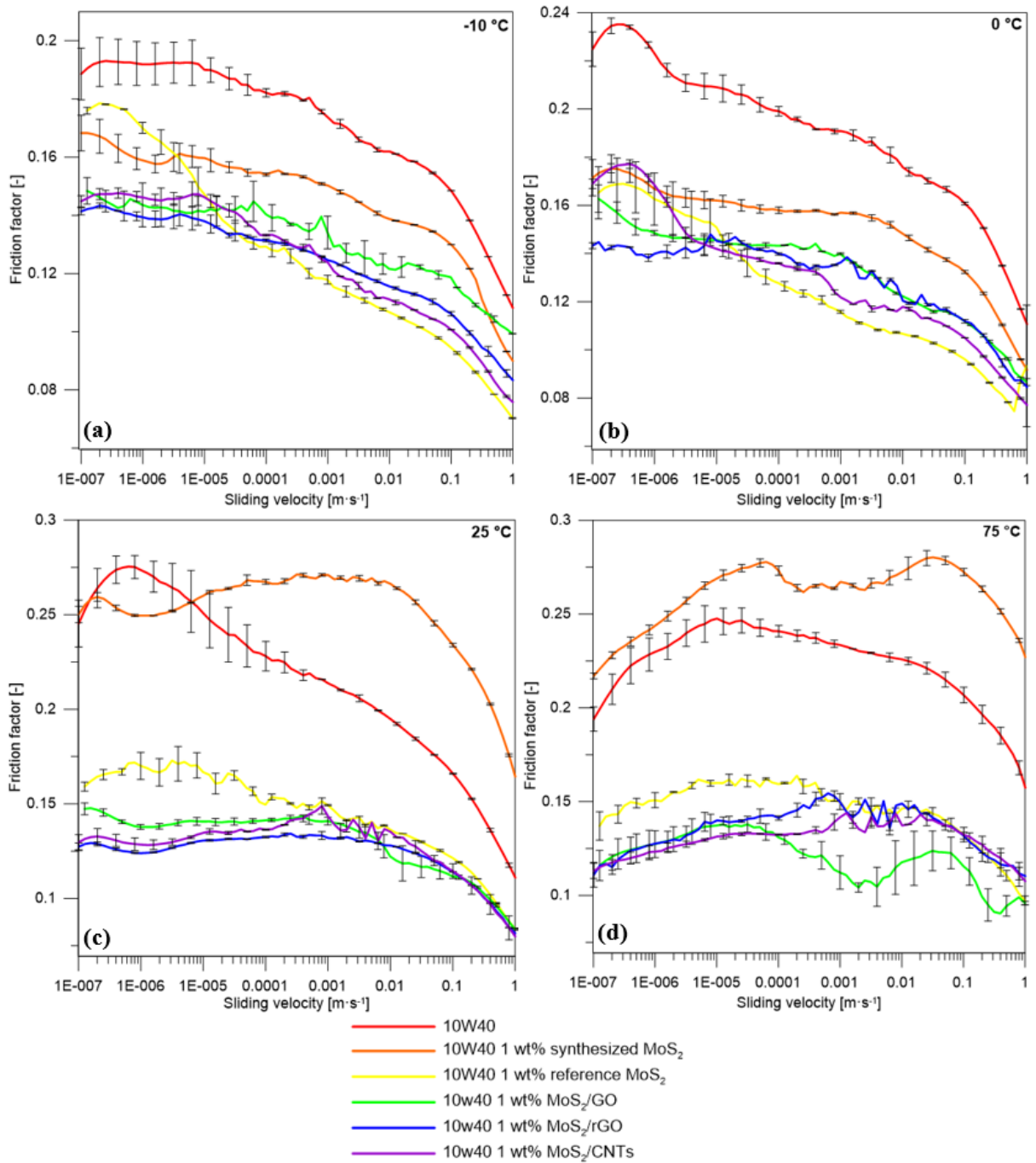


Figure 34. Stribeck curves of 10W-40 oil, nanosuspensions of 10W-40 + 1 wt.% of reference MoS₂, synthesized MoS₂, MoS₂/GO, MoS₂/rGO, and MoS₂/CNTs at temperatures of (a) -10, (b) 0, (c) 25, and (d) 75 °C [P5]

8.2 Rheological properties of MoS₂-based additives

Viscosity is a crucial parameter of the engine oil. Ensuring the appropriate viscosity value allows for good engine efficiency in various operating conditions. An important aspect in the field of oil additives is that their use does not significantly affect the rheological properties of the base oil. Changing the viscosity of the base oil can influence its features and change the SAE classification. Therefore, studying the tribological and rheological properties of the oil modified with additives is essential. The publication [P5] describes the methods for conducting the rheological measurements.

The viscosity curves of the base oil and nanosuspensions at various temperatures (−10, 0, 25, and 75 °C) are presented in Figure 35. All tested oils are shear-thinning fluids. The addition of synthesized MoS₂ increased the viscosity of the base oil at each temperature. At lower temperatures (i.e., −10 and 0 °C), adding hybrid nanostructures obtained by the wet chemical synthesis using impinging jet reactor slightly lowered the base oil viscosity. However, at higher temperatures, the differences in the viscosity of the base oil and the samples containing MoS₂/CNMs are insignificant. The slight decrease in the oil viscosity may lead to the improvement of its hydrodynamic properties.

At 75°C and low shear rates, the nanosuspensions with the addition of MoS₂/CNTs and MoS₂/GO exhibited deviations, possibly because at low viscosity, the non-uniform geometry of the carbon nanotubes and graphene oxide may have affected the results. This phenomenon is not observed at higher shear rates. Therefore, engine operation will not be affected at this temperature as engines run at higher revs. More details about the rheological properties of the prepared nanosuspensions can be found in [P5].

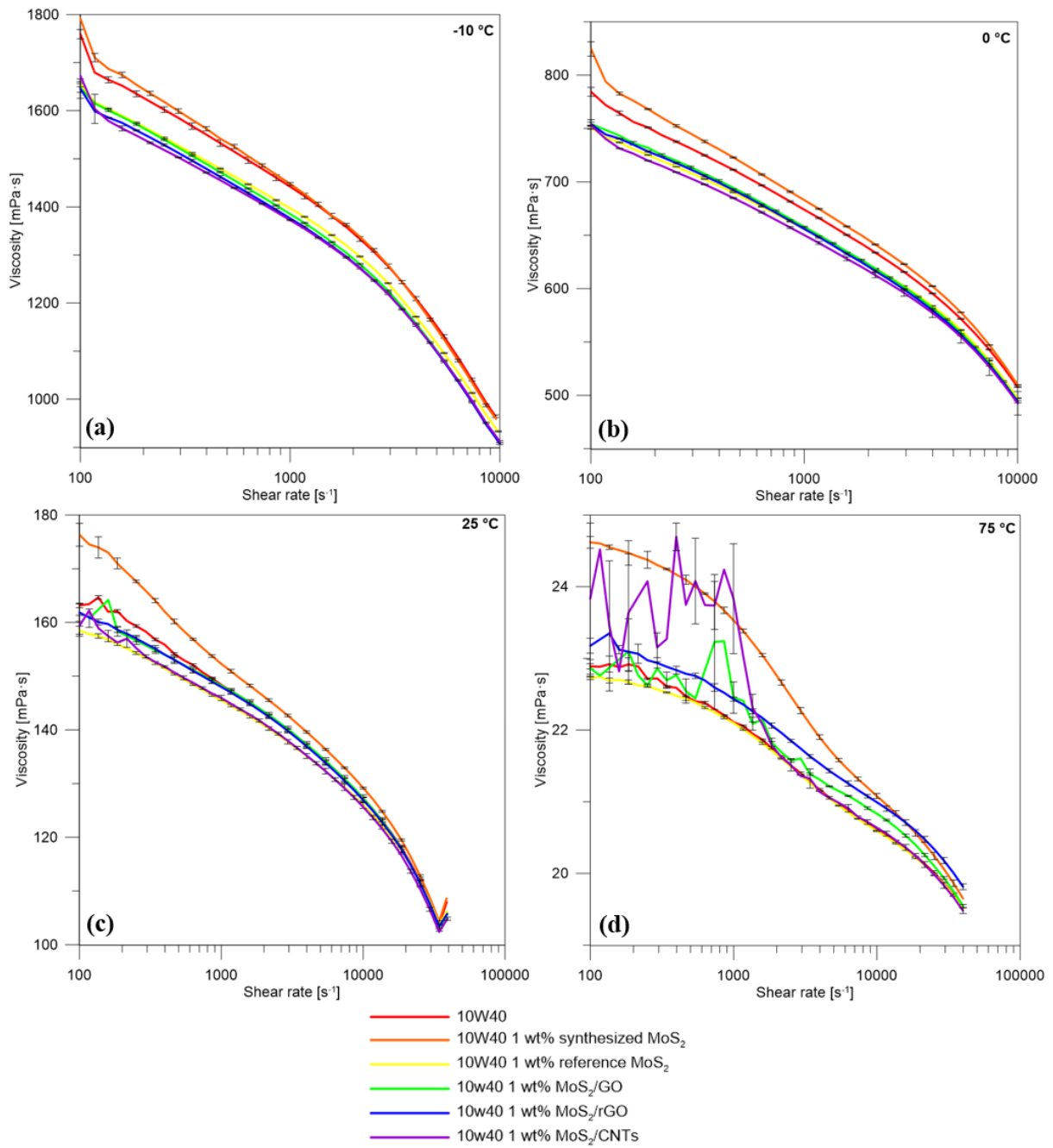


Figure 35. Rheograms of 10W-40 oil, nanosuspensions of 10W-40 + 1 wt.% of reference MoS₂, synthesized MoS₂, MoS₂/GO, MoS₂/rGO, and MoS₂/CNTs at temperatures of (a) -10, (b) 0, (c) 25, and (d) 75 °C [P5]

On the basis of the oil viscosity curves, it is possible to formulate a mathematical model that describes their rheological behaviors. In publication [P6], the mathematical model was formulated considering the effects of viscosity heating. The obtained rheograms were corrected in the region of high shear rates, where viscous heating effects become significant, using the model of the non-isothermal Couette flow (Figure 36). Moreover, the consistency k and flow behavior n indexes of the Ostwald-de Waele model (Equation 26) were determined.

$$\tau = k \cdot \dot{\gamma}^n \tag{26}$$

where τ is shear stress [Pa]; k is flow consistency index [Pa·sⁿ]; $\dot{\gamma}$ is shear rate [s⁻¹]; n is flow behavior index [-].

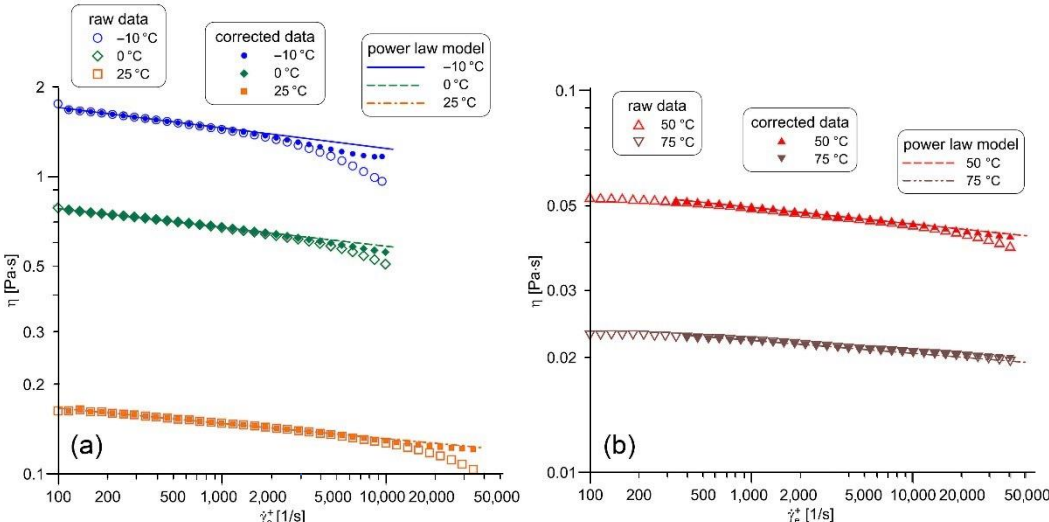


Figure 36. Temperature correction of the apparent viscosity of the base oil 10W-40 at (a) low cup temperatures; (b) high cup temperatures [P6]

Using the non-isothermal Couette flow model allowed to significantly reduce viscous heating effects and correct the oils' rheograms in the region of high shear rates. The Ostwald–de Waele model adequately describes the rheological properties of the tested oils in a wide range of shear rates and temperatures. Refined viscosity curves of the base oil 10W-40 and the nanosuspensions are presented in Figure 37. More details about temperature correction can be found in [P6].

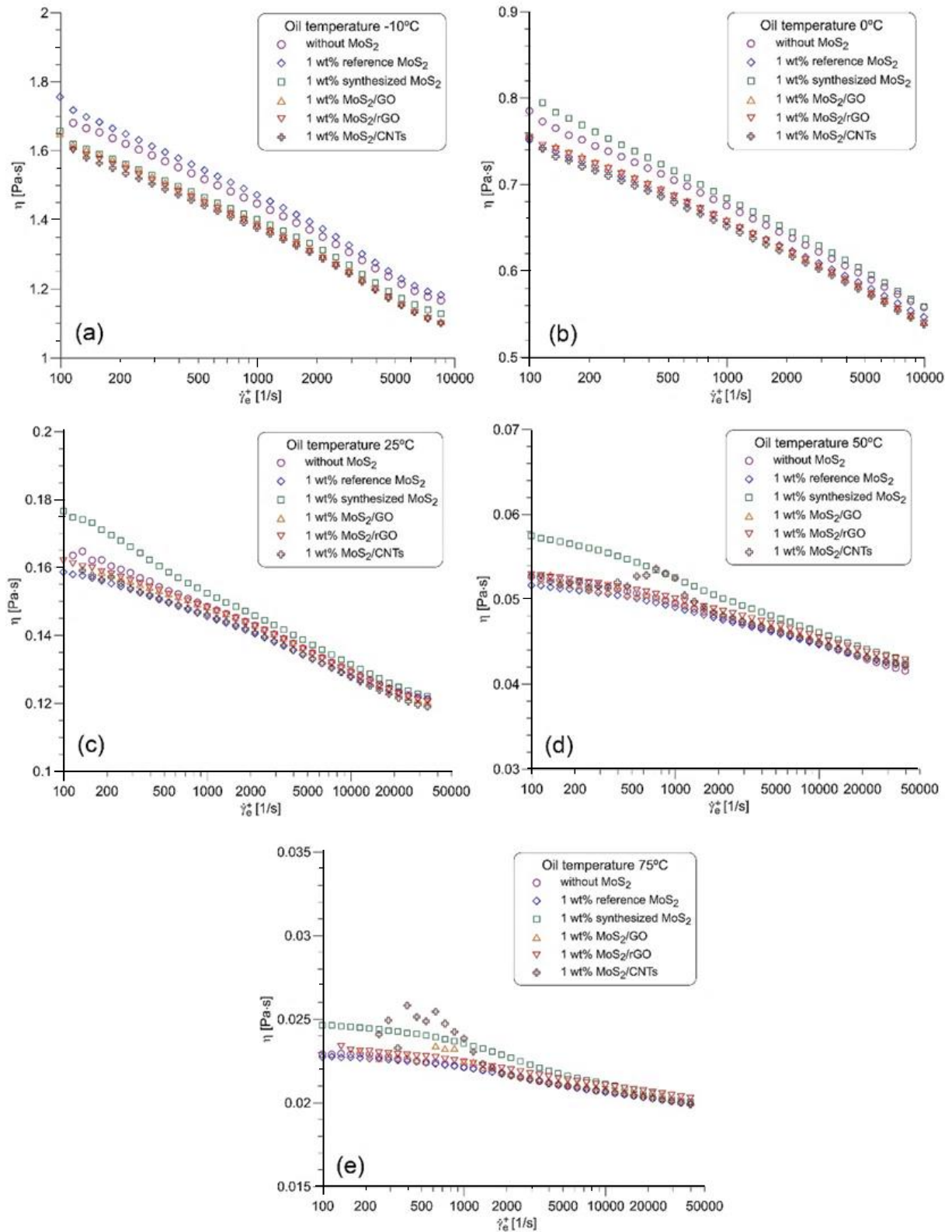


Figure 37. Refined viscosity curves of the base oil 10W-40 and the nanosuspensions with MoS₂ and MoS₂/CNMs at (a) -10, (b) 0, (c) 25, (d) 50, (e) 75 °C [P6]

8.3 Particle size distribution in the engine exhaust gas

Using oil with enhanced properties increases engine efficiency and reduces the pollution caused by emitted gases. Therefore, to check whether oils modified with hybrid nanostructures are suitable for use in a real internal combustion engine, research was carried out on the distribution of solid particles in the exhaust of a power generator. This section follows previous research and supplements the results of the publication [P5].

For this purpose, hybrid nanostructure based on carbon nanotubes with an assumed weight ratio of 5/1 and annealed at 550 °C was synthesized according to [P4]. CNTs were chosen for further research due to the larger amounts of oil needed to fill the power generator and the abundant resources of this material. Before starting the engine tests, the effect of suspension concentration was also investigated. Tribological properties of various concentrations (i.e., 0.05, 0.1, 0.2, 0.4, 0.5, 0.6, 0.7, 0.8, 1.0 wt.%) of nanosuspensions containing MoS₂/CNTs at various temperatures (-10, 0, 25, 75, and 100 °C) were checked. The 10W-40 engine oil was used as the base oil. The same setup and methodology were used in [P5] to carry out the tribological measurements.

Due to the readability of the results, Figure 38 presents only the friction factor for a representative sliding velocity equal to 0.63 m/s. At higher temperatures (75 and 100 °C), the decrease in friction factor of each suspension compared to base oil can be observed. The best results were obtained for 0.5 and 1 wt.% MoS₂/CNTs. For 1 wt.% nanosuspension, the decrease in the friction factor at 75 and 100°C was 40% and 39%, respectively, compared to pure oil (Figure 38 a and b). The differences in tribological properties of the oils are less significant at 25 and 0 °C (Figure 38 c and d). However, at -10 °C (Figure 38 e), the hybrid nanostructure did not change or even deteriorated the oil tribological properties. At this temperature, the oil viscosity increases significantly, which may change the mobility of the additives in the suspension. The non-linear relationship between the measured friction factor of the tested oils and the additive content may be caused by many factors. First, the results correspond only to a fragment of the Stribeck curves. Furthermore, there is an optimal relationship between the amount of friction-reducing agent added and its tendency to agglomerate, which causes further sedimentation. From the obtained results, the 0.5 and 1 wt.% nanosuspensions were considered the best and taken for further research.

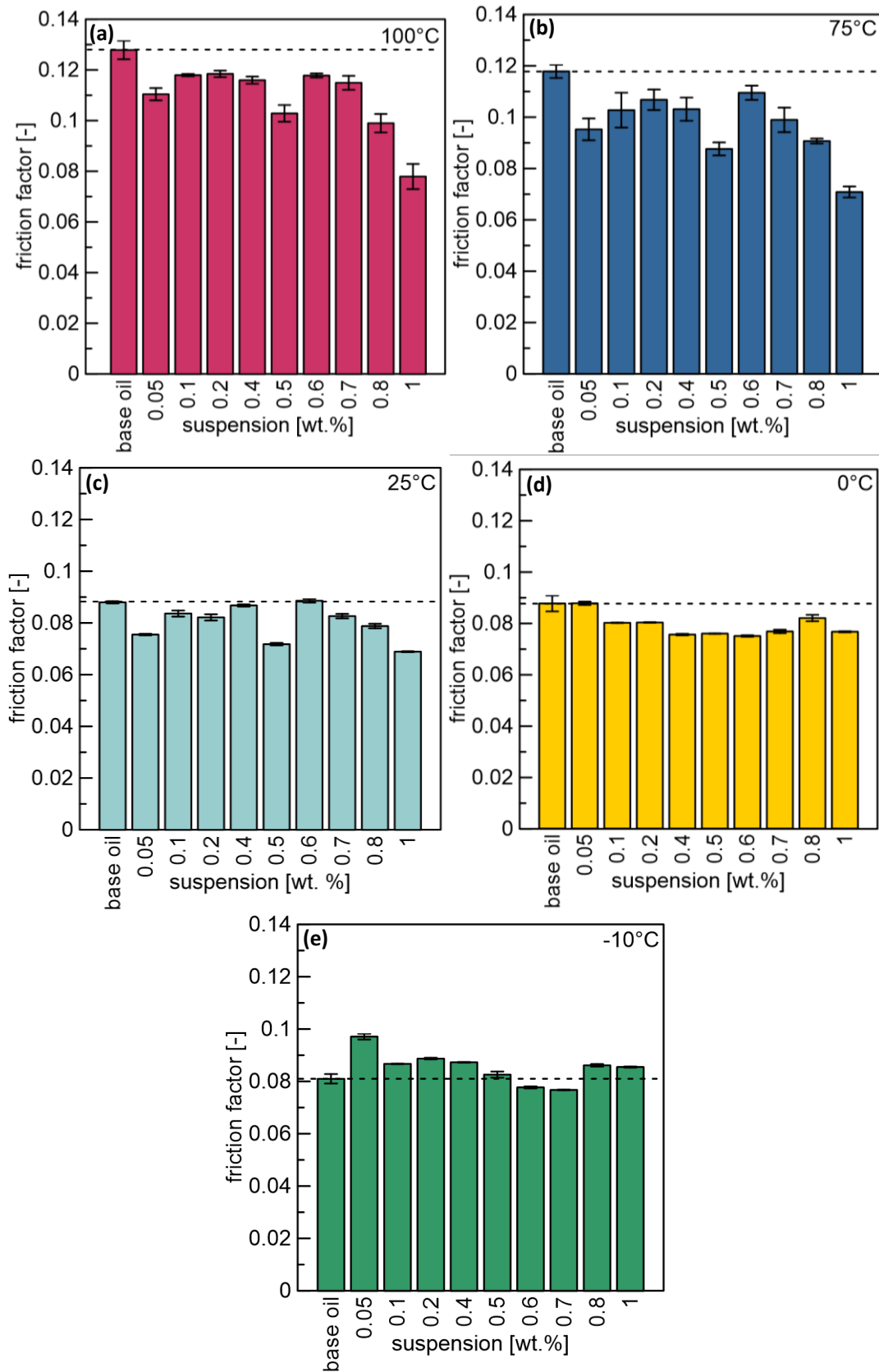


Figure 38. Friction factor at a sliding velocity of 0.63 m/s for each suspension containing MoS₂/CNTs and base oil at (a) 100, (b) 75, (c) 25, (d) 0, and (e) -10 °C

Although in short-term studies, the best properties were shown by the 1% nanosuspension, after a longer time, it was noticed that the sample was sedimenting. Due to the fear of destroying the engine, i.e., the power generator, 0.5wt.% of the suspension was used for further research.

To measure the distribution of particulate matter in the engine exhaust, fast aerosol particle emission spectrometry (FAPES) from the Grimm Aerosol Technic GmbH system was used [92, 93]. The exhaust gases were produced by a 5.5 kW Honda EM 5500CX power generator. The flue gases were then led to the combustion chamber, where the measuring probe was located. The test began with determining the background (engine off) for 3 min. The PSD was examined during further 3 minutes of engine idle operation. Subsequently, the load was turned on for another 2 minutes, and the measurements were continued. An electric heater with a capacity of 2 kW was used as the load. The schematic illustration of the system used is shown in Figure 39. Measurements were made for an engine that was running with 400 ml of the base oil and 0.5 wt.% nanosuspension containing MoS₂/CNTs.

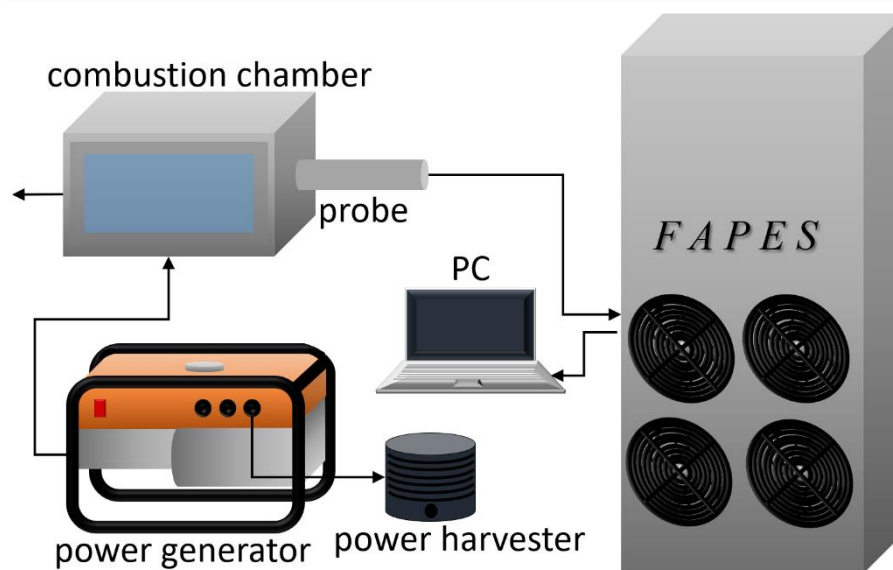


Figure 39. The scheme of the system used for the solid particle size distribution of engine exhaust

The results obtained from FAPES are in the form of normalized particle size distributions ($\frac{dN}{d \ln(D_p)}(D_p)$). On their basis, the normal distributions were adjusted as a function of the logarithm of the particle size (Figure 40 a and b). Moreover, the results were converted into PSDs by number (Figure 40 c) and volume (Figure 40 d) using Equations 27-30. The primary particles measured by FAPES are assumed to be spherical. Therefore fractal particles are formed only after deposition on the surface, according to [92]. That is why the volume shape factor of particles is equal to $\frac{\pi}{6}$.

$$d \ln D_p = \frac{d \ln D_p}{dD_p} \cdot dD_p = \frac{dD_p}{D_p} \quad (27)$$

$$\frac{dN}{d \ln(D_p)} = \frac{dN}{dD_p} D_p \quad (28)$$

$$\frac{dN}{dD_p} = \frac{dN}{d \ln(D_p)} \frac{1}{D_p} \quad (29)$$

$$\frac{dV}{dD_p} = \frac{dN}{dD_p} \frac{\pi}{6} D_p^3 \quad (30)$$

where D_p is particle diameter [m]; N is particle concentration [$\# \cdot m^{-3}$]; V is particle volume [m^3].

The obtained PSDs confirmed that the MoS₂/CNTs used as engine oil additives positively impacted the quality of the engine exhaust. Adding MoS₂/CNTs to the base oil improved its lubricating properties, reduced oil consumption, and the nucleation of NPs formed during engine operation. The number and total volume of particles contained in the exhaust gases are significantly smaller when the engine worked with 0.5 wt.% nanosuspension than with the base oil. This effect is visible in both operating conditions. The total volume of solid particles in the exhaust gas was reduced by 91% during idling and 49% during the load running.

Due to the good properties of the oil containing the reference MoS₂, presented in [P5], tests were also carried out with the engine using a 0.5 wt.% suspension with this additive. However, it was impossible to perform the test because the engine could not run with this suspension. This is probably due to the reference particles being too large. Therefore, the hybrid nanostructures MoS₂/CNMs have an advantage over both MoS₂ synthetic and reference.

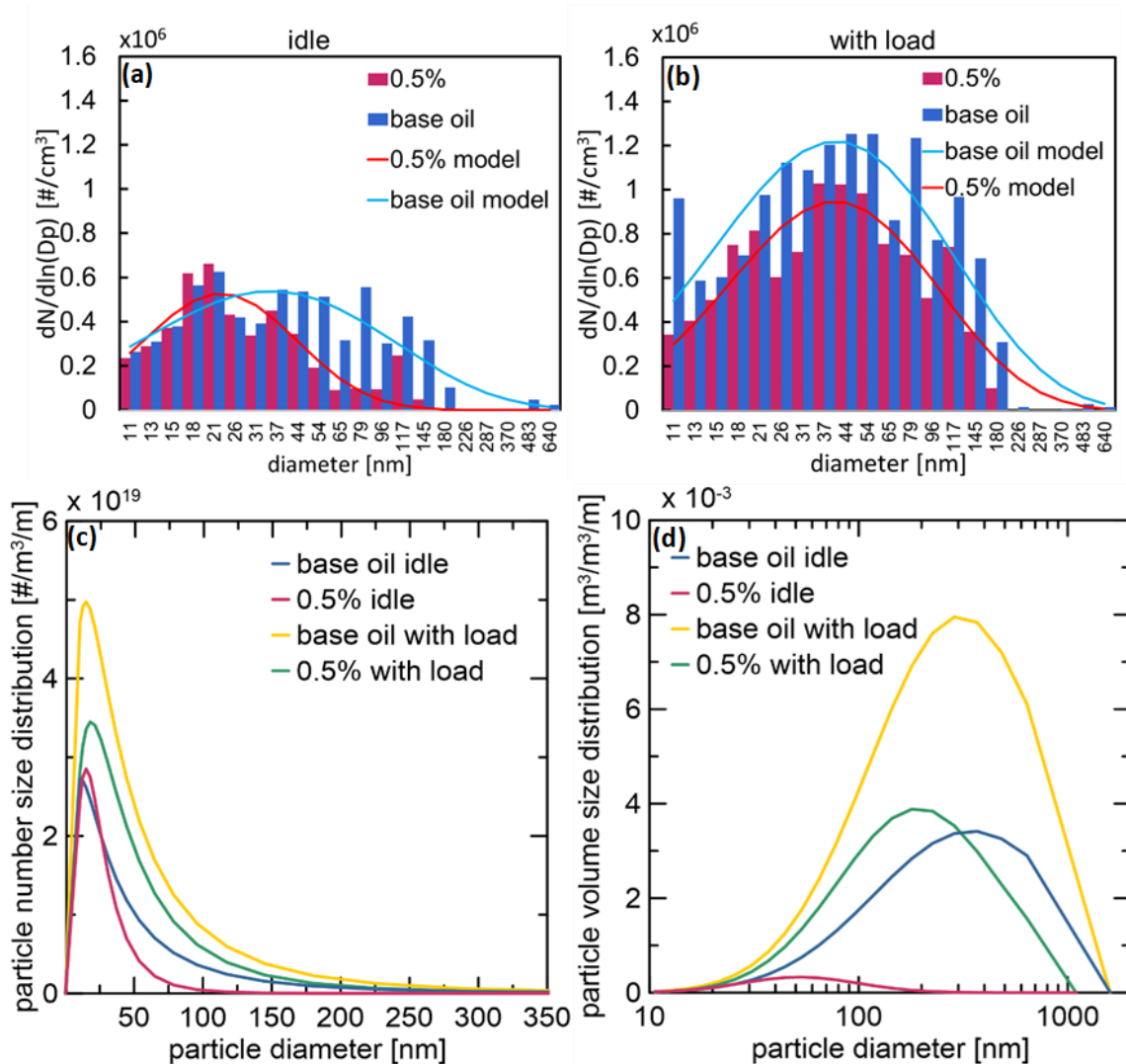


Figure 40. Normalized PSD measured using FAPES (a) at the idle run and (b) with load, (c) particle number size distribution, and (d) particle volume size distribution of engine exhaust

The presented results in the publications [P5-P6] and section 8.3 confirmed the thesis [T4] assumed in this doctoral dissertation. The use of carbon nanomaterials as support for MoS₂ particles also enhances its lubricating properties. Due to the size reduction and synergistic effect between these two unique materials, hybrid nanostructures improve the tribological properties and stability of the modified oils. Moreover, hybrid nanostructures MoS₂/CNMs prepared via this novel method can be successfully used as nanoadditives for engine oil to mitigate the gasoline engines' harmful effects on the environment.

9. Conclusions

This doctoral dissertation presents a new method of obtaining hybrid nanostructures based on molybdenum disulfide and carbon nanomaterials. It focuses on determining the influence of process parameters on the morphology and structure of the product of the wet chemical synthesis performed in impinging jet reactors. Molybdenum disulfide particles are produced as a result of the primary homogeneous nucleation. While hybrid nanostructures are formed in the process of heterogeneous nucleation, during which MoS₂ nanoparticles precipitate on the surface of carbon nanomaterials. The foreign substance present in the supersaturated solution reduces the nucleation energy, so heterogeneous nucleation occurs earlier than homogeneous nucleation. Wet chemical synthesis can be carried out in commonly used tank reactors, but also in impinging jet reactors. The high mixing intensity is related to the formation of an area with a high energy dissipation rate in the contact zone of the inlet streams. This allows obtaining materials with the desired and repeatable properties in a relatively inexpensive, continuous, controlled, and scalable way. The comprehensive analysis of this research is presented in [P1, P2, P3]. These results are consistent with the assumed two first theses [T1-T2] presented in this dissertation. Subsequently, the developed hybrid nanostructures were tested in two important applications.

Due to the potential use of molybdenum disulfide as a catalyst for the hydrogen evolution reaction, the electrochemical properties of the developed hybrid nanostructures were investigated. The addition of carbon nanomaterials enhances MoS₂ catalytic properties by promoting its charge transport, reducing particle size, and exposing the active sites. The presented results in [P4] confirmed the thesis [T3]. Moreover, wet chemical synthesis enables the production of an amorphous product. The mostly amorphous MoS₂ (annealed at 550 °C) showed superior catalytic properties than its crystalline form. The maximum current density obtained at a potential of 0.2 V vs. RHE for the best hybrid sample was 16 times higher than in the case of pure MoS₂ synthesized and commercially available.

Furthermore, molybdenum disulfide is commonly used as a lubricant, which is why it was tested how MoS₂/CNMs affect the lubricating properties of engine oil. The use of carbon nanomaterials as the support for MoS₂ growth also enhances its lubricating properties. Due to the size reduction and synergetic effect between these two unique materials, hybrid nanostructures improve the tribological properties of the base oils. A complete tribological and rheological analysis of the modified oils is provided in [P5, P6]. Moreover, MoS₂/CNMs

mitigate the gasoline engines' harmful effects on the environment. Studies of the size distribution of particulate matter in the engine exhaust gas showed that the use of oil with MoS₂/CNMs allowed to reduce the total volume of particulate matter in the exhaust gas by 91% and 49% under idling conditions and with load compared to work with the base oil. The results confirmed the thesis [T4] assumed in this doctoral dissertation.

The research presented in this doctoral thesis fits into the European Union's plan to achieve climate neutrality by 2050, along with the interim emission reduction target of 55% by 2030. In order to achieve the above goals, it is therefore necessary to decrease greenhouse gas emissions, which can be done by investing in renewable energy, energy efficiency, or other clean, low-carbon technology. Among the renewable energy technologies, hydrogen stands out as the fuel of the future. To help commercialize green hydrogen, its production costs should be reduced. One of the solutions may be finding a cheaper, noble metal-free catalyst for the hydrogen evolution reaction in water electrolysis. An alternative to the commonly used expensive catalysts may be hybrid nanostructures MoS₂/CNMs. The hydrogen produced via water electrolysis can be further used in low-temperature fuel cells, which I also dealt with during my research work [94]. However, the transition period between the widespread use of green hydrogen and the present, which the EU says is around 20-30 years, requires a focus on current issues. One of them is the reduction of emissions from internal combustion engines. To extend the life of the engine and mitigate its negative impact on the environment, oil with nanoadditives can be used. Again, MoS₂/CNMs can be distinguished from other lubricating additives.

List of Figures

Figure 1. Types of hydrogen and methods of its production.....	25
Figure 2. Graphene and graphene oxide structure [11]	29
Figure 3. Single-wall carbon nanotube and multi-wall carbon nanotube structures [40]	31
Figure 4. Molybdenum disulfide structure [47]	32
Figure 5. Crystalline forms of MoS ₂ [55].....	33
Figure 6. Preparation of hybrid nanostructures MoS ₂ /CNMs and bulk MoS ₂	34
Figure 7. Water splitting (water electrolysis)	36
Figure 8. Mechanism of hydrogen evolution on the electrode surface in (a) acidic and (b) alkaline solutions.....	38
Figure 9. Comparison of catalyst activity based on the comparison of η_{10} values.....	40
Figure 10. An example of Nyquist plot.....	42
Figure 11. Exchange current density as a function of Gibbs energy for selected materials [71]	42
Figure 12. Stribeck curve and illustrations of the three lubricant regimes.....	45
Figure 13. (a) Flow curves and (b) viscosity curves for different types of fluids	47
Figure 14. Schematic presentation of wet chemical synthesis	51
Figure 15. Diffractograms of (a) purified particles [P1], (b) annealed at 850 °C [P1], and 550 °C [P4] particles of MoS ₂ obtained by wet chemical synthesis	52
Figure 16. Thermogravimetric analysis of purified MoS ₂ particles heated in the flow of air and argon [P1].....	53
Figure 17. Particle size distributions (by (a-b) number, (c-d) surface area, (e-f) volume) for MoS ₂ particles prepared with citric (CA) and formic acid (FA) after each step of preparation [P2].....	54

Figure 18. Raman spectra of MoS ₂ prepared with the use of citric (CA) and formic acid (FA) [P2]	55
Figure 19. Scheme of (a) semi-batch and (b) continuous flow reactor used for the MoS ₂ production through the wet chemical synthesis [P1]	56
Figure 20. PSD of the MoS ₂ obtained in the continuous flow reactor (a) agglomerates and (b) primary particles, and in the semi-batch system (c) agglomerates and (d) primary particles depending on the initial Mo concentration [P1]	57
Figure 21. (a) S-type and (b) T-type reactors [P2]	58
Figure 22. Mixing areas with turbulence intensity above 70% in the T-reactor for various flow velocities of CA (a) 20, (b) 40, and (c) 60 ml/min and in the S-reactor for (d) 20, (e) 40, and (f) 60 ml/min [P2]	59
Figure 23. Influence of the process conditions on the particle mean size (a) initial molybdenum concentration at 20 °C and with a flow velocity of 20 ml/min, (b) reagent flow velocity at 20 °C and with Mo concentration of 0.2 M, (c) reaction temperature with a flow velocity of 20 ml/min and with Mo concentration of 0.2 M [P2]	60
Figure 24. Schemes of the wet chemical synthesis carried out in (a) semi-batch and (b) continuous flow reactor (i.e., impinging jet reactor) [P3]	61
Figure 25. Images of MoS ₂ /GO formed in the semi-batch reactor in weight ratios of (a) 10:1, (b) 30:1, (c) 50:1 in SE and BF-STEM modes [P3]	62
Figure 26. Images of MoS ₂ /GO formed in the impinging jet reactor in weight ratios of (a) 10:1, (b) 30:1, (c) 50:1 in SE and BF-STEM mode [P3]	63
Figure 27. Diffractograms of MoS ₂ , MoS ₂ /GO prepared in the semi-batch reactor and impinging jet reactor [P3]	64
Figure 28. LSV curves of (a) MoS ₂ and hybrid nanostructures (b) MoS ₂ /rGO; (c) MoS ₂ /GO; (d) MoS ₂ /CNTs with assumed weight ratios of 5/1, 30/1, 50/1 annealed at 550 and 850 °C [P4]	68
Figure 29. STEM images of MoS ₂ /GO 50/1 550 °C [P4]	69

Figure 30. STEM images of MoS ₂ /CNTs 5/1 550 °C [P4]	69
Figure 31. LSV curve of reference MoS ₂	70
Figure 32. STEM images of reference MoS ₂ [P5]	70
Figure 33. Chronoamperometric measurements of (a) reference and (b) amorphous MoS ₂ , hybrid nanostructures based on (c) GO and (d) CNTs.....	71
Figure 34. Stribeck curves of 10W-40 oil, nanosuspensions of 10W-40 + 1 wt.% of reference MoS ₂ , synthesized MoS ₂ , MoS ₂ /GO, MoS ₂ /rGO, and MoS ₂ /CNTs at temperatures of (a) -10, (b) 0, (c) 25, and (d) 75 °C [P5]	76
Figure 35. Rheograms of 10W-40 oil, nanosuspensions of 10W-40 + 1 wt.% of reference MoS ₂ , synthesized MoS ₂ , MoS ₂ /GO, MoS ₂ /rGO, and MoS ₂ /CNTs at temperatures of (a) -10, (b) 0, (c) 25, and (d) 75 °C [P5].....	78
Figure 36. Temperature correction of the apparent viscosity of the base oil 10W-40 at (a) low cup temperatures; (b) high cup temperatures [P6]	79
Figure 37. Refined viscosity curves of the base oil 10W-40 and the nanosuspensions with MoS ₂ and MoS ₂ /CNMs at (a) -10, (b) 0, (c) 25, (d) 50, (e) 75 °C [P6]	80
Figure 38. Friction factor at a sliding velocity of 0.63 m/s for each suspension containing MoS ₂ /CNTs and base oil at (a) 100, (b) 75, (c) 25, (d) 0, and (e) -10 °C	82
Figure 39. The scheme of the system used for the solid particle size distribution of engine exhaust.....	83
Figure 40. Normalized PSD measured using FAPES (a) at the idle run and (b) with load, (c) particle number size distribution, and (d) particle volume size distribution of engine exhaust	85

List of Tables

Table 1. The estimated hydrogen yield	72
--	----

References

1. Parlament Europejski. Ograniczanie emisji gazów cieplarnianych w UE: krajowe cele na 2030 r. (2022). at
<
3. Singla, M. K., Nijhawan, P. & Oberoi, A. S. Hydrogen fuel and fuel cell technology for cleaner future: a review. *Environmental Science and Pollution Research* **28**, <https://doi.org/10.1007/s11356-020-12231-8> (2021)
4. Tollefson, J. Hydrogen vehicles: Fuel of the future?. *Nature* **464**, <https://doi.org/10.1038/4641262a> (2010)
5. Velazquez Abad, A. & Dodds, P. E. Green hydrogen characterisation initiatives: Definitions, standards, guarantees of origin, and challenges. *Energy Policy* **138**, <https://doi.org/10.1016/j.enpol.2020.111300> (2020)
6. Kakoulaki, G., Kougias, I., Taylor, N., Dolci, F., Moya, J. & Jäger-Waldau, A. Green hydrogen in Europe – A regional assessment: Substituting existing production with electrolysis powered by renewables. *Energy Convers Manag* **228**, <https://doi.org/10.1016/j.enconman.2020.113649> (2021)
7. Dresselhaus, M. S. & Terrones, M. Carbon-based nanomaterials from a historical perspective. *Proceedings of the IEEE* **101**, <https://doi.org/10.1109/JPROC.2013.2261271> (2013)
8. Aqel, A., El-Nour, K. M. M. A., Ammar, R. A. A. & Al-Warthan, A. Carbon nanotubes, science and technology part (I) structure, synthesis and characterisation. *Arabian Journal of Chemistry* **5**, <https://doi.org/10.1016/j.arabjc.2010.08.022> (2012)

9. Choudhary, N., Hwang, S. & Choi, W. Carbon Nanomaterials: A Review. *Handbook of Nanomaterials Properties*. doi:10.1007/978-3-642-31107-9_37 (2014)
10. Chen, D., Feng, H. & Li, J. Graphene oxide: Preparation, functionalization, and electrochemical applications. *Chem Rev* **112**, <https://doi.org/10.1021/cr300115g> (2012)
11. Tadzysak, K., Wychowanec, J. K. & Litowczenko, J. Biomedical applications of graphene-based structures. *Nanomaterials* **8**, <https://doi.org/10.3390/nano8110944> (2018)
12. Gao, W., Alemany, L. B., Ci, L. & Ajayan, P. M. New insights into the structure and reduction of graphite oxide. *Nat Chem* **1**, <https://doi.org/10.1038/nchem.281> (2009)
13. Jiao, K., Wang, X., Wang, Y. & Chen, Y. Graphene oxide as an effective interfacial layer for enhanced graphene/silicon solar cell performance. *J Mater Chem C Mater* **2**, <https://doi.org/10.1039/C4TC00705K> (2014)
14. Sharma, H. & Mondal, S. Functionalized graphene oxide for chemotherapeutic drug delivery and cancer treatment: A promising material in nanomedicine. *Int J Mol Sci* **21**, <https://doi.org/10.3390/ijms21176280> (2020)
15. Polak, D., Zielińska, I., Szwaś, M., Kogut, I. & Małolepszy, A. Modification of ceramic membranes with carbon compounds for pharmaceutical substances removal from water in a filtration—Adsorption system. *Membranes (Basel)* **11**, <https://doi.org/10.3390/membranes11070481> (2021)
16. Zhu, C., Liu, P. & Mathew, A. P. Self-Assembled TEMPO Cellulose Nanofibers: Graphene Oxide-Based Biohybrids for Water Purification. *ACS Appl Mater Interfaces* **9**, <https://doi.org/10.1021/acsami.7b06358> (2017)
17. Tarcan, R., Todor-Boer, O., Petrovai, I., Leordean, C., Astilean, S. & Botiz, I. Reduced graphene oxide today. *J Mater Chem C Mater* **8**, <https://doi.org/10.1039/c9tc04916a> (2020)
18. Stobinski, L., Lesiak, B., Malolepszy, A., Mazurkiewicz, M., Mierzwa, B., Zemek, J., Jiricek, P. & Bieloshapka, I. Graphene oxide and reduced graphene oxide studied by the XRD, TEM and electron spectroscopy methods. *J Electron Spectros Relat Phenomena* **195**, <https://doi.org/10.1016/j.elspec.2014.07.003> (2014)

19. Toh, S. Y., Loh, K. S., Kamarudin, S. K. & Daud, W. R. W. Graphene production via electrochemical reduction of graphene oxide: Synthesis and characterisation. *Chemical Engineering Journal* **251**, <https://doi.org/10.1016/j.cej.2014.04.004> (2014)
20. Alam, S. N., Sharma, N. & Kumar, L. Synthesis of Graphene Oxide (GO) by Modified Hummers Method and Its Thermal Reduction to Obtain Reduced Graphene Oxide (rGO)*. *Graphene* **06**, <https://doi.org/10.4236/graphene.2017.61001> (2017)
21. Xie, X., Zhou, Y. & Huang, K. Advances in microwave-assisted production of reduced graphene oxide. *Front Chem* **7**, <https://doi.org/10.3389/fchem.2019.00355> (2019)
22. Konios, D., Stylianakis, M. M., Stratakis, E. & Kymakis, E. Dispersion behaviour of graphene oxide and reduced graphene oxide. *J Colloid Interface Sci* **430**, <https://doi.org/10.1016/j.jcis.2014.05.033> (2014)
23. Zakrzewska, B., Dembinska, B., Zoladek, S., Rutkowska, I. A., Żak, J., Stobinski, L., Małolepszy, A., Negro, E., di Noto, V., Kulesza, P. J. & Miecznikowski, K. Prussian-blue-modified reduced-graphene-oxide as active support for Pt nanoparticles during oxygen electroreduction in acid medium. *Journal of Electroanalytical Chemistry* **875**, <https://doi.org/10.1016/j.jelechem.2020.114347> (2020)
24. Pisarkiewicz, T., Maziarz, W., Małolepszy, A., Stobiński, L., Michoń, D. & Rydosz, A. Multilayer structure of reduced graphene oxide and copper oxide as a gas sensor. *Coatings* **10**, <https://doi.org/10.3390/coatings10111015> (2020)
25. Dubey, P. K., Tripathi, P., Tiwari, R. S., Sinha, A. S. K. & Srivastava, O. N. Synthesis of reduced graphene oxide-TiO₂ nanoparticle composite systems and its application in hydrogen production. *Int J Hydrogen Energy* **39**, <https://doi.org/10.1016/j.ijhydene.2014.03.104> (2014)
26. Arora, N. & Sharma, N. N. Arc discharge synthesis of carbon nanotubes: Comprehensive review. *Diam Relat Mater* **50**, <https://doi.org/10.1016/j.diamond.2014.10.001> (2014)
27. Kumar, M. & Ando, Y. Chemical vapor deposition of carbon nanotubes: A review on growth mechanism and mass production. *J Nanosci Nanotechnol* **10**, <https://doi.org/10.1166/jnn.2010.2939> (2010)

28. Scott, C. D., Arepalli, S., Nikolaev, P. & Smalley, R. E. Growth mechanisms for single-wall carbon nanotubes in a laser-ablation process. *Appl Phys A Mater Sci Process* **72**, <https://doi.org/10.1007/s003390100761> (2001)
29. Thostenson, E. T., Ren, Z. & Chou, T. W. Advances in the science and technology of carbon nanotubes and their composites: A review. *Compos Sci Technol* **61**, [https://doi.org/10.1016/S0266-3538\(01\)00094-X](https://doi.org/10.1016/S0266-3538(01)00094-X) (2001)
30. Khalil, W., Mohamed, A., Bayoumi, M. & Osman, T. A. Tribological properties of dispersed carbon nanotubes in lubricant. *Fullerenes Nanotubes and Carbon Nanostructures* **24**, <https://doi.org/10.1080/1536383X.2016.1188804> (2016)
31. Dorri Moghadam, A., Omrani, E., Menezes, P. L. & Rohatgi, P. K. Mechanical and tribological properties of self-lubricating metal matrix nanocomposites reinforced by carbon nanotubes (CNTs) and graphene - A review. *Compos B Eng* **77**, <https://doi.org/10.1016/j.compositesb.2015.03.014> (2015)
32. Yu, B., Liu, Z., Zhou, F., Liu, W. & Liang, Y. A novel lubricant additive based on carbon nanotubes for ionic liquids. *Mater Lett* **62**, <https://doi.org/10.1016/j.matlet.2008.01.128> (2008)
33. Sehrawat, P., Julien, C. & Islam, S. S. Carbon nanotubes in Li-ion batteries: A review. *Mater Sci Eng B Solid State Mater Adv Technol* **213**, <https://doi.org/10.1016/j.mseb.2016.06.013> (2016)
34. Pan, H., Li, J. & Feng, Y. P. Carbon nanotubes for supercapacitor. *Nanoscale Res Lett* **5**, <https://doi.org/10.1007/s11671-009-9508-2> (2010)
35. Wang, C., Waje, M., Wang, X., Tang, J. M., Haddon, R. C. & Yan, Y. Proton Exchange Membrane Fuel Cells with Carbon Nanotube Based Electrodes. *Nano Lett* **4**, <https://doi.org/10.1021/nl034952p> (2004)
36. Dubey, R., Dutta, D., Sarkar, A. & Chattopadhyay, P. Functionalized carbon nanotubes: synthesis, properties and applications in water purification, drug delivery, and material and biomedical sciences. *Nanoscale Adv* **3**, <https://doi.org/10.1039/d1na00293g> (2021)

37. Zhou, Y., Fang, Y. & Ramasamy, R. P. Non-covalent functionalization of carbon nanotubes for electrochemical biosensor development. *Sensors (Switzerland)* **19**, <https://doi.org/10.3390/s19020392> (2019)
38. Ma, P. C., Siddiqui, N. A., Marom, G. & Kim, J. K. Dispersion and functionalization of carbon nanotubes for polymer-based nanocomposites: A review. *Compos Part A Appl Sci Manuf* **41**, <https://doi.org/10.1016/j.compositesa.2010.07.003> (2010)
39. Bandyopadhyaya, R., Nativ-Roth, E., Regev, O. & Yerushalmi-Rozen, R. Stabilization of Individual Carbon Nanotubes in Aqueous Solutions. *Nano Lett* **2**, <https://doi.org/10.1021/nl010065f> (2002)
40. Sahu, A., Jain, A. & Gulbake, A. THE ROLE OF CARBON NANOTUBES IN NANOBIOMEDICINES. *Int J Pharm Pharm Sci* **9**, <https://doi.org/10.22159/ijpps.2017v9i6.18522> (2017).
41. Fu, Q., Han, J., Wang, X., Xu, P., Yao, T., Zhong, J., Zhong, W., Liu, S., Gao, T., Zhang, Z., Xu, L. & Song, B. 2D Transition Metal Dichalcogenides: Design, Modulation, and Challenges in Electrocatalysis. *Advanced Materials* **33**, <https://doi.org/10.1002/adma.201907818> (2021)
42. Spalvins, T. Lubrication with sputtered MoS₂ films: Principles, operation, and limitations. *J Mater Eng Perform* **1**, <https://doi.org/10.1007/BF02652388> (1992)
43. Fusaro, R. L. Lubrication and failure mechanisms of molybdenum disulfide films. 2: Effect of substrate roughness. (1978)
44. Vazirisereshk, M. R., Martini, A., Strubbe, D. A. & Baykara, M. Z. Solid lubrication with MoS₂: A review. *Lubricants* **7**, <https://doi.org/10.3390/LUBRICANTS7070057> (2019)
45. Serles, P., Gaber, K., Pajovic, S., Colas, G. & Filleter, T. High Temperature Microtribological Studies of MoS₂ Lubrication for Low Earth Orbit. *Lubricants* **8**, <https://doi.org/10.3390/lubricants8040049> (2020)
46. An, V., Irtegov, Y. & de Izarra, C. Study of tribological properties of nanolamellar WS₂ and MoS₂ as additives to lubricants. *J Nanomater* **2014**, <https://doi.org/10.1155/2014/865839> (2014)

47. Radisavljevic, B., Radenovic, A., Brivio, J., Giacometti, V. & Kis, A. Single-layer MoS₂ transistors. *Nat Nanotechnol* **6**, <https://doi.org/10.1038/nnano.2010.279> (2011)
48. Gant, P., Huang, P., Pérez de Lara, D., Guo, D., Frisenda, R. & Castellanos-Gomez, A. A strain tunable single-layer MoS₂ photodetector. *Materials Today* **27**, <https://doi.org/10.1016/j.mattod.2019.04.019> (2019)
49. Singh, E., Kim, K. S., Yeom, G. Y. & Nalwa, H. S. Atomically thin-layered molybdenum disulfide (MoS₂) for bulk-heterojunction solar cells. *ACS Appl Mater Interfaces* **9**, <https://doi.org/10.1021/acsami.6b13582> (2017)
50. Li, Z., Meng, X. & Zhang, Z. Recent development on MoS₂-based photocatalysis: A review. *Journal of Photochemistry and Photobiology C: Photochemistry Reviews* **35**, <https://doi.org/10.1016/j.jphotochemrev.2017.12.002> (2018)
51. Sun, K., Guo, H., Jiao, F., Chai, Y., Li, Y., Liu, B., Mintova, S. & Liu, C. Design of an intercalated Nano-MoS₂ hydrophobic catalyst with high rim sites to improve the hydrogenation selectivity in hydrodesulfurization reaction. *Appl Catal B* **286**, <https://doi.org/10.1016/j.apcatb.2021.119907> (2021)
52. He, Z. & Que, W. Molybdenum disulfide nanomaterials: Structures, properties, synthesis and recent progress on hydrogen evolution reaction. *Appl Mater Today* **3**, <https://doi.org/10.1016/j.apmt.2016.02.001> (2016)
53. Mao, J., Liu, P., Du, C., Liang, D., Yan, J. & Song, W. Tailoring 2D MoS₂ heterointerfaces for promising oxygen reduction reaction electrocatalysis. *J Mater Chem A Mater* **7**, <https://doi.org/10.1039/C9TA01321K> (2019)
54. Mao, J., Wang, Y., Zheng, Z. & Deng, D. The rise of two-dimensional MoS₂ for catalysis. *Front Phys* **13**, <https://doi.org/10.1007/s11467-018-0812-0> (2018)
55. Strachan, J., Masters, A. F. & Maschmeyer, T. 3R-MoS₂ in Review: History, Status, and Outlook. *ACS Appl Energy Mater* **4**, <https://doi.org/10.1021/acsaem.1c00638> (2021)
56. Zeng, M. & Li, Y. Recent advances in heterogeneous electrocatalysts for the hydrogen evolution reaction. *J Mater Chem A Mater* **3**, Preprint at <https://doi.org/10.1039/c5ta02974k> (2015)

57. Jawaid, A., Nepal, D., Park, K., Jespersen, M., Qualley, A., Mirau, P., Drummy, L. F. & Vaia, R. A. Mechanism for Liquid Phase Exfoliation of MoS₂. *Chemistry of Materials* **28**, <https://doi.org/10.1021/acs.chemmater.5b04224> (2016)
58. Peng, J. & Weng, J. One-pot solution-phase preparation of a MoS₂/graphene oxide hybrid. *Carbon* **94**, <https://doi.org/10.1016/j.carbon.2015.07.035> (2015)
59. Liu, H. F., Wong, S. L. & Chi, D. Z. CVD Growth of MoS₂-based Two-dimensional Materials. *Chemical Vapor Deposition* **21**, <https://doi.org/10.1002/cvde.201500060> (2015)
60. Liu, N., Wang, X., Xu, W., Hu, H., Liang, J. & Qiu, J. Microwave-assisted synthesis of MoS₂/graphene nanocomposites for efficient hydrodesulfurization. *Fuel* **119**, <https://doi.org/10.1016/j.fuel.2013.11.045> (2014)
61. Duraisamy, S., Ganguly, A., Sharma, P. K., Benson, J., Davis, J. & Papakonstantinou, P. One-Step Hydrothermal Synthesis of Phase-Engineered MoS₂/MoO₃ Electrocatalysts for Hydrogen Evolution Reaction. *ACS Appl Nano Mater* **4**, <https://doi.org/10.1021/acsanm.0c03274> (2021)
62. Du, H., Liu, D., Li, M., al Otaibi, R. L., Lv, R. & Zhang, Y. Solvothermal synthesis of MoS₂ nanospheres in DMF-water mixed solvents and their catalytic activity in hydrocracking of diphenylmethane. *RSC Adv* **5**, <https://doi.org/10.1039/C5RA08424E> (2015)
63. Song, H., Wang, B., Zhou, Q., Xiao, J. & Jia, X. Preparation and tribological properties of MoS₂/graphene oxide composites. *Appl Surf Sci* **419**, <https://doi.org/10.1016/j.apsusc.2017.05.022> (2017)
64. Deokar, G., Vancsó, P., Arenal, R., Ravaux, F., Casanova-Cháfer, J., Llobet, E., Makarova, A., Vyalikh, D., Struzzi, C., Lambin, P., Jouiad, M. & Colomer, J. F. MoS₂-Carbon Nanotube Hybrid Material Growth and Gas Sensing. *Adv Mater Interfaces* **4**, <https://doi.org/10.1002/admi.201700801> (2017)
65. Wu, H., Feng, C., Zhang, L., Zhang, J. & Wilkinson, D. P. Non-noble Metal Electrocatalysts for the Hydrogen Evolution Reaction in Water Electrolysis. *Electrochemical Energy Reviews* **4**, <https://doi.org/10.1007/s41918-020-00086-z> (2021)

66. Zhu, J., Hu, L., Zhao, P., Lee, L. Y. S. & Wong, K. Y. Recent Advances in Electrocatalytic Hydrogen Evolution Using Nanoparticles. *Chem Rev* **120**, <https://doi.org/10.1021/acs.chemrev.9b00248> (2020)
67. Ghassemi, M., Kamvar, M. & Steinberger-Wilckens, R. in *Fundamentals of Heat and Fluid Flow in High Temperature Fuel Cells*, doi:10.1016/b978-0-12-815753-4.00004-x (2020)
68. Shinagawa, T., Garcia-Esparza, A. T. & Takanabe, K. Insight on Tafel slopes from a microkinetic analysis of aqueous electrocatalysis for energy conversion. *Sci Rep* **5**, <https://doi.org/10.1038/srep13801> (2015)
69. Bao, F., Kemppainen, E., Dorbandt, I., Bors, R., Xi, F., Schlatmann, R., van de Krol, R. & Calnan, S. Understanding the Hydrogen Evolution Reaction Kinetics of Electrodeposited Nickel-Molybdenum in Acidic, Near-Neutral, and Alkaline Conditions. *ChemElectroChem* **8**, <https://doi.org/10.1002/celec.202001436> (2021)
70. Dupont, M., Hollenkamp, A. F. & Donne, S. W. Electrochemically active surface area effects on the performance of manganese dioxide for electrochemical capacitor applications. *Electrochim Acta* **104**, <https://doi.org/10.1016/j.electacta.2013.04.007> (2013)
71. Gao, X., Zhou, G., Wang, H., Yin, J., Zhang, L., Xiao, F., Siddharth, K., Zhu, S. & Shao, M. Defect engineering of molybdenum-based materials for electrocatalysis. *Catalysts* **10**, <https://doi.org/10.3390/catal10111301> (2020)
72. Li, Y., Wang, H., Xie, L., Liang, Y., Hong, G. & Dai, H. MoS₂ nanoparticles grown on graphene: An advanced catalyst for the hydrogen evolution reaction. *J Am Chem Soc* **133**, <https://doi.org/10.1021/ja201269b> (2011)
73. Wu, L., Longo, A., Dzade, N. Y., Sharma, A., Hendrix, M. M. R. M., Bol, A. A., de Leeuw, N. H., Hensen, E. J. M. & Hofmann, J. P. The Origin of High Activity of Amorphous MoS₂ in the Hydrogen Evolution Reaction. *ChemSusChem* **12**, <https://doi.org/10.1002/cssc.201901811> (2019)
74. Tang, W., Jian, J., Chen, G., Bian, W., Yu, J., Wang, H., Zhou, M., Ding, D. & Luo, H. Carbon Nanotube Supported Amorphous MoS₂ via Microwave Heating Synthesis for

- Enhanced Performance of Hydrogen Evolution Reaction. *Energy Material Advances*, DOI:10.34133/2021/8140964 (2021)
75. Huang, H., Huang, W., Yang, Z., Huang, J., Lin, J., Liu, W. & Liu, Y. Strongly coupled MoS₂ nanoflake-carbon nanotube nanocomposite as an excellent electrocatalyst for hydrogen evolution reaction. *J Mater Chem A Mater* **5**, <https://doi.org/10.1039/C6TA09612C> (2017)
 76. Garbacz, H. & Motyka, M. Chapter 10 – Tribology. *Nanocrystalline Titanium*. <https://doi.org/10.1016/B978-0-12-814599-9.00010-9> (2018)
 77. Hutchings, I. & Shipway, P. *Tribology: Friction and wear of engineering materials: Second Edition*. *Tribology: Friction and Wear of Engineering Materials: Second Edition* (2017)
 78. Adams, D. R. *Tribology and Dynamics of Engine and Powertrain: Fundamentals, Applications and Future Trends*, doi:10.1533/9781845699932.2.251(2010)
 79. Barnes, H. A., Hutton, J. F. & Walters, K. in *An Introduction to Rheology* (1989)
 80. Tanner, R. I. ENGINEERING RHEOLOGY. *CEA, Chemical Engineering in Australia ChE* **7**, (1982)
 81. Dörr, N., Agocs, A., Besser, C., Ristić, A. & Frauscher, M. Engine Oils in the Field: A Comprehensive Chemical Assessment of Engine Oil Degradation in a Passenger Car. *Tribol Lett* **67**, <https://doi.org/10.1007/s11249-019-1182-7> (2019)
 82. Anton Paar GmbH. SAE Viscosity Grades. at <<https://wiki.anton-paar.com/en/sae-viscosity-grades/>>
 83. Danilov, A. M., Bartko, R. v. & Antonov, S. A. Current Advances in the Application and Development of Lubricating Oil Additives. *Petroleum Chemistry* **61**, <https://doi.org/10.1134/S0965544121010035> (2021)
 84. Xie, H., Jiang, B., He, J., Xia, X. & Pan, F. Lubrication performance of MoS₂ and SiO₂ nanoparticles as lubricant additives in magnesium alloy-steel contacts. *Tribol Int* **93**, <https://doi.org/10.1016/j.triboint.2015.08.009> (2016)

85. Song, W., Yan, J. & Ji, H. Tribological Study of the SOCNTs@MoS₂ Composite as a Lubricant Additive: Synergistic Effect. *Ind Eng Chem Res* **57**, <https://doi.org/10.1021/acs.iecr.8b00740> (2018)
86. Wojtalik, M., Wojtas, K., Gołębiowska, W., Jarząbek, M., Orciuch, W. & Łukasz, M. Molybdenum Disulphide Precipitation in Jet Reactors: Introduction of Kinetics Model for Computational Fluid Dynamics Calculations. *Molecules* **27(12)**, <https://doi.org/10.3390/molecules27123943> (2022)
87. Wojtas, K., Makowski, Ł., Orciuch, W. & Bałdyga, J. Comparison of Subgrid Closure Methods for Passive Scalar Variance at High Schmidt Number. *Chem Eng Technol* **38**, <https://doi.org/10.1002/ceat.201400646> (2015)
88. Wojtas, K., Orciuch, W. & Makowski, Ł. Large eddy simulations of reactive mixing in jet reactors of varied geometry and size. *Processes* **8**, <https://doi.org/10.3390/pr8091101> (2020)
89. Wojtas, K., Makowski, Ł. & Orciuch, W. Barium sulfate precipitation in jet reactors: Large eddy simulations, kinetics study and design considerations. *Chemical Engineering Research and Design* **158**, <https://doi.org/10.1016/j.cherd.2020.03.019> (2020)
90. Wojtas, K., Orciuch, W., Wysocki, Ł. & Makowski, Ł. Modeling and experimental validation of subgrid scale scalar variance at high Schmidt numbers. *Chemical Engineering Research and Design* **123**, <https://doi.org/10.1016/j.cherd.2017.05.003> (2017)
91. Wu, W., Niu, C., Tian, Q., Liu, W., Niu, G., Zheng, X., Li, C., Jia, Y., Wei, C. & Xu, Q. Amorphous-MoO_{3-x}/MoS₂ heterostructure: In situ oxidizing amorphization of S-vacancy MoS₂ for enhanced alkaline hydrogen evolution. *Chemical Communications* **56**, <https://doi.org/10.1039/D0CC05888B> (2020)
92. Penconek, A., Jackiewicz, A. & Moskal, A. Penetration of diesel exhaust particles (DEPs) through fibrous filters produced using melt-blown technology. *KONA Powder and Particle Journal*, <https://doi.org/10.14356/kona.2015008> (2015)

93. Penconek, A., Drayk, P. & Moskal, A. Penetration of diesel exhaust particles through commercially available dust half masks. *Annals of Occupational Hygiene* **57**, <https://doi.org/10.1093/annhyg/mes074> (2013)
94. Jałowiecka, M., Bojarska, Z., Małolepszy, A. & Makowski, Ł. Mass transport enhancement in direct formic acid fuel cell with a novel channel design. *Chemical Engineering Journal*, **451**, <https://doi.org/10.1016/j.cej.2022.138474>. (2023)